

The nature of the Diffuse Gamma-Ray Background

Mattia Fornasa

School of Physics and Astronomy, University of Nottingham, University Park NG7 2RD, UK

Miguel A. Sánchez-Conde

*Oskar Klein Centre for Cosmoparticle Physics, Department of Physics, Stockholm University,
SE-10691 Stockholm, Sweden*

Abstract

We review the current understanding of the diffuse gamma-ray background (DGRB). The DGRB is what remains of the total measured gamma-ray emission after the subtraction of the resolved sources and of the diffuse Galactic foregrounds. It is interpreted as the cumulative emission of sources that are not bright enough to be detected individually. Yet, its exact composition remains unveiled. Well-established astrophysical source populations (e.g. blazars, misaligned AGNs, star-forming galaxies and millisecond pulsars) all represent guaranteed contributors to the DGRB. More exotic scenarios, such as dark matter annihilation or decay, may contribute as well. In this review, we describe how these components have been modeled in the literature and how the DGRB can be used to provide valuable information on each of them. We summarize the observational information currently available on the DGRB, paying particular attention to the most recent measurement of its intensity energy spectrum by the *Fermi* LAT Collaboration. We also discuss the novel analyses of the auto-correlation angular power spectrum of the DGRB and of its cross-correlation with tracers of the large-scale structure of the Universe. New data sets already (or soon) available are expected to provide further insight on the nature of this emission. By summarizing where we stand on the current knowledge of the DGRB, this review is intended both as a useful reference for those interested in the topic and as a means to trigger new ideas for further research.

Keywords:

Email addresses: `fornasam@gmail.com` (Mattia Fornasa), `sanchezconde@fysik.su.se` (Miguel A. Sánchez-Conde)

Contents

Table of acronyms	2
1 Introduction	3
2 The intensity energy spectrum	6
2.1 The new <i>Fermi</i> LAT measurement of the Diffuse Gamma-Ray Background	6
2.2 The astrophysical components of the Diffuse Gamma-Ray Background . .	7
2.2.1 Blazars	9
2.2.2 Misaligned Active Galactic Nuclei	15
2.2.3 Star-forming galaxies	16
2.2.4 Millisecond pulsars	22
2.2.5 Other astrophysical components	25
2.3 The Dark Matter component of the Diffuse Gamma-Ray Background . . .	29
2.3.1 The case of annihilating Dark Matter	30
2.3.2 The case of decaying Dark Matter	39
3 The angular power spectrum of anisotropies	41
3.1 The <i>Fermi</i> LAT measurement of gamma-ray anisotropies	42
3.2 Deducing the nature of the DGRB from its anisotropies	44
4 The photon count distribution	52
5 The cross-correlation with independent probes	55
5.1 The cross-correlation with galaxy catalogs	55
5.2 The cross-correlation with cosmic shear	62
5.3 The cross-correlation with other tracers	66
6 The science of the Diffuse Gamma-Ray Background	67
7 Acknowledgments	73

Table of acronyms

1FGL	<i>Fermi</i> LAT First Source Catalog
2FGL	<i>Fermi</i> LAT Second Source Catalog
2FPC	<i>Fermi</i> LAT Second Catalog of gamma-ray pulsars
2LAC	<i>Fermi</i> LAT Second Catalog of Active Galactic Nuclei
2MASS	2 Micron All-Sky Survey
3FGL	<i>Fermi</i> LAT Third Source Catalog
AGN	Active Galactic Nucleus
APS	Angular Power Spectrum
CFHTLenS	Canada-France-Hawaii Telescope Lensing Survey
CMB	Cosmic Microwave Background
CR	Cosmic Ray
CTA	Cherenkov Telescope Array
DES	Dark Energy Survey
DESI	Dark Energy Spectroscopic Instrument
DGRB	Diffuse Gamma-Ray Background
DM	Dark Matter

eBOSS	extended Baryon Oscillation Spectroscopy Survey
EBL	Extragalactic Background Light
FRI	Fanaroff-Riley Class I
FRII	Fanaroff-Riley Class II
FSRQ	Flat-Spectrum Radio Quasar
HMF	Halo Mass Function
HOD	Halo Occupation Distribution
HSP	High-Synchrotron Peak
IC	Inverse Compton
IR	InfraRed
ISP	Intermediate-Synchrotron Peak
JWST	James Webb Space Telescope
LF	Luminosity Function
LOFAR	Low-Frequency Array
LSP	Low-Synchrotron Peak
LSS	Large-Scale Structure
MAGN	Misaligned Active Galactic Nucleus
MSP	MilliSecond Pulsar
MW	Milky Way
NFW	Navarro-Frenk-White
NuSTAR	Nuclear Spectroscopic Telescope Array
NVSS	NRAO VLA Sky Survey
PDF	Probability Distribution Function
PSF	Point Spread Function
SDSS	Sloan Digital Sky Survey
SED	Spectral Energy Distribution
SFG	Star-Forming Galaxy
SFR	Star-Forming Rate
SKA	Square Kilometer Array
UHECR	Ultra-High-Energy Cosmic Ray
UV	UltraViolet
WIMP	Weakly Interacting Massive Particle
WISE	Wide-field Infrared Survey Explorer
WMAP	Wilkinson Microwave Anisotropy Probe

1. Introduction

The first full-sky image of gamma-ray emission was obtained in 1972 by the OSO-3 satellite. It consisted of 621 events detected above 50 MeV [1]. Since then, telescopes with lower sensitivities and better angular and energy resolutions have significantly improved our understanding of the gamma-ray Universe. The all-sky maps produced by the Fermi Large Area Telescope¹ (*Fermi* LAT from now on) after more than 6 years of data taking contain more than 5 million events above 1 GeV. These maps exhibit a rich morphology: along the Galactic plane, the diffuse Galactic foreground is the most evident feature and, overall, it accounts for $\sim 80\%$ of the detected gamma rays. This diffuse radiation is produced by the interaction of cosmic rays (CRs) with the Galactic interstellar radiation field and with the nuclei of the Galactic interstellar medium. Also,

¹<http://fermi.gsfc.nasa.gov/>

the Third *Fermi* LAT catalog (3FGL) reported the detection of 3033 sources throughout the sky [2]. Extended gamma-ray emitters are discussed in Ref. [3]. Other structures, e.g. the Fermi bubbles [4], represent more complex phenomena, whose emission is not fully understood yet.

In order to reproduce the data from the *Fermi* LAT it is necessary to include one additional contribution, i.e. a diffuse and *nearly* isotropic emission called the Diffuse Gamma-Ray Background (DGRB) [1, 5, 6, 7, 8, 9]. The DGRB is thought to be predominantly of extragalactic origin: gamma-ray sources with a flux smaller than the sensitivity of *Fermi* LAT are not detected individually, producing instead a cumulative diffuse glow that contributes to the DGRB. Unresolved blazars [10, 11, 12, 13, 14, 15, 16, 17, 18, 19, 20, 21, 22, 23, 24, 25], misaligned Active Galactic Nuclei (MAGNs) [26, 27, 28, 29], star-forming galaxies (SFGs) [30, 31, 32, 33, 34, 35] and millisecond pulsars (MSPs) [36, 37, 38] are guaranteed components to the DGRB. More uncertain source classes, e.g. galaxy clusters [39] or Type Ia supernovae [40, 41], may also play a role, together blue with diffuse phenomena, e.g. the radiation produced by the interaction of Ultra-High-Energy Cosmic Rays (UHECRs) with the Extragalactic Background Light (EBL) [42, 43].² It is possible to estimate how much different source classes contribute to the DGRB, but its exact composition remains one of the main unanswered questions of gamma-ray astrophysics. Finding a definitive answer would constrain the faint end of the luminosity function of the DGRB contributors. Indeed, the study of the DGRB may represent the only source of information about those objects that are too faint to be detected individually.

The DGRB may also shed some light on exotic Physics as, e.g., on the nature of Dark Matter (DM): a huge experimental effort is currently devoted to the so-called indirect detection of DM, i.e. the search for particles (e.g. gamma rays, neutrinos, positrons or anti-protons) produced by the annihilations or decays of DM. Such a signal would constitute the first evidence that DM can interact non-gravitationally and it would represent an enormous step forward in our understanding of its nature [44, 45, 46, 47]. Targets like the center of the Milky Way (MW), local satellite galaxies or nearby galaxy clusters are considered optimal, thanks to the intensity of the expected DM signal and/or to the absence of significant competing backgrounds. Yet, no signal has been robustly associated with DM. Then, if DM annihilates or decays producing gamma rays and such a signal has not been detected up to now, it is most probably unresolved and it contributes to the DGRB. Looking for the features of a DM component in the DGRB, one can, then, hope to finally unravel the long-standing mystery of the nature of DM [48, 49, 50, 51, 52, 53, 54, 55, 56, 57, 58, 59, 45, 60, 61, 62, 63, 64, 65].

The most recent measurement of the intensity of the DGRB has been performed by the *Fermi* LAT, in the range between 100 MeV and 820 GeV [9] (see also Refs. [1, 5, 6, 7, 8] for the previous measurements). Valuable information on the nature of the DGRB can be extracted from its intensity energy spectrum. Its steepness could indicate whether a particular class of sources dominates the emission. Moreover, the transition between two energy regimes dominated by different classes could, in principle, give rise

²Different names have been used in the literature to denote the DGRB, e.g. Extragalactic Gamma-Ray Background or Isotropic Gamma-Ray Background. We believe the denomination used in this review is more precise since, as we will see in the following sections, the DGRB may be not entirely extragalactic and since it exhibits a certain amount of anisotropy. We also note that, in Ref. [9], the *Fermi* LAT Collaboration uses the name Extragalactic Gamma-Ray Background to characterize the cumulative emission of *all* sources (both resolved and unresolved), while Isotropic Gamma-Ray Background refers to the unresolved component only, i.e. what we call DGRB (see Sec. 2).

to breaks and features in the energy spectrum. Yet, since the intensity of the DGRB is only sensitive to the sum of its contributions, ultimately there is only a limited amount of information that can be extracted from it.

Fortunately, due to its excellent sensitivity and exemplary angular resolution, the *Fermi* LAT marked the beginning of an era in which the intensity energy spectrum is no longer the only observational data available for the study of the DGRB. In 2012, the first measurement of anisotropies in the DGRB was reported [66], and the detection of a non-null auto-correlation angular power spectrum (APS) provided complementary constraints on the composition of the DGRB [67, 68, 63]. Moreover, in Ref. [69], the authors used the photon-count probability distribution measured after 11 months of *Fermi* LAT data to constrain the contribution of unresolved blazars to the DGRB. More recently, the cross-correlation of the DGRB anisotropies with observables tracing the Large Scale Structure (LSS) of the Universe has also been considered. In Ref. [70] the authors measured the 2-point correlation of the DGRB with 5 different galaxy catalogs and they reported a signal with 4 of them. Ref. [71], instead, cross-correlated the DGRB with the cosmic shear observed by the Canada France Hawaii Telescope Lensing Survey (CFHTLenS) and found no significant detection. These works, together with Refs. [72, 73, 74, 75], have proved that the study of the cross-correlation of the DGRB with the LSS is a very powerful strategy that may provide access to components of the DGRB that are only subdominant in the intensity energy spectrum or in the auto-correlation APS. In particular, the technique has the potential to deliver the first detection of DM-induced gamma-ray emission.

In the near future, the data on the DGRB is expected to further increase, due to the extended run of the *Fermi* LAT and to the fore-coming Cherenkov Telescope Array (CTA) [76, 77]. Other frequencies and other messengers will also be crucial to improve our modeling of the DGRB and to extract complementary information about its nature. The scenario is rapidly evolving and the study of the DGRB is quickly becoming a standard tool for the characterization of unresolved astrophysical sources and of a potential DM-induced gamma-ray signal.

Therefore, we believe that this is the right moment to summarize where we stand in our understanding of the DGRB. In this article we will survey the data available on the DGRB at present and we will discuss how these observations have been used to constrain the nature of the emission. We will also enumerate the classes of sources or emission mechanisms that have been proposed as contributors to the DGRB. By sketching a snapshot of the state-of-art on the DGRB *circa* 2015, we intend to provide the community with a reference point from which to build on.

We end by noting that the DGRB is intrinsically an analysis- and time-dependent quantity. Indeed, its intensity depends on the sensitivity of the telescope employed to detect it and on its instrumental capability to resolve sources. Even with the same detector, an increase in statistics or, in general, any improvement in the detection sensitivity will result in a different DGRB. In the following sections, every time we mention the DGRB we will make sure to specify which measurement of the DGRB we refer to.

The paper is organized as follows: in Sec. 2 we focus on the intensity of the DGRB. Sec. 2.1 reviews the recent measurement of the DGRB energy spectrum by the *Fermi* LAT, while Secs. 2.2 and 2.3 are devoted to the description of the sources that have been proposed as contributors to the emission: astrophysical objects are studied in Sec. 2.2, while Sec. 2.3 discusses the case of the DM-induced emission. Sec. 3 reviews the *Fermi* LAT measurement of the auto-correlation APS of anisotropies and its impact on our understanding of the DGRB. The topic of Sec. 4 is the measurement and the

interpretation of the photon count probability distribution, while in Sec. 5 we investigate the cross-correlation with probes of LSS, namely galaxy catalogs in Sec. 5.1, cosmic shear in Sec. 5.2 and other observables in Sec. 5.3. Finally, we present our conclusions in Sec. 6.

2. The intensity energy spectrum

The subject of this section is the intensity energy spectrum of the DGRB. The first subsection (Sec. 2.1) summarizes the most recent measurement of this observable, i.e. the one performed by the *Fermi* LAT in Ref. [9]. The following subsections (Sec. 2.2 and Sec. 2.3) present the different source classes and emission mechanisms that have been proposed to interpret the observed emission. For each population we summarize how the DGRB energy spectrum has been used to learn about the properties of the gamma-ray emitters.

2.1. The new *Fermi* LAT measurement of the Diffuse Gamma-Ray Background

The *Fermi* LAT [78] on board the NASA *Fermi* satellite started its scientific operation on August 2008 and, since then, it has revolutionized our knowledge of the most violent phenomena in the Universe. The *Fermi* LAT covers 4 decades in energy, from few dozens of MeV up to the TeV regime. It has an unprecedented sensitivity (~ 30 times better than its predecessor EGRET) and an extremely large field of view reaching almost one fifth of the sky. Its angular resolution is of about 0.8° at 1 GeV and better than 0.2° above 10 GeV.³ Such superb capabilities allowed the discovery of hundreds of new gamma-ray sources and an impressive cartography of the Galactic CR-induced gamma-ray diffuse emission that reaches, for the first time, energies greater than 10 GeV [79].

In addition to these achievements, the analysis of 10 months of data delivered the first *Fermi* LAT measurement of the DGRB energy spectrum at Galactic latitudes, b , greater than 10 degrees [8]. Such a measurement was performed between 200 MeV and 102 GeV and it represents the third independent observation of the DGRB, after the one by the SAS-2 satellite in 1978 between 40 and 300 MeV [80] and that by EGRET between 40 MeV and 10 GeV in 1998 [6]. The energy spectrum of the DGRB as measured by the *Fermi* LAT in Ref. [8] is featureless and it can be well described by a single power law with a spectral index of 2.41 ± 0.05 . This is significantly softer than both the DGRB initially reported by EGRET [6] and the revised estimate of Ref. [81] from the same data set.⁴

More recently, a new measurement of the DGRB energy spectrum has been performed by the *Fermi* LAT [9]. The analysis used 50 months of data with $|b| > 20^\circ$, it employed a dedicated event selection and it took advantage of improvements in the determination of the CR background and of the diffuse Galactic foreground. The measurement, denoted by red data points in Fig. 1, now extends down to 100 MeV and up to 820 GeV. It represents the most complete and accurate picture that we currently possess of the DGRB intensity. Interestingly, the DGRB now exhibits a high-energy exponential cut-off at 279 ± 52 GeV (for the baseline model of Galactic diffuse foreground used in Ref. [9]), and it is well described by a single power law with a spectral index of 2.31 ± 0.02 at lower

³These values refer to the 68% containment radius.

⁴However, note that, in the re-analysis of Ref. [81], the energy spectrum is well described by a single power law *only* up to 2 GeV.

energies. The cut-off is compatible with the attenuation expected from the interaction of high-energy photons with the EBL [82, 83, 84, 85, 86, 87, 88] over cosmological distances [25]. The largest systematic uncertainty (represented by the red shaded region in Fig. 1) ranges between a factor of $\sim 15\%$ and 30% (depending on the energy range considered) and it comes from the modeling of the Galactic diffuse emission.

For the purposes of this review, it is convenient to briefly summarize here the main steps followed in Ref. [9] to measure the DGRB. Two different sets of selection cuts are applied to the gamma-ray data, optimized over different energy ranges, namely below and above 12.8 GeV. Different selection criteria are required because of the energy dependence in the composition of the CR-induced backgrounds and the way CRs interact with the detector. For the low-energy data sample, the all-sky Galactic diffuse emission is modeled as a sum of templates obtained with GALPROP⁵ and the point-like sources are modeled following the information in the Second *Fermi* LAT catalog (2FGL). Additional templates are used to model subdominant contributions from the Loop I large-scale Galactic structure and from electrons interacting with the Solar radiation field through Inverse Compton (IC). A fully isotropic template is also included, in order to describe the DGRB and the residual CR contamination. The fit to the data determines the normalizations of the different templates and it is performed independently in each energy bin considered. At the highest energies, where the statistic is scarce, the normalizations of the templates for the Galactic diffuse emission are fixed to the best-fit values obtained at intermediate energies (between 6.4 and 51.2 GeV). The spectral shapes of their emission are also fixed to those predicted by GALPROP. Above 12.8 GeV, then, the normalizations of the point-like sources and of the isotropic template are the only free parameters in the fit.

Monte Carlo simulations are used to estimate the residual CR contamination. The energy spectrum of the DGRB is, finally, obtained by subtracting the CR contamination from the isotropic component determined in the template fitting. The systematic error induced by the imperfect knowledge of the Galactic diffuse emission is estimated by repeating the whole procedure for three benchmark models of Galactic foreground and for different values of the parameters controlling the propagation of CRs in the MW (see Ref. [9] for further details).

2.2. The astrophysical components of the Diffuse Gamma-Ray Background

In this section we describe the classes of astrophysical sources and emission mechanisms that have been proposed as contributors to the DGRB over the years. Well-established astrophysical populations, whose brightest members have been robustly detected, represent “guaranteed” components to the DGRB. They are discussed in Sec. 2.2.1, Sec. 2.2.2, Sec. 2.2.3 and Sec. 2.2.4, which are devoted, respectively, to blazars, MAGNs, SFGs and MSPs. Then, in Sec. 2.2.5, we turn to more speculative scenarios. We do not discuss the possibility of a DM-induced contribution to the DGRB, since that is the subject of the following section (Sec. 2.3).

We start by presenting a formalism that will be adopted throughout the manuscript for the description of a generic population of sources. The sources are supposed to be characterized by a measurable quantity Y . In most cases Y will be the blue gamma-ray luminosity L_γ of the source but, in some instances, it will indicate another parameter such as, e.g., the mass of the galaxy or of the DM halo hosting the gamma-ray emitter. The differential gamma-ray flux $d\Phi/dEd\Omega$ (i.e. the number of photons per unit area,

⁵A CR propagation code available from <http://galprop.stanford.edu>. See also Ref. [79].

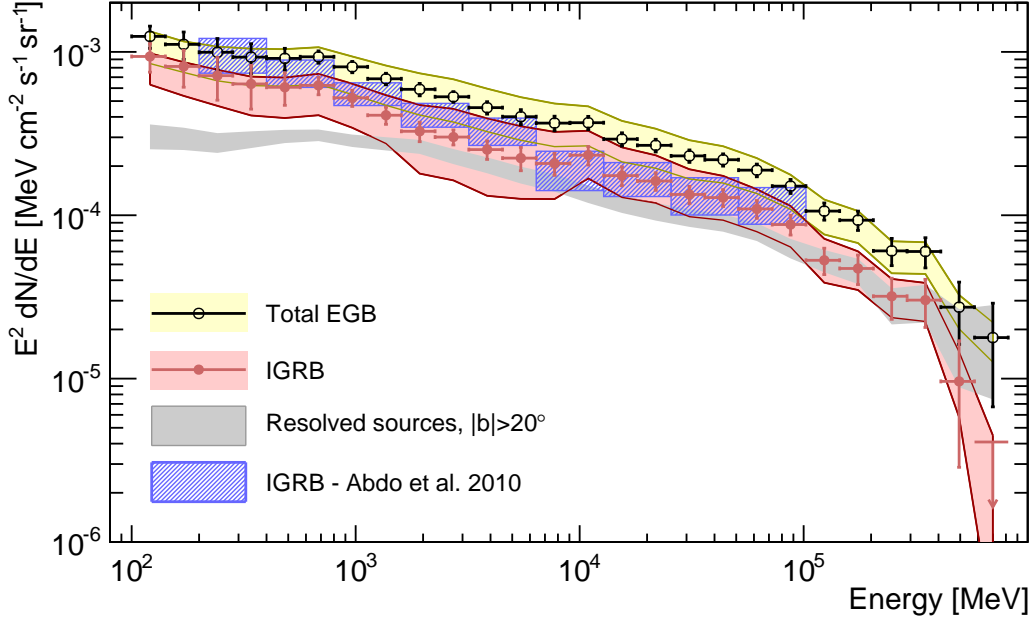


Figure 1: In red, the DGRB intensity energy spectrum, labeled “Isotropic Gamma-Ray Background (IGRB)” in the figure. Model A from Ref. [9] is used for the diffuse Galactic foreground. The spectrum is compared to the previous *Fermi* LAT measurement of the DGRB from Ref. [8] (blue bands) and to the total “Extragalactic Gamma-ray Background (EGB)” (black data points). The latter is defined here as the sum of the DGRB and of the resolved sources at $|b| > 20^\circ$ (shown in gray). The comparison shows that, above 100 GeV, $\sim 50\%$ of the Extragalactic Gamma-ray Background is now resolved into individual LAT sources. Yellow and red shaded bands represent the systematic error associated with the uncertainties in the modeling of the Galactic diffuse emission. Taken from Ref. [9].

time, energy and solid angle) expected from the *unresolved* objects in such a population can be written as follows:

$$\frac{d\Phi}{dE d\Omega}(E_0) = \int_{z_{\min}}^{z_{\max}} dz \int_{Y_{\min}}^{Y_{\max}} dY \int_{\Gamma_{\min}}^{\Gamma_{\max}} d\Gamma \frac{dN}{dV dY d\Gamma}(z, Y, \Gamma) \frac{dV}{dz d\Omega} F_{E_0}(z, Y, \Gamma) \times \left(1 - \frac{\Omega(z, Y, \Gamma)}{\Omega_{\max}}\right) e^{-\tau_{\text{EBL}}(E_0, z)}, \quad (1)$$

where z is the redshift and Γ is a parameter that characterizes the shape of the energy spectrum of the sources. The domain of integration will depend on the particular population considered. The factor $dN/dV dY d\Gamma$ indicates the comoving number density of sources per unit Y and Γ , while $dV/dz d\Omega$ is the comoving volume per unit redshift and solid angle. The factor $F_{E_0}(z, Y, \Gamma)$ is the gamma-ray flux (at energy E_0) produced by the source identified by the value Y , located at redshift z and with an energy spectrum characterized by Γ . If sources are described by their gamma-ray luminosity ($Y = L_\gamma$), F_{E_0} can be written as follows:

$$F_{E_0} = \frac{(1+z)^2 L_\gamma}{4\pi D_L(z)^2} g_{E_0}(\Gamma), \quad (2)$$

where $D_L(z)$ is the luminosity distance at redshift z and $g_{E_0}(\Gamma)$ parametrizes the gamma-ray energy spectrum. For other choices of Y , the relation between Y and F_{E_0} needs to

be specified case per case.

Thus, the first line of Eq. (1) indicates the cumulative emission expected from all the sources located between z_{\min} and z_{\max} and with characteristics between $(Y_{\min}, \Gamma_{\min})$ and $(Y_{\max}, \Gamma_{\max})$. The quantity $\Omega(z, Y, \Gamma)$ is called sky coverage and it is defined as the area Ω_{\max} surveyed by the telescope multiplied by the detection efficiency. It represents the probability for a source characterized by parameters (z, Y, Γ) to be detected and it encodes the sensitivity of the instrument, i.e. $\Omega(z, Y, \Gamma)$ is equal to zero if the source is too faint to be detected. It also accounts for any potential selection effect. An estimate of $\Omega(z, Y, \Gamma)$ for the high-latitude blazars in the first *Fermi* LAT catalog (1FGL) is provided in Ref. [18]. Then, the factor $(1 - \Omega(z, Y, \Gamma)/\Omega_{\max})$ in Eq. (1) has the effect of selecting only the sources that remain undetected. Finally, the exponential $e^{-\tau_{\text{EBL}}(E_0, z)}$ accounts for the effect of the EBL attenuation.

It is also convenient to define a generic expression for the differential source count distribution dN/dS , i.e. the number of sources per unit solid angle and per unit flux S :

$$\frac{dN}{dS} = \int_{z_{\max}}^{z_{\min}} dz \int_{\Gamma_{\min}}^{\Gamma_{\max}} d\Gamma \frac{dN}{dV dY d\Gamma}(z, Y, \Gamma) \frac{dV}{dz d\Omega} \frac{dY}{dS} \frac{\Omega(z, Y, \Gamma)}{\Omega_{\max}}, \quad (3)$$

where S is the gamma-ray flux associated with the source characterized by (z, Y, Γ) .⁶ Note that the factor $\Omega(z, Y, \Gamma)/\Omega_{\max}$ has now the effect of selecting only the resolved objects. The number of sources (per solid angle) with a flux larger than \bar{S} , i.e. the *cumulative* source count distribution $N(> \bar{S})$, can be obtained by integrating Eq. (3) above \bar{S} .

2.2.1. Blazars

Blazars are among the brightest gamma-ray sources in the sky. They are interpreted as Active Galactic Nuclei (AGNs) with the relativistic jet directed towards the observer [89, 90]. The emission coming from the jet normally outshines the radiation associated with the accretion onto the supermassive Black Hole at the center of the nucleus. The Spectral Energy Distribution (SED) is bimodal: the low-energy peak is located between ultraviolet (UV) and radio frequencies and it corresponds to the synchrotron emission produced by the electrons that are accelerated in the jet. Instead, the high-energy peak reaches the gamma-ray band and it is produced by IC of the same population of synchrotron-emitting electrons. The seed photons for the IC emission come either from the synchrotron radiation itself (i.e., the so-called synchrotron self-Compton) or from the accretion disk (external Compton). Blazars can be divided in two categories: BL Lacs and Flat Spectrum Radio Quasars (FSRQs). Sources belonging to the first class have a nuclear non-thermal emission so strong that the rest-frame equivalent width of the strongest optical emission line is narrower than 5 Å, while FSRQs have broader lines and a spectral index $\alpha_r < 0.5$ in the radio band. Blazars have also been classified according to the frequency of their synchrotron peak, ν_S [91, 92]: low-synchrotron-peaked (LSP) blazars have a peak in the infrared (IR) or far-IR band, ($\nu_S < 10^{14}$ Hz), intermediate-synchrotron-peaked (ISP) blazars for ν_S in the near-IR or UV (10^{14} Hz $\leq \nu_S < 10^{15}$ Hz) and high-synchrotron-peaked (HSP) blazars for $\nu_S \geq 10^{15}$ Hz, i.e. in the UV band or higher. From the study of the 886 blazars present in the Second *Fermi* LAT AGN catalog (2LAC) [93] it was confirmed that FSRQs (which are almost entirely LSPs) are

⁶Normally S is the gamma-ray flux above some energy E_{\min} and, therefore, it is related to $F_{E_0}(z, Y, \Gamma)$ as $S = \int_{E_{\min}} F_{E_0}(z, Y, \Gamma) dE_0$.

generally brighter than BL Lacs. Also, it was possible to determine a correlation between the steepness of their energy spectrum (in the gamma-ray band) and the position of the synchrotron peak, suggesting that FSRQs (with a low ν_s) have softer spectra than BL Lacs [93].

Since the EGRET era, blazars were suspected to play a significant role in explaining the DGRB emission, with estimates ranging from 20% to 100% [94, 10, 11, 12, 13, 15, 95, 30, 16]. Fewer AGNs were known before the *Fermi* LAT (66 in the third EGRET catalog [96], mainly FSRQs), preventing reliable population studies to be performed entirely at gamma-ray energies. Predictions for the emission of unresolved blazars were obtained by means of well-established correlations between the gamma-ray luminosity L_γ and the luminosity at lower frequencies, either in the radio or in the X-ray band [94, 11]. Thus, the strategy followed in these early works was to characterize the blazar population in those low-frequency regimes, where the statistical sample was much larger, and then export the information up to the gamma-ray range by means of the aforementioned correlation between luminosities.

Ref. [16] considers the correlation between L_γ and the luminosity in X-rays, L_X . The $L_\gamma - L_X$ connection is a consequence of the relation between the emission of the jet (which can be linked to L_γ) and the mass accretion onto the supermassive Black Hole [97, 98, 99, 100]. This, in turn, correlates with the X-ray luminosity of the accretion disk L_X . Ref. [16] considers L_γ as the Y -parameter in Eqs. (1) and (3). The dependence on Γ in the factor $dN/dVdL_\gamma d\Gamma$ is taken care of by the so-called “blazar sequence” [101, 102, 103], which predicts how the shape of the blazar SED changes as a function of their luminosity. Then, integrating Eq. 1 over Γ , the blazar sequence selects, for each L_γ , the only SED compatible with L_γ . On the other hand, $dN/dVdL_\gamma$ is the gamma-ray luminosity function (LF), $\Phi_\gamma(z, L_\gamma)$. Given the $L_\gamma - L_X$ relation, $\Phi_\gamma(z, L_\gamma)$ can be inferred from the X-ray LF $\Phi_X(L_X, z)$:

$$\Phi_\gamma(L_\gamma, z) = \kappa \frac{dL_X}{dL_\gamma} \Phi_X(L_X, z). \quad (4)$$

The factor κ indicates the fraction of AGNs observed as blazars and a parametrization for $\Phi_X(z, L_X)$ is available in Refs. [104, 105, 106]. X-ray AGNs are found to evolve positively (i.e. they are more abundant as redshift increases) until a certain redshift peak z_c , above which the X-ray LF decreases [104, 105, 106]. It was found that allowing z_c to vary with L_X (i.e., what is called a luminosity-dependent density evolution) provides a better description of the blazars observed by EGRET than other evolution schemes, e.g., pure luminosity evolution or pure density evolution [13].

Parameter κ in Eq. (4) is left free in the analysis of Ref. [16], together with the faint-end slope γ_1 of the X-ray LF and the proportionality coefficient between L_γ and L_X .⁷ These parameters are determined by a maximum-likelihood fit to the differential source count dN/dS of the blazars detected by EGRET. The best-fit model is, then, used to determine the contribution of unresolved blazars to the DGRB through Eq. (1). Ref. [16] finds that unresolved blazars can explain approximately 45% of the DGRB measured by EGRET in Ref. [7] at 100 MeV.

Similar results are obtained in other works that follow the same formalism: Refs. [13,

⁷More precisely, the assumed proportionality is between L_X and the so-called “bolometric luminosity”, i.e. a measure of the total emission power of the source. However, under the hypothesis of the blazar sequence, L_γ can be uniquely derived from the bolometric luminosity.

[107, 52] also consider a luminosity-dependent density evolution for the X-ray LF but they assume a common power-law energy spectrum at gamma-ray frequencies, instead of the SED predicted by the blazar sequence. In Ref. [19] the formalism outlined before is fitted to both the blazar dN/dS computed from the 1FGL [108] and to the first *Fermi* LAT measurement of the DGRB in Ref. [8] (see also Ref. [109]). The result of the fit proves that it is possible to explain both observables with one single population of blazars.⁸ Their predictions are re-calibrated in Ref. [68], where the model is fitted against the 1FGL dN/dS and the *Fermi* LAT measurement of the DGRB auto-correlation APS of anisotropies from Ref. [66] (see Sec. 3). Ref. [68] finds that the DGRB intensity energy spectrum and the auto-correlation APS cannot be *simultaneously* explained in terms of unresolved blazars, since a model that fits both the abundance of resolved blazars (i.e., their dN/dS) and the DGRB intensity energy spectrum would exceed the measured auto-correlation APS. Alternatively, unresolved blazars can reproduce the measured anisotropies but, then, their emission only accounts for a maximum of 4.3% of the DGRB intensity in Ref. [8], above 1 GeV.

Instead of using the $L_\gamma - L_X$ correlation discussed above, Ref. [11] relates L_γ to the radio luminosity, L_r . The gamma-ray LF is inferred from the radio LF, similarly to what done in Eq. (4). The radio LF is taken from Ref. [110]. A power-law energy spectrum is assumed at gamma-ray frequencies, while the distribution of spectral indexes $dN/d\Gamma$ is calibrated to reproduce the sources detected by EGRET. Ref. [11] finds that unresolved blazars can fit reasonably well the EGRET DGRB energy spectrum reported in Ref. [6]. Other works exploit the $L_\gamma - L_r$ relation with similar findings: Ref. [111] determines the properties of the blazar population by fitting their measured radio LF (assuming it follows a pure luminosity evolution), while in Ref. [20] the fit is performed with the cumulative source distribution $N(> S)$ of 1FGL blazars. The authors of Ref. [20] also caution about the use of the sky coverage determined in Ref. [18], since it may be affected by systematic uncertainties in the low-flux regime due to low statistics.

With the advent of the *Fermi* era, direct population studies at gamma-ray frequencies became possible, without the need to rely on correlations with lower frequencies. Following the formalism of Eqs. (1) and (3), in Ref. [18] the Y parameter is taken to be the flux S above 100 MeV. The energy spectra of the blazars are assumed to be power laws with indexes Γ characterized by a Gaussian probability distribution independent of S . The gamma-ray LF $dN/dVdS$ is combined with the factor $dV/dz d\Omega$ in Eq. (3) into $dN/dz dS d\Omega$, which is assumed to be the same for all the sources considered and to depend on S as a broken power law. No correlation with other frequencies is required. The parameters of the broken power law (as well as the mean and standard deviation of the Gaussian distribution for Γ) are inferred through a maximum-likelihood fit to the blazars in the 1FGL with $|b| > 20^\circ$. The best-fit point has a break at $S = (5.99 \pm 0.91) \times 10^{-8} \text{cm}^{-2} \text{s}^{-1}$ and slopes of 1.58 ± 0.08 and 2.44 ± 0.11 above and below the break [18]. The model is, then, used to determine the cumulative emission of unresolved sources. Results indicate that unresolved blazars (with $S_{\min} = 0$) account for 23% of the DGRB detected by *Fermi* LAT in Ref. [8].

Ref. [22] improves the analysis in Ref. [18], attacking one of its main limitations, i.e. the fact that the broken power law considered for $dN/dz dS d\Omega$ is assumed *a priori* and it is not inferred from a specific evolution scheme. In Ref. [22], the analysis is restricted to FSRQs: sources are identified by their L_γ (i.e., $Y \equiv L_\gamma$), their redshift and

⁸The best-fit point obtained in Ref. [19] favors a γ_1 much larger than the one found in Ref. [16] for EGRET blazars.

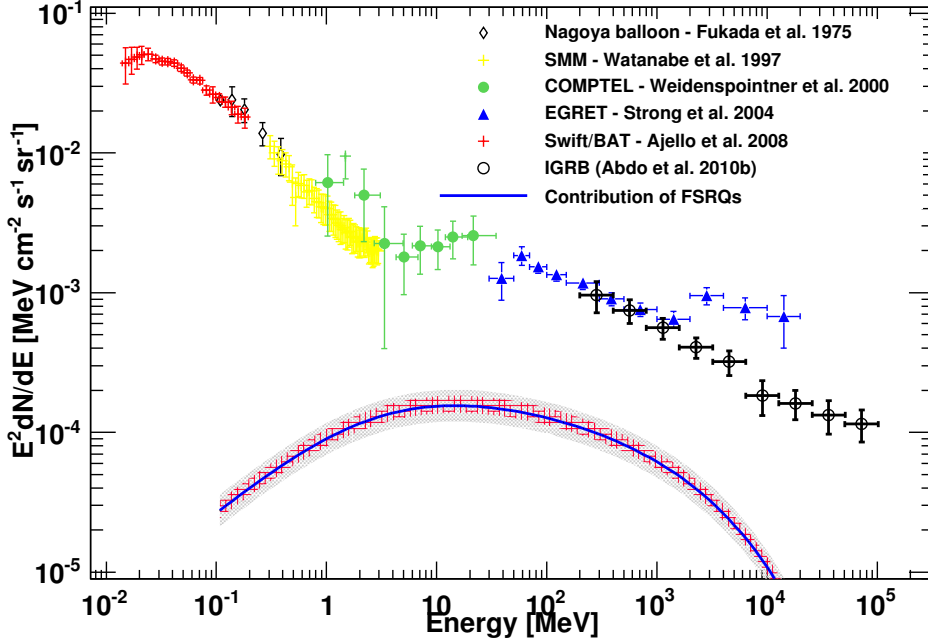


Figure 2: Contribution of unresolved FSRQs to the DGRB as determined by integrating the LF coupled to the SED model derived in Ref. [22]. The red hatched band around the best-fit point prediction (solid blue line) shows the 1σ statistical uncertainty, while the gray band represents the systematic uncertainty. Note that, in the figure, the DGRB measured by the *Fermi* LAT in Ref. [8] (black data points) is referred to as “IGRB”. Taken from Ref. [22].

the slope of the power-law fit to their energy spectrum. $dN/dVdL_\gamma d\Gamma$ is split into the gamma-ray LF and the spectral index distribution $dN/d\Gamma$. The former is described by a parametric expression inspired by the results in the radio and X-ray bands, while a Gaussian distribution is assumed for $dN/d\Gamma$, with no dependence on L_γ . A maximum-likelihood fit is performed to determine the parameters of the model. 186 FSRQs in the 1FGL and with $|b| \geq 15^\circ$ are considered in the fit. Results establish that FSRQs evolve positively until a z_c that depends on L_γ , i.e. a luminosity-dependent density evolution performs better than other evolution formalisms. The best-fit model corresponds to an unresolved emission which accounts for $9.3^{+1.6}_{-1.0}\%$ of the *Fermi* LAT DGRB in Ref. [8], between 0.1 and 100 GeV (see Fig. 2).⁹ The contribution peaks below the GeV scale and it becomes more subdominant at higher energies.

Performing a similar population study for BL Lacs is hampered by the fact that it is more difficult to obtain a measure of spectroscopic redshift for these objects due to the lack of strong emission lines: indeed, approximately 55% of the BL Lacs in the 2LAC do not have an associated z . This issue is somehow alleviated in Ref. [23] by considering photometric redshift estimates [113], lower [114] or upper limits on z [113, 114] and

⁹In Ref. [22] only sources with $L_\gamma \geq 10^{44} \text{ erg s}^{-1}$ are considered when computing the emission of unresolved FSRQs. Such a value corresponds approximately to the fainter blazar in the 1FGL. Thus, the quoted contribution of FSRQs to the DGRB implicitly assumes that no sources are present below $10^{44} \text{ erg s}^{-1}$ and, therefore, it should be considered as a lower limit to the total emission of unresolved FSRQs.

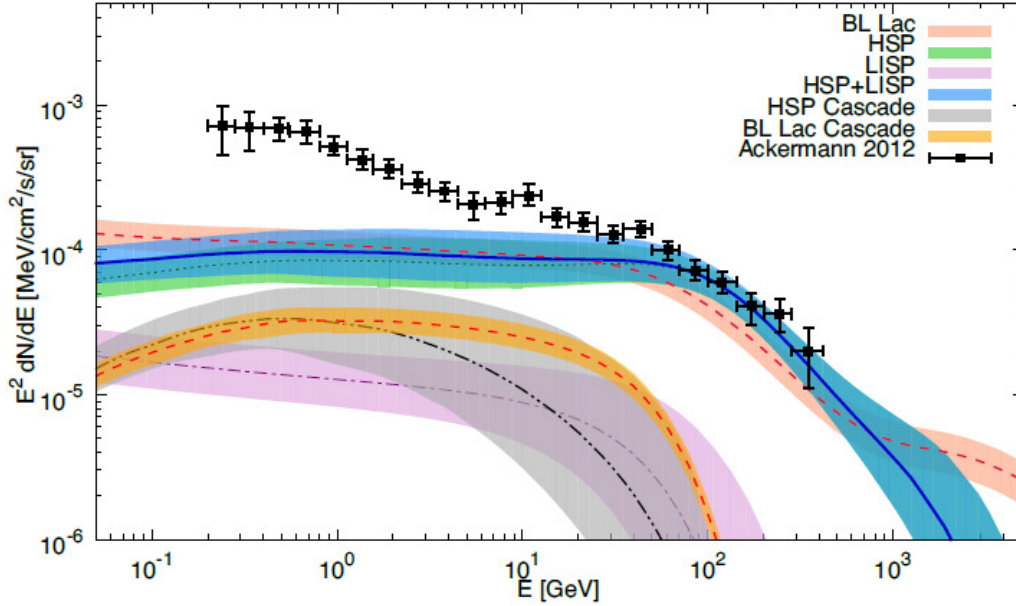


Figure 3: Diffuse gamma-ray emission from unresolved BL Lacs. Predictions for the best-fit model in Ref. [24] are shown embedded in their 1σ uncertainty bands: the summed contribution from LSPs and ISPs is plotted by means of the purple dot-dashed line and the purple band, the one from HSP BL Lacs by the green band and green dotted line (almost overlapped with the blue band), the one from the sum of the two by blue band and solid blue line and the contribution from BL Lacs considered as a unique population is depicted by the pink band and dashed pink line. The DGRB data are taken from Ref. [112] and are displayed as black points. The gray band and double-dot-dashed black line (orange band and dashed red line) represent the cascade emission from the HSP BL Lacs (the whole BL Lac population). Taken from Ref. [24].

host-galaxy spectral fitting [114]. The 211 BL Lacs studied in Ref. [23] are taken from Ref. [18] and analyzed by means of the same pipeline applied in Ref. [22] to FSRQs: the Y parameter in Eq. (1) is again L_γ but the mean of the Gaussian distribution of spectral indexes depends now linearly on $\log_{10}(L_\gamma)$. Only sources with $L_\gamma \geq 7 \times 10^{43} \text{ erg s}^{-1}$ are considered. The best-fit model suggests that the number density of faint BL Lacs (probably HSPs) decreases with redshift, while BL Lacs with $L_\gamma \geq 10^{45.8} \text{ erg s}^{-1}$ are more numerous at large redshift, i.e. more similar to the positive evolution FSRQs. The redshift estimates adopted for the BL Lacs without spectroscopic information are crucial to constrain the evolution of their LF. Results indicate that unresolved BL Lacs contribute to $7.7^{+2.0}_{-1.3}\%$ of the *Fermi* LAT DGRB in Ref. [8], between 0.1 and 100 GeV. Due to the large density of low-luminosity hard sources at low redshift, the emission of unresolved BL Lacs is expected to be harder than that of FSRQs and, thus, BL Lacs may play a more significant role at higher energies.

This hypothesis was tested by Ref. [24], where the authors considered a set of 148 BL Lacs with redshift and synchrotron peak frequency ν_s obtained from the 2FGL [115]. Their model for the gamma-ray LF is fitted to the observed cumulative source distribution $N(> S)$, the gamma-ray LF and the redshift distribution dN/dz of the detected sources. The energy spectra of the sources are obtained from a combination of *Fermi* LAT and Imaging Air Cherenkov Telescopes data. A luminosity-dependent density evolution is found to provide the best fit to the data. Pure power laws, log-parabolae and power laws with exponential cut-offs are considered as possible SEDs, with the last one corresponding to the most accurate description of the BL Lacs in the

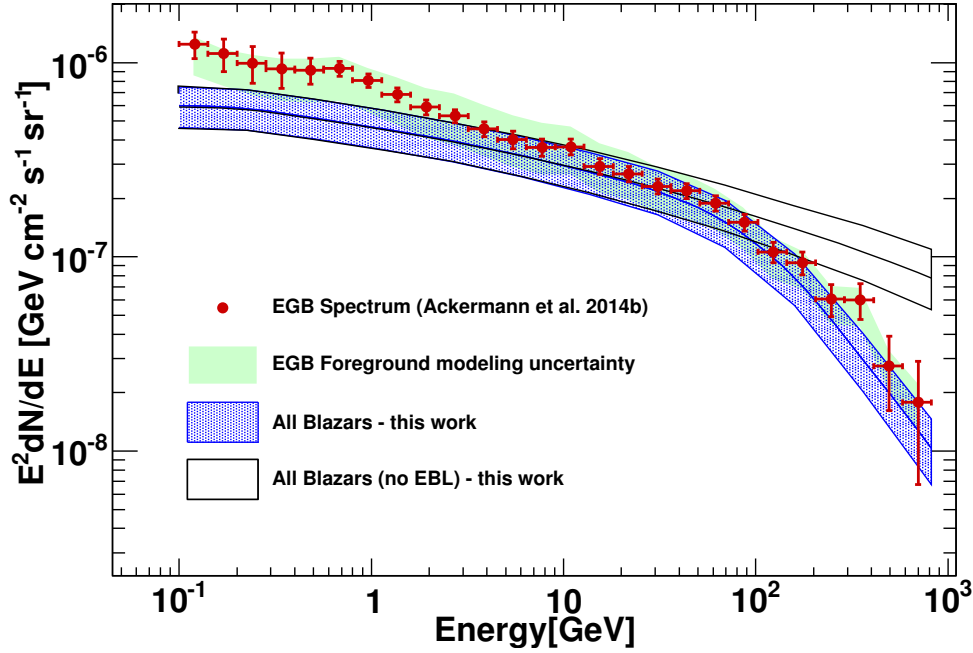


Figure 4: Diffuse emission arising from blazars (with or without EBL absorption), in comparison with the intensity of the total emission from sources (both resolved and unresolved), called here “EGB” (red data points, from Ref. [9]). Taken from Ref. [25]

sample. The sources were considered as either one single population, or split into HSPs and a second sub-class including ISPs and LSPs. In their best-fit model, HSPs dominates the dN/dS below $S = 5 \times 10^{-9} \text{cm}^{-2} \text{s}^{-1}$ and their SED extends to much higher energies than in the ISP+LSP class (the best-fit cut-off energy is 910 GeV for HSPs and 37 GeV for the class of ISPs and LSPs). That is the reason why the cumulative emission from HSPs (computed from Eq. (1) above $L_\gamma \geq 10^{38} \text{erg s}^{-1}$) can extend up to very high energies and it is able to explain the whole DGRB emission reported in Ref. [112] above few tens of GeV (see Fig. 3). Between 0.1 and 100 GeV, unresolved BL Lacs account for $\sim 11\%$ of the *Fermi* LAT DGRB in Ref. [112], in agreement with Ref. [23].

Ref. [25] repeated the analysis of Ref. [23] on a sample of 403 blazars from 1FGL, this time considering both FSRQs and BL Lacs as one single population by allowing the spectral index distribution to depend on L_γ . A double power-law energy spectrum, proportional to $[(E_0/E_b)^{1.7} + (E_0/E_b)^{2.6}]^{-1}$, is assumed and the energy scale E_b is found to correlate with the index Γ obtained when the SED is fitted by a single power law. The same LF used in Ref. [23] and based on a luminosity-dependent density evolution is implemented in Ref. [25], together with other evolution schemes. They all provide an acceptable description of the blazar population, even if the luminosity-dependent density evolution is the one corresponding to the largest log-likelihood. The predicted cumulative emission of blazars (FSRQs and BL Lacs, resolved and unresolved) can be seen in the Fig. 4 as a dotted blue band, compared to the total emission from resolved and unresolved sources taken from Ref. [9] (labeled “EGB” here, red data points). Blazars (both resolved and unresolved) accounts for the $50_{-11}^{+12}\%$ of the total emission from resolved and unresolved sources, above 100 MeV. Unresolved blazars, on the other hand, are

responsible for approximately 20% of the new *Fermi* LAT measurement of the DGRB in Ref. [9], in the 0.1-100 GeV energy band.

2.2.2. Misaligned Active Galactic Nuclei

Under the AGN unification scenario, the parameter that discriminates among different classes of AGNs is the viewing angle [89]. A value of 14° separates blazars (with the jet pointing towards the observer) from non-blazars, i.e. MAGNs. Among MAGNs it is possible to further distinguish between radio galaxies (with a viewing angle larger than 44°) and radio quasars [116]. Radio galaxies are classified either as Fanaroff-Riley Type I or Type II (FRI and FRII, respectively) according to their morphology [117]. The emission of FRIs peaks at the center of the AGN and it is dominated by two-sided decelerating jets. On the other hand, FRIIs are brighter and they are characterized by edge-brightened radio lobes with bright hotspots, while jets and core (when detected) are subdominant. FRIs and FRIIs are normally interpreted as the misaligned counterparts of BL Lacs and FSRQs, respectively. Indeed, the detection of MAGNs in the 1FGL and 2FGL confirms that, similar to the case of BL Lacs and FSRQs, FRIs have harder spectra than FRIIs [118].

The mechanisms of gamma-ray production in MAGNs are less clear than for blazars: the SED exhibits a bimodal structure, with the low-frequency peak due to synchrotron radiation, while at higher energies, the bulk of gamma-ray emission may be due to synchrotron self-Compton [119]. External IC may also contribute [120]. If present, external IC would be localized within one parsec from the center of the AGN, while synchrotron self-Compton emission is produced outside that region [119, 120]. Furthermore, spatially coincident with the radio lobes, there may also be emission from IC off the Cosmic Microwave Background (CMB) [27, 26] (see the discussion at the end of this section).

With no Doppler boost, MAGNs are expected to be less bright but more abundant than blazars, making them potentially important contributors to the DGRB [28]. 15 MAGNs were reported in Ref. [118], precluding the possibility of deriving their gamma-ray LF directly from gamma-ray observations, as done with blazars. Yet, the LF of MAGNs is well known at radio frequencies. As done in the previous section, once a correlation between their radio and gamma-ray luminosities is established, it is possible to deduce the gamma-ray properties of MAGNs by studying the sources in the radio band.

Ref. [28] considers L_γ (between 0.1 and 10 GeV) for 10 MAGNs detected by the *Fermi* LAT in Ref. [118]. The author studies the possibility of a linear correlation between $\log_{10}(L_\gamma)$ and $\log_{10}(L_r)$, where L_r is the radio luminosity. The slope of the observed correlation is very similar to the one found by Ref. [121] for blazars. Then, $\Phi_\gamma(z, L_\gamma)$ is determined in terms of the radio LF, $\Phi_r(z, L_r)$, as $\Phi_\gamma(z, L_\gamma) = \kappa \Phi_r(z, L_r) dL_r / dL_\gamma$. This is similar to Eq. (4) for blazars. Ref. [28] takes Φ_r from Ref. [122] and the value of κ is tuned to reproduce the number of sources observed by the *Fermi* LAT. All MAGNs are assumed to share the same energy spectrum, i.e. a power law with an index of 2.39. Such a value is the mean spectral index among the 10 MAGNs considered. The emission from unresolved MAGNs is, finally, estimated from Eq. (1), for $L_\gamma \geq 10^{39} \text{ erg s}^{-1}$. The result indicates that $\sim 25\%$ of the DGRB measured by *Fermi* LAT in Ref. [8] above 100 MeV can be explained in terms of unresolved MAGNs.

Ref. [29] improves the analysis in Ref. [28] by properly estimating the uncertainties involved: the authors consider L_γ (defined above 100 MeV) of 12 MAGNs in the 2FGL and the correlation with L_r at 5 GHz. They make use of the total radio luminosity, $L_{r,\text{tot}}$, and the so-called “radio core luminosity” $L_{r,\text{core}}$, defined as the emission from

the central arcsecond-scale region of the source. Both the $\log_{10}(L_\gamma) - \log_{10}(L_{r,\text{core}})$ and $\log_{10}(L_\gamma) - \log_{10}(L_{r,\text{tot}})$ relations are considered. The gamma-ray LF is inferred from the radio LF as follows:

$$\Phi_\gamma(z, L_\gamma) = \kappa_i \Phi_{r,i} \frac{\log_{10}(L_{r,i})}{\log_{10}(L_\gamma)}, \quad (5)$$

where i stands for “total” or “core”.¹⁰ If $L_{r,\text{tot}}$ is used, $\Phi_{r,\text{tot}}$ is taken from Ref. [122]. On the other hand, it is not possible to build the core radio LF directly from radio observation, due to the scarce data available [123]. In Ref. [29], a relation is assumed between $L_{r,\text{core}}$ and $L_{r,\text{tot}}$ [124], so that $\Phi_{r,\text{core}}$ can be derived from $\Phi_{r,\text{tot}}$. The factor κ_i in Eq. (5) is tuned to reproduce the number of observed MAGNs. Different values for κ are obtained in Ref. [29], depending on which LF is considered (total radio or core radio) and on how the uncertainties in the $\log_{10}(L_\gamma) - \log_{10}(L_{r,i})$ correlations are treated. Finally, the emission from unresolved MAGNs is computed as in Eq. (1), assuming a Gaussian distribution for the spectral indexes. The results (for $L_\gamma > 10^{41} \text{ erg s}^{-1}$) are summarized in Fig. 5. For the best-fit model, the contribution of MAGNs accounts for $\sim 25\%$ of the *Fermi* LAT DGRB in Ref. [8] above 100 MeV. The value agrees very well with that given in Ref. [28]. Yet, in Ref. [29], the prediction is embedded in an uncertainty band with a size of almost one order of magnitude. Such large uncertainty mainly comes from the possible different values for κ .

Given the complex morphology of the emission in radio galaxies, it is possible that different regions in the source emit gamma rays which are not accounted for by the analyses presented above. Ref. [27] considers a scenario in which the non-thermal electrons responsible for the synchrotron emission in the radio lobes of FRIIs could emit gamma rays by IC off the CMB. Indeed, gamma-ray emission spatially coincident with the radio lobes of Centaurus A has been recently observed by the *Fermi* LAT [125]. Such a component would peak at around 1 MeV and could explain up to 10% of the DGRB in Ref. [8] below 1 GeV.

Similarly, Ref. [26] considers the X-ray-emitting kpc-scale jets of FRIs as possible contributors to the DGRB. The established synchrotron origin of those X-rays suggests that the same non-thermal electrons could also emit gamma rays through IC with the ambient photons of the host galaxy. However, even assuming this is common for all FRIs, the contribution adds up to only $\sim 1\%$ of the DGRB reported in Ref. [7].

2.2.3. Star-forming galaxies

The majority of the gamma-ray emission detected by the *Fermi* LAT is associated with the MW [79]. This diffuse Galactic foreground is produced by the interaction of Galactic CRs (mainly protons and electrons) with the Galactic interstellar medium and interstellar radiation field. Other SFGs similar to the MW are expected to shine in gamma rays thanks to the same emission mechanisms. Up to now, the *Fermi* LAT has only detected a few SFGs other than the MW: M31 and M33 [126], the Large and Small Magellanic Clouds [127, 128] in the Local Group and the Circinus Galaxy [129], M82, NGC 253 [130, 131], NGC 1068 and NGC 4945 [33]. Ref. [132] also reported the detection of gamma-ray emission from NGC 2146. Being intrinsically faint but numerous, SFGs are expected to contribute significantly to the DGRB.

Massive stars in SFGs emit the majority of their light in the UV band. The emission is then absorbed by interstellar dust and re-emitted as IR light. The IR luminosity can be

¹⁰The luminosity functions in Ref. [29] are defined per units of $\log(L)$, hence the factor $\log_{10}(L_{r,i})/\log_{10}(L_\gamma)$ in Eq. (5) as compared to Eq. (4).

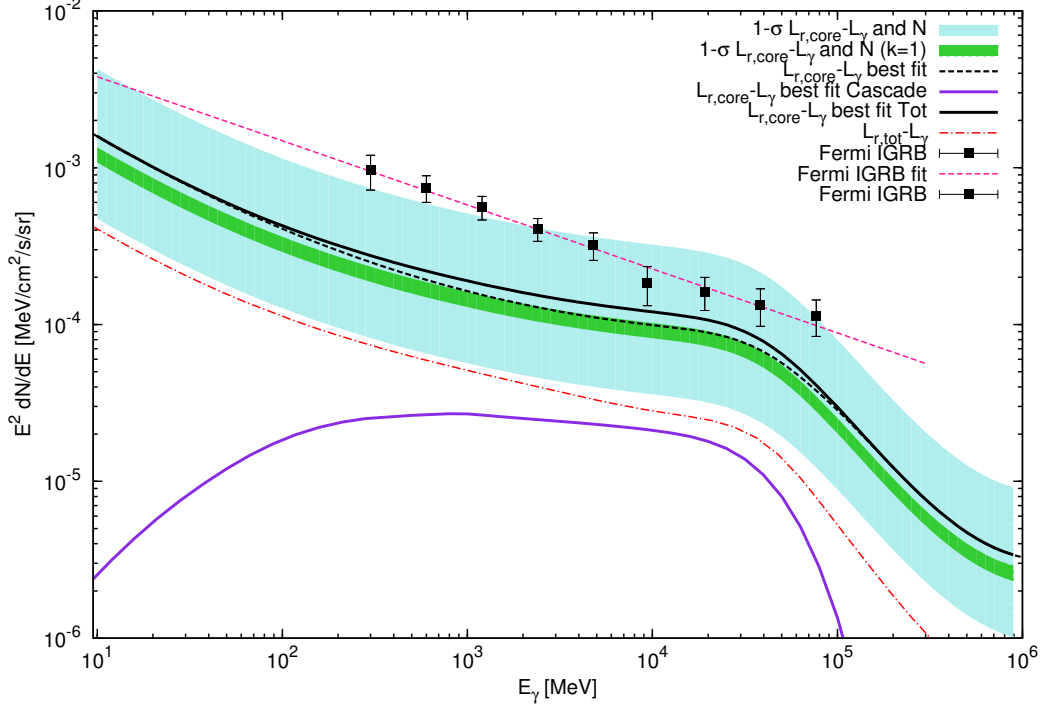


Figure 5: Diffuse gamma-ray flux due to MAGNs as a function of the gamma-ray energy. The dashed black line is obtained from the best-fit to the $L_{r,\text{core}} - L_\gamma$ correlation. The cyan shaded area is derived by allowing for the uncertainty on the $L_{r,\text{core}} - L_\gamma$ correlation and by including all the models that are less than 1σ away from the best-fit point. The green band corresponds to the case with $\kappa = 1$ at 1σ confidence level. The red dot-dashed curve shows the diffuse flux obtained when assuming a correlation between the total radio luminosity and the gamma-ray luminosity. The black squares corresponds to the DGRB measured by the *Fermi* LAT in Ref. [8] and the magenta dashed curve represents the best-fit to the data. Taken from Ref. [29].

used as a good tracer of the star-forming rate (SFR) ψ , i.e. the amount of mass converted in stars per unit time [133]. The same massive stars finally explode into core-collapse supernovae, leaving behind supernova remnants which are considered to be the main sources of accelerated CRs on galactic scales [134]. The leptonic component of these CRs is responsible for the synchrotron radio emission observed from SFGs and they may also contribute at gamma-ray frequencies when interacting with the interstellar radiation field of the host galaxy (through IC or bremsstrahlung). However, such leptonic gamma-ray emission is expected to be subdominant with respect to the hadronic one [35], since CR protons have an intrinsically larger injection rate than CR electrons [135, 34]. Hadronic gamma-ray emission mainly comes from inelastic interactions of CR protons with the nuclei of the interstellar medium, producing neutral pions that decay into gamma rays with an energy spectrum that peaks at around 300-400 MeV.

The so-called “initial mass function” determines the relative number of stars produced in any star-formation event in a galaxy, as a function of the stellar mass [136, 137]. Under the assumption of an universal high-mass end of the initial mass function, the SFR of a galaxy is proportional to the rate of supernova explosions and, thus, to the CR abundance and the CR-induced emission [138, 34]. Then, it is expected that, in a generic galaxy, the gamma-ray and radio luminosities (both associated with CRs) are correlated with the IR emission, which depends on the SFR.

The cumulative gamma-ray flux produced by IC of CR electrons in *all* SFGs at *all* redshifts is computed in Ref. [35]. In this work, the emission of a generic galaxy is modeled based on a template which is tuned to reproduce the emission of the MW. The cumulative gamma-ray flux depends on the abundance of SFGs. Ref. [35] assumes that, at a certain redshift, the total emission scales as the so-called cosmic SFR $\dot{\rho}_\star(z)$, i.e. the mass converted to stars per unit time and comoving volume:

$$\dot{\rho}_\star(z) = \int d\psi \psi \frac{dN}{dV d\psi}, \quad (6)$$

where $dN/dV d\psi$ is the comoving density of galaxies per unit SFR. Parametric fits for $\dot{\rho}_\star(z)$ are available from the observation of the total luminosity density at various wavelengths [139, 140, 141]. Ref. [35] finds that the IC-induced emission is always subdominant with respect to the hadronic one. The two become comparable only above 100 GeV.

Indeed, the majority of the studies on the SFGs focus on their hadronic emission and they neglect the contribution from primary electrons. The hadronic gamma-ray luminosity of a SFG, as a function of the observed energy E_0 , can be written as follows:

$$L_\gamma(E_0) = \int \Gamma_{\pi^0 \rightarrow \gamma\gamma}(E_{\text{em}}) n_{\text{H}} dV = \Gamma_{\pi^0 \rightarrow \gamma\gamma}(E_{\text{em}}) N_{\text{H}}, \quad (7)$$

where E_{em} is the energy in the emitter frame, $\Gamma_{\pi^0 \rightarrow \gamma\gamma}$ is the pionic gamma-ray production rate per interstellar hydrogen atom and n_{H} is density of hydrogen atoms in the interstellar medium [31, 20]. Integrated over the volume of the medium, N_{H} gives the total number of hydrogen atoms, which can be expressed in terms of the total interstellar gas mass M_{gas} in the galaxy as $X_{\text{H}} M_{\text{gas}}/m_p$. $X_{\text{H}} \sim 0.7$ is the hydrogen mass fraction and m_p is the mass of the proton. As for $\Gamma_{\pi^0 \rightarrow \gamma\gamma}$ in Eq. (7), it is the product of the flux Φ_p of CR protons (averaged over the volume of the galaxy) and the cross section for the production of gamma rays [142, 143].

The distribution and propagation of CR protons is governed by the diffuse-loss equation, which depends on their injection rate, diffusion, energy losses and possible inelastic interactions (see Ref. [34] for a recent review). Different scenarios are possible depending on the strength of those terms. Here we only mention two possibilities that provide good descriptions to different typologies of galaxies. The first is the so-called *escape regime* and it corresponds to a situation in which the energy losses of CR protons are dominated by their escape from the diffuse region of the galaxy. An equilibrium is reached between the energy losses and the acceleration of CR protons so that their flux is proportional to the product of the SFR of the galaxy and the CR escape path-length, Λ_{esc} : $\Phi_p \propto \Lambda_{\text{esc}} \psi$. Consequently, $L_\gamma \propto M_{\text{gas}} \psi$ [144, 145, 31]. The escape regime provides a good description of the diffuse foreground of the MW. This motivates the use of the gamma-ray production rate of the MW, $\Gamma_{\pi^0 \rightarrow \gamma\gamma}^{\text{MW}}$, to normalize the proportionality relation between L_γ and $M_{\text{gas}} \psi$. Then Eq. (7) becomes:

$$L_\gamma(\psi, M_{\text{gas}}) = X_{\text{H}} \Gamma_{\pi^0 \rightarrow \gamma\gamma}^{\text{MW}} \frac{M_{\text{gas}}}{m_p} \frac{\psi}{\psi_{\text{MW}}}, \quad (8)$$

where ψ_{MW} is the SFR of the MW. This relation provides a good description of the so-called *quiescent* or *normal* SFGs, characterized by properties similar to those of the MW.

The second scenario considered for the modeling of SFGs is the so-called *calorimetric*

regime: in this case the energy losses of CR protons is mainly due to their inelastic interactions. This means that protons lose all their energy into pions and SFGs act effectively as calorimeters. Their gamma-ray luminosity, then, can be computed from the amount of energy available to CRs. Under the paradigm that supernova remnants are the primary source of CRs, the energy available in the form of CRs for a calorimetric SFG is proportional to the supernova rate, multiplied by the energy E_{SN} released per supernova and by the fraction η of that energy going into CR protons (i.e. the so-called acceleration efficiency) [138, 33]. In turn, the supernova rate is proportional to the SFR, so that, finally,

$$L_{\gamma}(\psi) \propto \psi E_{\text{SN}} \eta. \quad (9)$$

Starburst galaxies are well modeled as proton calorimeters: normally brighter and less numerous than quiescent galaxies, starburst ones are characterized by at least one region undergoing intense star formation. This is often induced by major merger events or by bar instabilities, leading to a large gas density [146].

Several works analyze quiescent and starburst SFGs separately. Refs. [144, 145, 31], e.g., focus on quiescent galaxies. Their contribution to the DGRB is computed by using a formalism similar to Eq. (1), where L_{γ} is considered as the Y -parameter. Then, by means of Eq. (8), L_{γ} is written as a function of M_{gas} and ψ . In Refs. [144, 145], the former is factorized out of the integral in dL_{γ} in Eq. (1), assuming that M_{gas} only depends on redshift. The integration in dL_{γ} now only depends on the SFR and it amounts to the cosmic SFR $\dot{\rho}_{\star}(z)$ in Eq. (6). The net result is that the cumulative emission of quiescent SFGs scales with redshift as the product of $\dot{\rho}_{\star}(z)$ and the average amount of gas. Refs. [144, 145] take $\dot{\rho}_{\star}(z)$ from Refs. [139, 140], respectively, and derive the average gas mass assuming that the total baryonic mass of a galaxy (stars and gas) remains constant time and that it can be computed de-evolving backwards the cosmic history of the SFR density [144, 145]. They find that quiescent SFGs can contribute significantly to the DGRB, especially below 1 GeV, but they are only subdominant at higher energies.

Ref. [31] assumes the same formalism than Ref. [144] but it relates the gas content of a galaxy to its SFR, using the following relation:

$$M_{\text{gas}}(\psi, z) = 2.8 \times 10^9 M_{\odot} (1 + z)^{-0.571} \left(\frac{\psi}{M_{\odot} \text{yr}^{-1}} \right)^{0.714}. \quad (10)$$

This is obtained by the so-called Kennicutt-Schmidt law [147, 148], which links the surface density of star formation to that of the gas. Then, the integration over L_{γ} in Eq. (1) is converted into one in SFR. In turn, the SFR is related to the IR luminosity, L_{IR} , assuming a direct proportionality between the two [149]. The contribution of SFGs now depends on the IR LF, Φ_{IR} . Ref. [31] considers the IR LF from Ref. [150]. Results are provided for both a pure luminosity evolution and a pure density evolution for Φ_{IR} . The difference between the two prescriptions amounts to approximately a factor of 2 (see the dashed and long-dashed lines in Fig. 6). An intermediate scenario that mediates between the two evolution schemes indicates that unresolved SFGs account for $\sim 50\%$ of the DGRB intensity reported in Ref. [8] below 10 GeV. Above that energy, the contribution of SFGs goes down rapidly due to the softness of the energy spectrum assumed, i.e. a power law with a slope of 2.75.

Ref. [20] proposes two alternatives to estimate M_{gas} : in the first one, the gas mass is not obtained from Eq. (10) but taken to be some fraction of the stellar mass M_{\star} . The latter can be constrained by combining the findings of Refs. [151, 152]. In the

second scenario, the mean gas mass is assumed to scale with the cosmic SFR divided by a parameter linking the SFR to the density of clouds of molecular hydrogen [153, 20]. The two methods differ by approximately a factor of 10 in their predictions for the contribution of SFGs to the DGRB. In the second one, SFGs are able to account for the whole DGRB of Ref. [8] between 200 MeV and 1 GeV.

Starburst SFGs have also been considered: Ref. [138] works under the hypothesis that these objects are in the calorimetric regime. From Eq. (9), their gamma-ray luminosity is proportional to the SFR which, in Ref. [138], is related to the IR luminosity. Thus, the total gamma-ray emission from unresolved starburst SFGs can be obtained simply by rescaling the total diffuse extragalactic IR background taken, e.g., from Ref. [154]. Unresolved starburst galaxies are found to account for $\sim 10\%$ of the DGRB detected by EGRET in Ref. [7], at least at the GeV scale (see the double-dotted-dashed line in Fig. 6). The main uncertainty affecting this prediction stems from the unknown starburst fraction, i.e. the fraction of the IR background emission associated with starburst galaxies in the calorimetric regime. Observations suggests that such a fraction is quite low at $z = 0$ but that it can approximate to 1 at earlier epochs, when the star formation is much more efficient [155, 156]. However, see also Refs. [157, 20, 158, 34] for different values.

Both quiescent and starburst SFGs are modeled at the same time in Ref. [32]. The relations between L_γ and ψM_{gas} and between L_γ and ψ for quiescent and starburst SFGs respectively (see Eqs. (8) and (9)) are determined by fitting the results of 4 SFGs detected by the *Fermi* LAT. On the other hand, the abundance of galaxies is inferred from simulated galaxy catalogs [159, 160]. Starburst SFGs are found to be always subdominant and the total (quiescent *and* starburst) gamma-ray emission is between 5.4% and 9.6% of the DGRB intensity reported by the *Fermi* LAT in Ref. [8] above 100 MeV (see the black solid line in Fig. 6).

In Ref. [34] the authors model the emission from the MW and from M82, which are considered as templates of quiescent and starburst SFGs, respectively. The results are used to determine L_γ for the two typologies of SFGs. Their total emission is assumed to evolve with redshift following $\dot{\rho}_*(z)$, modulated by functions $f_i(z)$ (where i stands for either “starburst” or “quiescent”) that fix the relative abundance of the two sub-classes. They find that SFGs can be responsible from 4% to 76% of the DGRB of Ref. [8] in the GeV range and that their contribution cannot reproduce the data below the GeV or above few tens GeV. In their fiducial model quiescent SFGs always dominate over starbursts.

Ref. [33] follows an alternative approach to compute the emission of unresolved SFGs. The authors consider the 8 SFGs detected by the *Fermi* LAT and 64 galaxies observed in radio and IR but for which only upper limits are available in the gamma-ray energy range. These are used to determine a correlation between $\log_{10}(L_\gamma)$ (defined between 0.1 and 100 GeV) and the IR luminosity $\log_{10}(L_{\text{IR}})$ (defined between 8 and 1000 μm). Similarly to what done for blazars and MAGNs, this correlation is used to infer the properties of SFGs in the gamma-ray band from the study performed at IR frequencies. In particular, it is assumed that the gamma-ray LF can be written in terms of Φ_{IR} , as $\Phi_\gamma(z, L_\gamma) = \Phi_{\text{IR}} d\log_{10}(L_{\text{IR}})/d\log_{10}(L_\gamma)$.

The contribution to the DGRB, then, is computed following Eq. (1), with $Y = L_\gamma$.¹¹ The IR LF is measured in Ref. [162] from data gathered by the Spitzer Space Telescope.

¹¹As done for MAGNs, gamma-ray and IR LF are defined here per unit of $\log(L_\gamma)$ and of $\log(L_{\text{IR}})$, respectively.

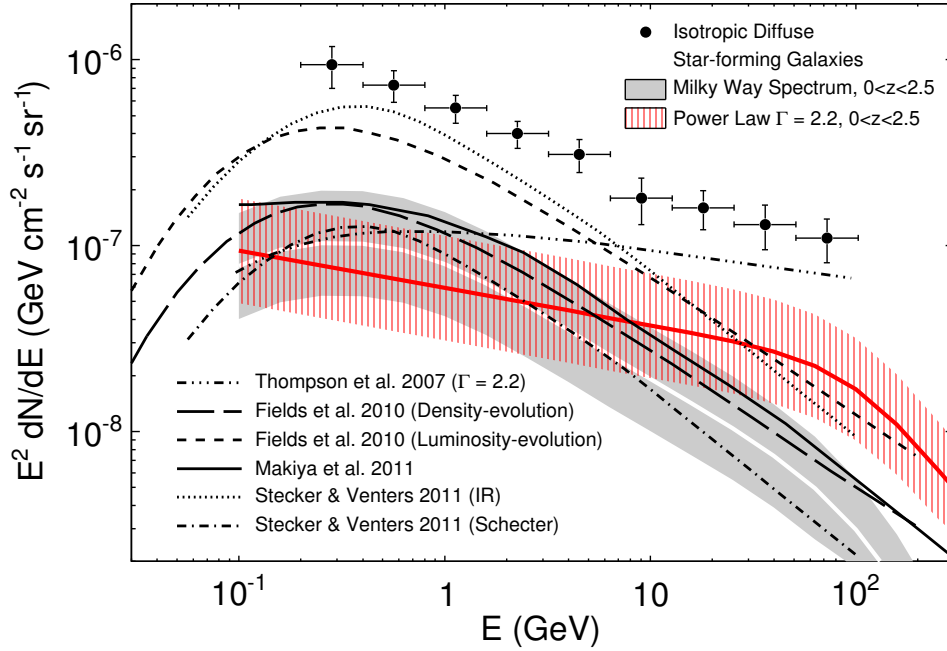


Figure 6: Estimated contribution of unresolved SFGs (both quiescent and starburst) to the DGRB emission measured by the *Fermi* LAT (black points, taken from Ref. [8]). Two different spectral models are used: a power law with a photon index of 2.2 (red line), and a spectral shape based on a numerical model of the global gamma-ray emission of the MW [135] (white line, inside gray band). The shaded regions indicate combined statistical and systematic uncertainties. Several other estimates for the intensity of unresolved SFGs are shown for comparison. For the double-dotted-dashed line starburst galaxies are treated as calorimeters of CR nuclei as in Ref. [138]. Ref. [31] (dashed and long-dashed line) considers the extreme cases of either pure luminosity and pure density evolutions. The solid black line shows predictions from Ref. [32], obtained from simulated galaxies and semi-analytical models of galaxy formation. Two recent predictions from Ref. [20] are plotted by dotted and dash-dotted black lines: the former assumes a scaling relation between IR and gamma-ray luminosities and the latter uses a redshift-evolving relation between the gas mass and the stellar mass of a galaxy. Taken from Ref. [33].

In Ref. [33] only objects below $z = 2.5$ are considered, since Φ_{IR} is not well determined for higher redshifts. The $L_{\text{IR}} - L_{\gamma}$ correlation is assumed to stand valid up to that redshift, even if only SFGs below $z \sim 0.05$ are used in Ref. [33] to derive it. Starburst galaxies are observed to have a harder energy spectrum than quiescent ones [163, 130], at least in the Local Group. Assuming that this is a general property, the steepness of the contribution of unresolved SFGs to the DGRB will depend on the fraction of starburst galaxies, which is unknown. Ref. [33] assumes that all SFGs share the same energy spectrum and it considers two extreme cases: a power-law with a slope of 2.2 (typical of starburst galaxies) and the spectrum of the diffuse foreground of the MW [135], which reproduces well the behavior of quiescent SFGs. Results are summarized in Fig. 6 by the red and gray bands, respectively. The figures show that unresolved SFGs can explain between 4% and 23% of the DGRB measured by the *Fermi* LAT in Ref. [8] above 100 MeV.

The results of Ref. [33] have been updated in Ref. [161], by improving the modeling of Φ_{IR} . Thanks to the recent detection of a larger number of high- z sources by the Herschel Space Observatory [164, 165, 166, 167], it is now possible to extend the LF

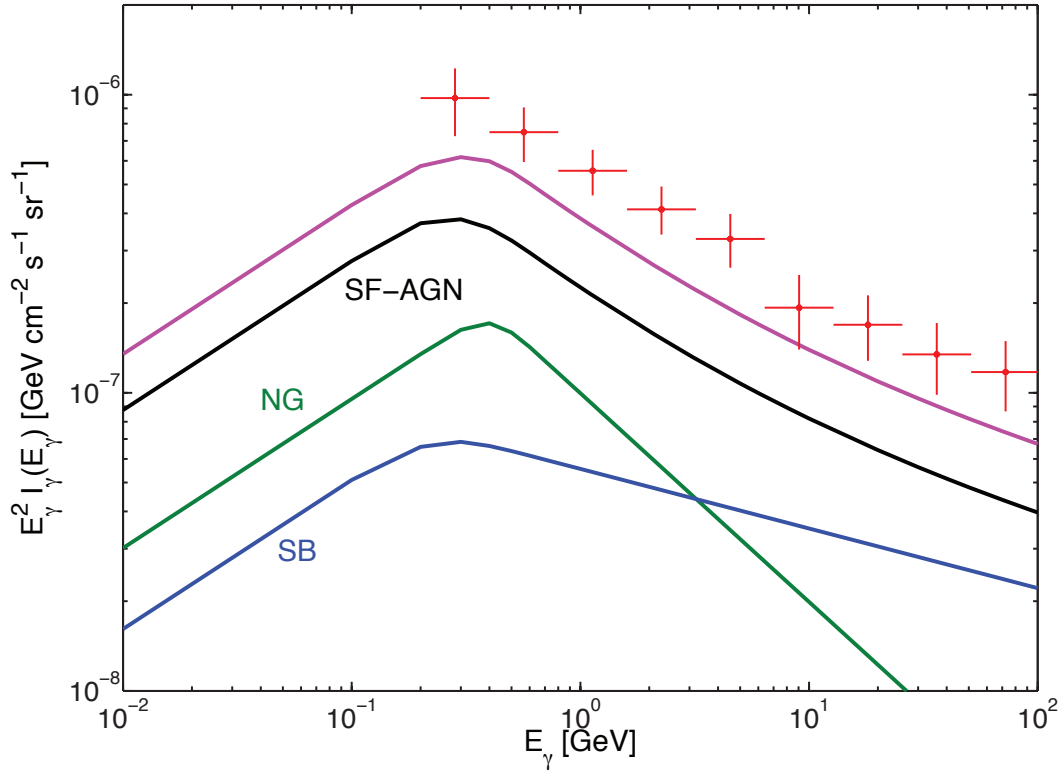


Figure 7: Diffuse gamma-ray emission as a function of the energy (without EBL attenuation) for the three different SFG contributions to the DGRB: quiescent SFGs (green, labeled “NG” in the figure), starburst SFGs (blue) and SFGs hosting an AGN (black). The solid pink indicates their sum. The DGRB from Ref. [8] is plotted in red. Taken from Ref. [161].

up to $z \simeq 4$ and to consider separately the contribution of different classes of SFGs. In particular, Herschel classifies its sources into quiescent galaxies, starburst ones and SFGs hosting an obscured or low-luminosity AGN.¹² At $z = 0$, starburst SFGs are found to be subdominant with respect to the other two classes, but the three families have different evolution and, by $z = 1$, the number of AGN-hosting SFGs is approximately twice the number of quiescent and starburst galaxies combined. Ref. [164] provides analytical fits to the LF of the three classes. From these, the emission of unresolved SFGs can be computed, assuming a broken power law as energy spectrum.¹³ The results are summarized in Fig. 7 and they show that unresolved SFGs are responsible for $\sim 50\%$ of the *Fermi* LAT DGRB of Ref. [8] in the range between 0.3 and 30 GeV. Note that the emission is dominated by SFGs hosting AGNs.

2.2.4. Millisecond pulsars

Pulsars are highly magnetized and rapidly spinning neutron stars, with a beam of radiation that periodically intersects the Earth. Their initial spin P decreases due to

¹²We note that, even if these SFGs host an AGN, their IR luminosities are expected to be dominated by the star-forming activity rather than the one associated with the AGN and, therefore, L_{IR} remains a useful tracer of the SFR.

¹³The low-energy slope is fixed to -1.5 in all cases, while the high-energy one is assumed to be -2.7 for quiescent galaxies and -2.2 for starburst ones. The class of AGN-hosting objects is additionally split into “starburst-like” and “quiescent-like” galaxies, with slopes of -2.2 and -2.7, respectively.

magnetic dipole braking [168], so that the time derivative of the period \dot{P} can be written as follows [36, 37, 169, 170, 38]:

$$\dot{P} = 9.8 \times 10^{-26} \left(\frac{B}{\text{G}} \right)^2 \left(\frac{P}{\text{s}} \right)^{-1}, \quad (11)$$

where B is the surface magnetic field. The loss of kinetic energy associated with the slowing down of the spinning, i.e. the so-called “spin-down luminosity” \dot{E} , is

$$\dot{E} = 4\pi^2 M \frac{\dot{P}}{P^3}, \quad (12)$$

where M is the moment of inertia of the neutron star. The spin-down luminosity is converted, with some efficiency, into radiation. MSPs were traditionally detected in radio, while, nowadays, thanks to the *Fermi* LAT, an increasingly large number of objects is observed also in the gamma-ray band. The shape of their gamma-ray energy spectra suggests that the emission comes from curvature radiation. This is a mechanism similar to synchrotron radiation, in which gamma rays are produced by relativistic charged particles following the curved force lines of a magnetic field [171, 172, 173]. Self-synchrotron Compton possibly also contributes [174].

Pulsars are classified in terms of their period and sources with $P < 15$ ms are referred to as MSPs. These are generally part of a binary system and their higher spin is the result of the large angular momentum transferred from the companion object [175, 176, 177, 178, 179]. Thanks to lower surface magnetic fields, MSPs have smaller \dot{P} and are, therefore, older than “normal” (i.e., young) pulsars. A longer life cycle may compensate the intrinsic lower birthrate so that MSPs are expected to be as abundant as normal pulsars [180]. Moreover, having had the time to orbit many times around the Galaxy, the distribution of MSPs is expected to be uncorrelated with their birth locations, potentially extending to high Galactic latitudes [36].

The conversion of energy loss \dot{E} into L_γ is parametrized by an empirical relation of the form

$$L_\gamma = \eta \dot{E}^\alpha \quad (13)$$

[181], where η is the called “conversion efficiency”. The case of $\alpha = 0.5$ is motivated in Refs. [182, 183, 181] and adopted in Refs. [184, 37, 169], even if some of those references also consider the case of $\alpha = 1$. Assuming that Eq. (13) is valid both for young pulsars and for MSPs, their luminosities are related by

$$\frac{L_\gamma^{\text{MSP}}}{L_\gamma^{\text{young}}} = \frac{\dot{P}_{\text{MSP}}}{\dot{P}_{\text{young}}} \left(\frac{P_{\text{MSP}}}{P_{\text{young}}} \right)^{-3}, \quad (14)$$

for $\alpha = 1$. Typical values are $P_{\text{MSP}} = 3$ ms, $P_{\text{young}} = 0.5$ ms, $\dot{P}_{\text{MSP}} = 10^{-19}$ and $\dot{P}_{\text{young}} = 10^{-15}$. These suggest that MSPs can be brighter than normal pulsars, by a factor of few tens. It is, therefore, reasonable to speculate that these sources can contribute significantly to the DGRB emission [36, 37, 185, 169, 38]. On the other hand, the cumulative emission of normal pulsars would be quite anisotropic and mainly localized along the Galactic plane, thus hardly compatible with the DGRB [186, 184].

The second *Fermi* LAT catalog of gamma-ray pulsars (2FPC) contains 117 sources, 40 of which are MSPs [170]. The number is too low to build a MSP LF only from *Fermi* LAT data. Also, given the uncertainties on the mechanisms of gamma-ray emission, it is not possible to postulate correlations with other frequencies, as done for blazars, MAGNs

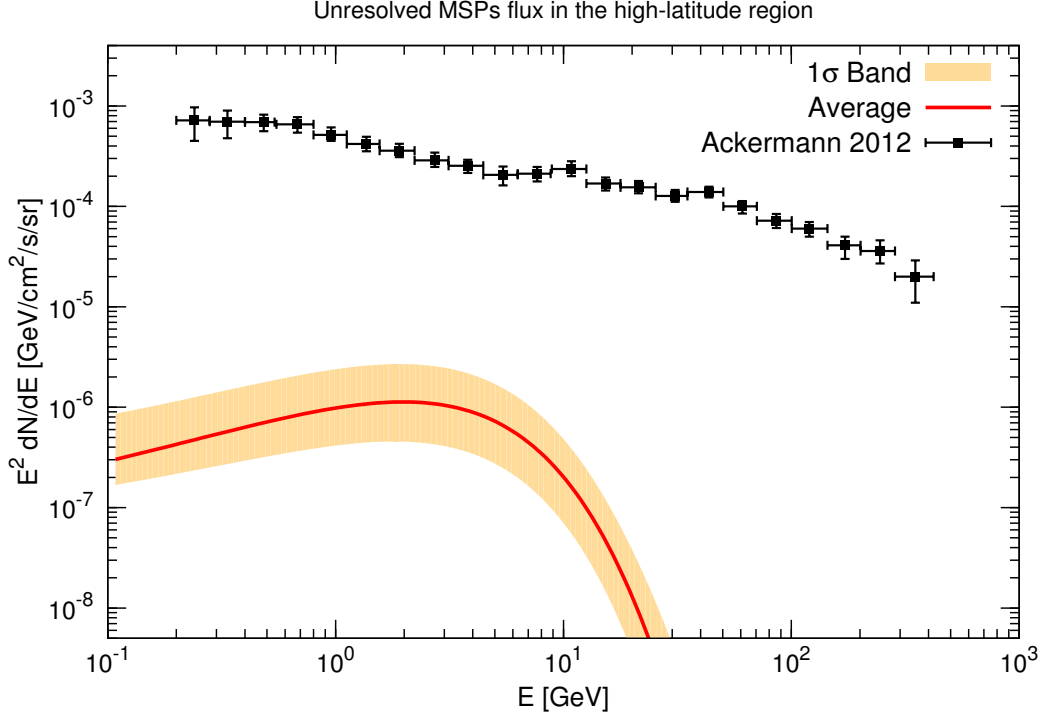


Figure 8: Prediction for the contribution of unresolved MSPs to the DGRB, as derived from 1000 Monte Carlo simulations of the MSP population of the MW. The red solid line represents the mean spectrum distribution (see Ref. [38] for further details), while the orange band corresponds to its 1σ uncertainty band. The black points refer to the preliminary DGRB measurement anticipated in Ref. [112]. Taken from Ref. [38].

and SFGs. This is the reason why Refs. [36, 37, 169, 38] rely on Monte Carlo simulations in order to properly describe the population of MSPs. Probability distributions of the most relevant quantities (e.g., radial and vertical position of the source, its period and surface magnetic field) are derived from the pulsars detected in radio [187, 180, 188]. At date, the largest catalog of pulsars is the Australia Telescope National Facility Pulsar catalog, containing 1509 sources, out of which 132 are MSPs [189]. Ref. [38] analyses the objects in the catalog and establishes that they are well described by the following prescriptions: *i*) a Gaussian distribution for the radial distance, R , from the center of the MW projected on the Galactic plane, i.e. $dN/dR \propto \exp[-(R - \langle R \rangle)/R_0]$, *ii*) an exponential distribution for the vertical distance, z , from the Galactic plane, i.e. $dN/dz \propto \exp(-z/z_0)$ [187, 184], *iii*) a log-Gaussian distribution for the period P (in contrast to previous works [36, 37, 169]) and *iv*) a log-Gaussian distribution for the magnetic field.

Ref. [38] also studies the relation between L_γ and \dot{E} . The data, however, are affected by quite large errors which prevent a statistically meaningful fit to the data. Thus, Ref. [38] identifies a benchmark case with $\alpha = 1$ that provides a qualitative good description of the data, and an uncertainty band that encompasses reasonably well the distribution of the data points. This completes the characterization of the MSP population and synthetic sources can be generated by randomly drawing from the assumed distributions. Each source is labeled as “resolved” or “unresolved” depending on whether its flux is larger or smaller than the sensitivity of the telescope at the position of the

source in the sky. Simulated sources are accumulated until the number of “resolved” ones equals the amount of detected MSPs: Refs. [184, 37] consider the MSPs detected in radio in the Australia Telescope National Facility catalog [190], while Refs. [169, 38] the sources detected by the *Fermi* LAT.¹⁴ This calibrates the Monte Carlo data and it allows the computation of the MSP contribution to the DGRB simply by summing over the “unresolved” sources. Their energy spectrum is fixed to a power law with an exponential cut-off, i.e a functional shape that reproduces well the MSPs in the 2FPC. The slopes and cut-off energies are assumed to have Gaussian distributions. The results of Ref. [38] are shown in Fig. 8, from which it is evident that MSPs are only a subdominant component to the DGRB, responsible for less than 1% of the intensity measured by the *Fermi* LAT in Ref. [8]. This value is lower than the previous estimates from Refs. [37, 169], in which a different modeling of the MSP population was adopted.

2.2.5. Other astrophysical components

Several other potential contributors to the DGRB have been proposed in the past. Some correspond to unresolved astrophysical populations not considered in the previous sections, while others are intrinsically diffuse processes. In this section, we focus on astrophysical scenarios, while a potential DM-induced emission will be discussed in detail in Sec. 2.3.

- **Clusters of galaxies:** it is believed that huge amounts of energy, of the order of $10^{61} - 10^{63}$ erg, is dissipated in the shocks associated with the assembly of clusters of galaxies [191, 192]. A fraction of this energy can go into the acceleration of CRs, even if the details of the acceleration mechanisms are still uncertain [193]. Accelerated CRs would produce gamma rays by means of *i*) the decay of pions produced by the interaction of CR protons with the intracluster medium and *ii*) IC scattering of primary CR electrons or of the electrons produced by the pion decays in point *i*). Yet, no gamma-ray emission has been detected from galaxy clusters. On the other hand, the interpretation of the observed radio emission as synchrotron radiation confirmed the presence of accelerated electrons and magnetic fields [194, 195]. However, not all known clusters emit in radio [196, 197] and it is not clear why some objects are radio-quiet.

The IC-induced gamma-ray emission [198, 199] depends on the abundance of CR electrons, on the intensity of the magnetic field and on the so-called acceleration efficiency ξ_e , i.e. the fraction of the thermal energy density produced by the shocks that is transferred to CR electrons. A Halo Model [200, 201], linking the properties of the shock to those of the DM halo hosting the cluster [202, 203], is often used to predict the IC-induced emission of clusters. Results can be tested with *N*-body simulations. An acceleration efficiency of $\xi_e = 0.05$ is typically assumed, following similar values measured in shocks surrounding supernova remnants. For this ξ_e , Ref. [202] finds that the cumulative IC-induced gamma-ray flux from unresolved clusters can explain, at most, 10% of the EGRET DGRB in Ref. [6]. Similar values are obtained by Refs. [204, 205, 206, 107, 207]. Yet, the non-detection of gamma rays from the observation of the Coma galaxy cluster suggests even lower efficiencies ($\xi_e < 1\%$) [208], which would further decrease the contribution of this source class to the DGRB.

¹⁴In this case the sensitivity of the *Fermi* LAT is taken from Ref. [170].

On the other hand, the gamma-ray emission expected from pion decay can be estimated as a function of the amount of gas in the intracluster medium, of the injected spectrum of CR protons and of the intensity of the magnetic fields [209]. Ref. [210] estimates that this hadronic gamma-ray emission can only account for less than few percents of the DGRB reported by EGRET in Ref. [6]. This result was later reduced to less than 1% of the *Fermi* LAT DGRB in Ref. [8], after that mock catalogs of clusters from Ref. [211] were considered in Ref. [208].

The most recent predictions for the emission of unresolved clusters come from Ref. [39]. In this paper, a correlation between the mass of the cluster and its gamma-ray luminosity is assumed and it is calibrated to reproduce the number of clusters detected in radio during the Radio Astronomy Observatory Very Large Array sky survey [212]. It is also required that results are compatible with the non-detection of the Coma cluster by the *Fermi* LAT [208] and of the Perseus cluster by MAGIC [213]. A second, more physically motivated, model for the distribution of CRs and of the intracluster medium distribution is also considered in Ref. [39]. In this case, the intracluster medium is reconstructed from X-ray observations and the CR spatial and spectral distributions are based on hydrodynamic N -body simulations [211]. The two scenarios agree in finding that the contribution of galaxy clusters to the DGRB is negligible.

- **Interactions of ultra-high-energy cosmic rays with background radiation:** UHECRs, with energies larger than 6×10^{19} eV are attenuated due to their pion-producing interactions with the CMB, i.e. the so-called Greisen-Zatsepin-Kuzmin cut-off [214, 215]). Pions trigger electromagnetic cascades, effectively transferring energy from the CRs to the GeV-TeV energy range. This can potentially contribute to the DGRB [216, 42, 43, 217]. Ref. [42] estimates this emission, showing that it is subject to large uncertainties. Indeed, the signal strongly depends on the evolution of the UHECRs with redshift, on their composition and on the intensity of the magnetic fields encountered during the propagation of the CRs. The uncertainty on the intensity of the emission spans more than two orders of magnitude below 10 GeV. The most optimistic prediction indicates that UHECRs can indeed represent a significant contribution to the EGRET DGRB in Refs. [6, 7]. However, above 10 GeV, the intensity of the signal reduce significantly so that it would not be able to explain the bulk of the sub-TeV DGRB detected by the *Fermi* LAT.
- **Type Ia supernovae:** Type Ia supernovae are generated in the thermonuclear explosions of white dwarfs near the Chandrasekhar mass [218, 219]. Gamma-ray emission results from the decay of the material (mainly ^{56}Ni) produced during the detonation. Refs. [220, 221, 40] compute the cumulative emission associated to this class of supernovae as a function of their event rate. The latter is either measured directly or related to the cosmic SFR, $\dot{\rho}_*(z)$, through a model of the delay time, i.e. the time required for a Type Ia supernova progenitor to become a supernova. The cumulative gamma-ray emission can contribute significantly to the DGRB only around the MeV scale (see also Ref. [222]).

On the other hand, Ref. [41] computes the emission associated with the decay of neutral pions produced in the interactions of CR protons with the interstellar medium of the galaxy hosting the supernova. This is a scenario very similar to the one described in Sec. 2.2.3 for SFGs. However, in Ref. [41], the authors consider

CRs accelerated in shocks induced by the explosions of Type Ia supernovae and not of the core-collapse supernovae, as done in Sec. 2.2.3. The predictions of Ref. [41] are affected by a significant uncertainty and they span a range between less than 10% and 100% of the DGRB reported by the *Fermi* LAT in Ref. [8] between 1-10 GeV.

- **Gamma-Ray Bursts:** gamma-ray bursts are very short and intense episodes of beamed gamma-ray emission with a bimodal SED [223, 224, 225]. As in the case of AGNs, the low- and high-frequency peak are associated, respectively, with synchrotron radiation and IC. The widely-accepted fireball internal-external shock model [226] allows to describe the phenomenology of the material inside the bursts and to predict the SED of the bursts. Refs. [227, 228] estimate the total contribution of unresolved gamma-ray bursts to the DGRB by adopting the LF given in Ref. [229]. Results suggest that this emission can explain only a small fraction of the EGRET DGRB in Ref. [6], becoming negligible at energies above ~ 40 GeV. Similar results have been obtained in Ref. [230] which estimates the contribution of unresolved gamma-ray bursts to be as large as 0.1% of the EGRET DGRB in Ref. [6] at the GeV scale.
- **Small Solar-system bodies:** our knowledge of comets populating the Oort Cloud is quite limited and it comes almost entirely from numerical simulations. We believe that more than 10^{12} objects, with sizes ranging from 1 to 50 km, may populate that region. These small Solar-system bodies emit gamma rays from the hadronic interactions of CRs impinging on them. Their abundance is the main unknown, with column densities of Solar-system bodies spanning over three orders of magnitude. As a consequence, a similar level of uncertainty affects the predictions for their cumulative gamma-ray emission. Their contribution to the DGRB may go from overpredicting the DGRB measured in Ref. [7] to being responsible for only few percents of it. See Ref. [231] and references therein.
- **Radio-quiet AGNs:** AGNs at sub-Eddington luminosities are characterized by radiatively inefficient accretions. Since the jet is not beamed enough to trigger non-thermal emission, the source emits mainly between IR and X-ray frequencies. Gamma rays can still be produced: one possibility is to have proton-proton interactions producing neutral pions in the hot gas surrounding the supermassive Black Hole. The intensity of the signal depends on the spin of the Black Hole, since more rapidly rotating objects correspond to larger X-to-gamma flux ratio [232, 233, 234]. Another possibility is a population of non-thermal electrons that can be accelerated in the hot corona around the AGN [235, 16]. The similarities between solar coronae and accretion disks [236] suggest that magnetic reconnection could be responsible for this acceleration [237]. The scenario is considered in Refs. [235, 16] where, using a luminosity-dependent-density evolution, the authors determine that this contribution can explain the whole DGRB measured by EGRET in Refs. [6, 7], but only below 1 GeV.
- **Imperfect knowledge of the Galactic foreground:** the authors of Ref. [238] reconsidered the measurement of the DGRB by EGRET and noted that some modifications on the modeling of Galactic CRs could decrease significantly the intensity of the DGRB. They also raised some doubts on the approach of template fitting. In particular, the effect of an extended halo of electrons around the MW

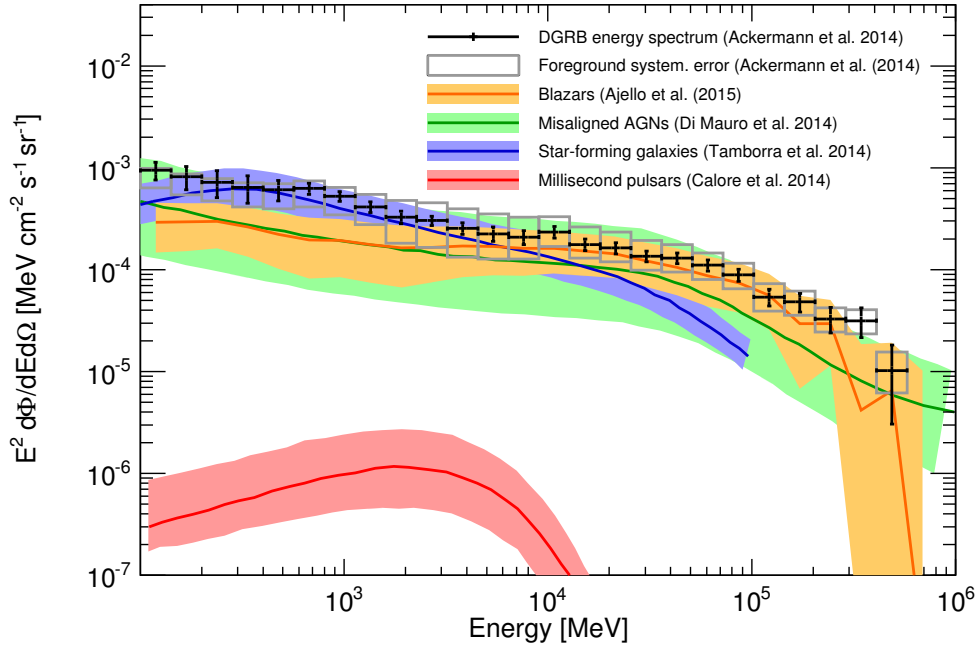


Figure 9: The energy spectrum of the DGRB (black points) as recently measured by the *Fermi* LAT [9]. Gray boxes around each data point denote the uncertainty associated with the Galactic diffuse emission. The solid color lines indicate the expected gamma-ray emission from unresolved sources, for 4 different well-established astrophysical populations: blazars (in orange), MAGNs (in green), SFGs (in blue) and MSPs (in red). Color bands represent the corresponding uncertainties on the emission of each population. Estimates are taken from Ref. [25] (blazars), Ref. [29] (MAGNs), Ref. [161] (SFGs) and Ref. [38] (MSPs).

(with a consequent IC gamma-ray emission extending to high latitudes) is considered. Furthermore, Ref. [239] investigates the possibility of a gas cloud with a mass of few $10^{10} M_{\odot}$, extending to hundreds of kpc from the center of the MW. This halo would be theoretically well motivated, as it would alleviate the problem of the missing baryons in spiral galaxies. A similar object around spiral galaxy NGC 1961 would also explain the diffuse X-ray detected in Ref. [240]. Hints of such large halo could be already present in hydrodynamical N -body simulations of our Galaxy [241, 242, 239]. The gamma-ray emission associated with pion decay in this hypothetical gas halo would be able to explain between 3% and 10% of the *Fermi* LAT DGRB in Ref. [8], depending on the exact size of the halo.

Other possibilities not considered in the list above include emission from massive black holes at $z \sim 100$ [243], from the evaporation of primordial black holes [244, 245], from the annihilations at the boundaries of cosmic matter and anti-matter domains [246] and from the decays of Higgs or gauge bosons produced from cosmic topological defects [247].

We conclude this section by discussing Fig. 9. The image gathers the most recent predictions for the “guaranteed” components to the DGRB, i.e. the emission associated with unresolved blazars, MAGNs, SFGs and MSPs (see sections from 2.2.1 to 2.2.4). They are taken from the results of Refs. [25, 29, 161, 38], respectively and they are

depicted in Fig. 9 by orange, green, blue and red lines, respectively.¹⁵ Each contribution is embedded in a band that denotes the level of uncertainty affecting the prediction. The largest is the one associated with MAGNs (light green band) spanning almost one order of magnitude. Black data points represent the new *Fermi* LAT measurement of the DGRB in Ref. [9] (see Sec. 2.1). The gray boxes around the data points indicate the systematic error associated with the modeling of the Galactic foreground. From the figure, it is clear that MSPs are subdominant and that the remaining 3 astrophysical components can potentially explain the whole DGRB, leaving very little room for additional contributions (see also Refs. [61, 248, 217]). Similar results have been recently obtained by Ref. [65]. This reference also shows that the goodness of the fit to the *Fermi* LAT DGRB energy spectrum in terms of astrophysical sources depends significantly on the model adopted for the diffuse Galactic foreground and on the slope of the energy spectrum of unresolved SFGs. In particular, a description of SFGs with a softer energy spectrum (similar to that of the Galactic foreground) can provide a better fit to the DGRB intensity.

2.3. The Dark Matter component of the Diffuse Gamma-Ray Background

The DGRB can also be used to investigate more exotic scenarios than those presented in the above subsections. In particular, it has already been shown that the DGRB is a powerful tool to investigate the nature of DM.

Discussing the very wide range of viable DM candidates is beyond the scope of this review (see, e.g., Ref. [249]). In the following, we only consider a family of candidates called Weakly Interacting Massive Particles (WIMPs), loosely characterized by a mass of the order of the GeV-TeV and by weak-scale interactions. This is a very well studied scenario since many extensions of the Standard Model of Particle Physics predict the existence of WIMPs [250, 251, 44, 252, 253]. It is also quite natural for WIMPs to reproduce the DM relic density observed, e.g., by Planck [254]. Yet, currently there is no observational confirmation of the existence of WIMPs.

WIMP DM can either annihilate or decay into Standard Model particles, including gamma rays. This is a general prediction of WIMP candidates and it represents an additional reason to focus only on WIMPs for this review. The specific mechanisms of gamma-ray emission (see, e.g., Ref. [44] for a review) depend on the DM candidate considered and include *i*) direct production of monochromatic gamma rays, *ii*) decay of neutral pions, produced by the hadronization of the primary annihilation/decay products, *iii*) final state radiation and *iv*) secondary emission by IC or bremsstrahlung of primarily produced leptons. Since no DM source has been unambiguously detected up to now, the entire DM-induced gamma-ray emission may be unresolved and, thus, it contributes to the DGRB. In Sec. 2.3.1 we discuss the potential DM contribution to the DGRB in the case of self-annihilating DM particles, while Sec. 2.3.2 is devoted to decaying DM. Note that some DM candidates can experience both annihilations and decays [255].

DM-induced gamma rays can be produced in the DM halo of the MW or in extragalactic DM structures and substructures. We refer to the two possibilities as the “Galactic” and “cosmological” DM components, respectively. The latter is isotropic by

¹⁵Ref. [25] only provides the total emission from resolved *and* unresolved blazars. Since we are interested in the unresolved component, the orange line in Fig. 9 is obtained by subtracting the emission of resolved sources from Ref. [9] from the total signal from blazars. The width of the light orange band is, then, computed summing the estimated errors of the two components in quadrature. Also, the abrupt end of the SFG component at ~ 100 GeV is not physical and simply comes from the lack of predictions above this energy in Ref. [161] only up to that energy.

construction, while the former is expected to exhibit some anisotropy, due to the particular location of the Earth in the DM halo of the MW. We remind that, as described in Sec. 2.1, the intensity of the DGRB is obtained by means of an isotropic template [9]. However, the Galactic DM signal can exhibit a significant anisotropy and, in that case, it cannot be considered part of the DGRB.¹⁶ In this section, we focus mainly on the contribution of the cosmological DM signal to the DGRB, discussing a possible Galactic DM component only towards the end of the section.

2.3.1. The case of annihilating Dark Matter

In the Λ CDM cosmological framework [254], initial matter fluctuations in the Early Universe are the seeds of the structures that populate today's Universe. These fluctuations grow by accreting new matter and form the first protostructures, which, then, collapse and eventually virialize into DM *halos*. Λ CDM predicts that, in later epochs, larger halos gradually assemble by accretion and merging of smaller halos. Under this scenario of structure formation, a cosmological gamma-ray signal is expected from the annihilations of DM particles taking place in *all* DM halos at *all* cosmic epochs.

The cosmological gamma-ray flux $d\Phi/dE_0 d\Omega$ (i.e. the number of photons per unit energy, time, area and solid angle) produced by DM annihilations at energy E_0 over all redshifts z is given by [48, 49, 51]:

$$\frac{d\Phi}{dE_0 d\Omega} = \frac{c \langle \sigma v \rangle (\Omega_{\chi,0} \rho_c)^2}{8\pi m_\chi^2} \int dz \frac{(1+z)^2}{H(z)} \zeta(z) e^{-\tau_{\text{EBL}}(E_0(1+z), z)} \sum_i B_i \left. \frac{dN^i}{dE} \right|_{E=E_0(1+z)} \quad (15)$$

where m_χ is the mass of the DM particle, $\langle \sigma v \rangle$ its annihilation cross section¹⁷ and the sum runs over all the possible annihilation channels, each of them corresponding to a specific branching ratio B_i and a differential photon yield dN^i/dE . $\Omega_{\chi,0}$ is the current DM density ratio, ρ_c the critical density of the Universe, and $H(z)$ and c are the Hubble parameter and the speed of light, respectively. The function $\tau_{\text{EBL}}(E, z)$ accounts for the absorption of gamma-ray photons due to interactions with the EBL. Finally, the quantity $\zeta(z)$ is the so-called *flux multiplier* and it indicates the variance of the fluctuations in the field of squared DM density. It is, therefore, a measure of the statistical clustering of DM in the Universe:

$$\zeta(z) = \langle \delta^2(z) \rangle = \frac{\langle \hat{\rho}_\chi^2(z) \rangle}{(\Omega_{\chi,0} \rho_c)^2}, \quad (16)$$

where $\hat{\rho}_\chi$ is the comoving DM density and the parentheses $\langle \cdot \rangle$ denote angular integration over all the possible pointings in the sky.

Two approaches have been proposed to calculate the flux multiplier. The first is based on the Halo Model [200, 201] and it relies on the knowledge of the abundance and of the internal properties of DM halos. The former is described by the Halo Mass Function (HMF), dn/dM , i.e. the comoving number of halos per unit mass, while the latter is encoded in the DM halo density profile. More specifically, in the Halo Model framework, $\zeta(z)$ is proportional to the integral of the HMF times the integral of the DM

¹⁶Small-scale anisotropies in the DGRB, on the other hand, are discussed in detail in Sec. 3.

¹⁷The annihilation cross section in Eq. (15) is assumed to be dominated by *s*-wave interactions. In the case of a dependence on the relative velocity of the annihilating DM particles, Eq. (15) has to be modified accordingly and the signal will, thus, depend on the velocity distribution of DM [256, 257].

density squared inside the halo [48, 49, 50, 64]:

$$\zeta(z) = \frac{1}{\rho_c} \int_{M_{\min}} dM \frac{dn}{dM} M \frac{\Delta(z)}{3} \langle F(M, z) \rangle, \quad (17)$$

where M_{\min} is the minimum halo mass. Typical values for M_{\min} range approximately between 10^{-12} and $10^{-3} M_{\odot}$ for supersymmetric DM candidates.¹⁸ Its exact value depends on the position of a cut-off in the power spectrum of matter fluctuations, above which the formation of DM structures is suppressed. This cut-off arises from the combined effect of kinetic decoupling and baryonic acoustic oscillations [258, 259, 260, 261], and its precise location ultimately depends on the Particle Physics nature of the DM candidate [262, 261, 263]. In addition, the mapping between the cut-off scale and M_{\min} is not well defined, depending on the assumed relation between mass and size of the small-mass halos [264]. These uncertainties are responsible for the huge variability of M_{\min} quoted above.

The factor $\Delta(z)$ in Eq. (17) is the so-called halo overdensity and it depends on the cosmology assumed and on the details of the gravitational collapse of the halo. The radius R_{Δ} at which the mean enclosed density of a DM halo is $\Delta(z)$ times ρ_c is called the *virial* radius, which can be taken as a measurement of the size of the halo. The DM distribution inside the halo is codified in the function $\langle F(M, z) \rangle$:

$$F(M, z) \equiv c_{\Delta}^3(M, z) \frac{\int_0^{c_{\Delta}} dx x^2 \kappa^2(x)}{\left[\int_0^{c_{\Delta}} dx x^2 \kappa(x) \right]^2}, \quad (18)$$

where $\kappa(x)$ is the DM density profile and $x = r/r_s$. r_s is a scale radius, whose precise definition depends on the assumed $\kappa(x)$. The quantity c_{Δ} is the so-called *concentration* [265, 266, 267] and it is defined as R_{Δ}/r_s . Note that $\langle F(M, z) \rangle$ in Eq. (17) is the function $F(M, z)$ from Eq. (18) averaged over a log-normal probability distribution assumed for c_{Δ} . Such a distribution accounts for halo-to-halo scatter on the value of c_{Δ} [265, 268, 269], which is a natural consequence of the stochastic process of structure formation in Λ CDM cosmology.

Information on the abundance and internal properties of DM halos is mainly extracted from N -body cosmological simulations (see, e.g., Ref. [270] and references therein). However, simulations do not resolve the whole halo hierarchy down to M_{\min} . The current resolution limit for MW-like DM halos is approximately at $10^5 M_{\odot}$ at $z = 0$ [271], i.e. several orders of magnitude above the expected value for M_{\min} . Thus, extrapolations of the relevant quantities (e.g., the HMF and $c_{\Delta}(M, z)$) are needed. Since $F(M, z)$ in Eq. (18) depends on the third power of the halo concentration, the way $c_{\Delta}(M, z)$ is extended below the mass resolution of simulations is crucial in the estimation of the cosmological DM signal. Above the mass resolution limit, $c_{\Delta}(M)$ can be well described by a power law [265, 272, 273, 266, 267]. Several works assume the same behavior to be valid down to M_{\min} [274, 56, 275, 276], thus assigning very large concentrations to the smallest halos. This translates into a very high gamma-ray flux expected from DM annihilations. Nevertheless, power-law extrapolations for $c_{\Delta}(M)$ are not physically motivated and they are now clearly ruled out both by recent high-resolution simulations of the smallest DM halos [277, 278, 279] and by theoretical predictions deeply rooted in the Λ CDM cosmological framework [267, 280, 281]. Indeed, simulation-based and theoretical estimates of

¹⁸The value $M_{\min} = 10^{-6} M_{\odot}$ has become a standard benchmark value in the field.

$c_{\Delta}(M, z)$ have been shown to agree now remarkably well over the full halo mass range, i.e. from Earth-like “microhalos” up to the scale of the heaviest galaxy clusters [280]. Compared to power-law extrapolations, these estimates exhibit a flattening of $c_{\Delta}(M)$ at low masses. This leads to substantially less concentrated low-mass halos and, thus, to a considerably smaller cosmological DM signal. Overall, predictions for the cosmological DM-induced emission can vary by few orders of magnitude depending on the adopted model for $c_{\Delta}(M, z)$ in Eq. (18), see, e.g., Refs. [56, 282].

Not unexpectedly, the variability of the predicted DM signal also depend on the particular choice of M_{\min} . For example, the cosmological signal increases by up to a factor of ~ 6 when M_{\min} goes from $10^{-3}M_{\odot}/h$ to $10^{-12}M_{\odot}/h$ [62]. This refers to the case of a power-law extrapolation of $c_{\Delta}(M)$ and, by construction, flux multipliers that rely on power-law extrapolations are particularly sensitive to the choice of M_{\min} . When adopting a $c_{\Delta}(M)$ that flattens at low halo masses, the flux multiplier changes by a factor of ~ 3 over the same range of M_{\min} [62, 64].

N -body cosmological simulations have also been employed to understand the HMF and its redshift evolution [283, 284]. Mock halo catalogs have been used to test the predictions of the Press-Schechter formalism, according to which the HMF can be written as follows [200, 285, 286, 287]:

$$\frac{dn}{dM}(M, z) = f(\sigma(M, z)) \frac{\rho_c \Omega_{\chi}(z)}{M} \frac{d \ln \sigma^{-1}(M, z)}{dM}, \quad (19)$$

where $\sigma(M, z)$ is the variance of the fluctuations of the DM density field (smoothed on a scale of mass M) and the exact expression for $f(x)$ depends on the mechanism assumed to describe the halo gravitational collapse. An accurate fitting formula for the HMF, inspired by Ref. [288], can be found in Ref. [289] for the cosmological model favored by the first data release of the Wilkinson Microwave Anisotropy Probe (WMAP). More recently, Ref. [267] have also adopted the functional form proposed in Ref. [289] and derived the parameters of the HMF compatible with the cosmological model preferred by Planck.¹⁹ Overall, the HMF at $z = 0$ can be qualitatively approximated by a power law with a slope between -1.9 and -2.0 and a sharp cut-off for halos more massive than $\sim 10^{14}M_{\odot}$. The uncertainty in the calculation of the cosmological DM signal induced by different possible parametrizations of the HMF is only marginal when compared to other sources of uncertainties. For instance, assuming the HMF of Ref. [288] instead of the one in Ref. [289] changes the total gamma-ray flux by a factor of about 20% (see also Ref. [282]).

High-resolution N -body simulations have also helped to establish the density profiles of DM halos in great detail. Ref. [291] determined that DM halos exhibit a density profile that is universal, i.e. independent of the halo mass. A Navarro-Frenk-White (NFW) profile, i.e. proportional to $\kappa \propto 1/r$ in the inner region and to a steeper r^{-3} at large radii, provides a good fit. More recently, the so-called Einasto profile was found to agree better with the results of N -body simulations, especially at intermediate halo radii [292, 293, 294]. Even if many other parametrizations have been proposed over the last years [295, 296, 297, 298, 299, 300], current N -body simulations agree on a slope $\lesssim -1$ for the DM density in the inner region. However, these “cuspy” profiles are derived from simulations that only contain DM, without including baryons. Indeed, high-resolution

¹⁹Note that the agreement of different fitting formulas with the simulations may depend on the algorithm used by the simulators to extract the mass of a halo from the raw particle data, with the caveat that different algorithms may lead to different results [290].

observations of the rotation curves of DM-dominated dwarfs and low-surface-brightness galaxies favor DM density profiles with a flat central core [301, 302, 303, 304, 305, 306, 307, 308, 309]. Phenomenological cored profiles, such as the Burkert one [302], were proposed to accommodate such results. More recently, hydrodynamical simulations have been performed, which realistically include the complexity of baryonic physics. They begin to reproduce the observed properties of galaxies successfully, e.g. in Refs. [310, 311]. Yet, the exact interplay between baryons and DM at all radial scales and for all halo masses is not fully understood, and the impact of complex baryonic phenomena (such as supernova feedback, stellar winds and baryonic adiabatic compression) on the DM density profile is still uncertain, particularly in the inner region [312, 313, 314, 315, 316, 317, 318, 319, 320]. Ref. [321] finds a difference of almost one order of magnitude in the cosmological flux when a Burkert profile is assumed for all DM halos instead of a NFW one.

In addition to DM halos, a natural prediction of Λ CDM is the existence of a large number of subhalos, i.e. halos gravitationally bound to a larger host halo and located within its virial radius. Since the annihilation luminosity of a halo is proportional to its DM density squared, the presence of small clumps with high DM densities has the effect of boosting the overall gamma-ray luminosity of the host halo [322, 323, 324, 274, 325, 326, 327, 56, 328, 329, 275, 330, 276, 279, 331, 280]. The additional contribution from substructures can be accounted for in the computation of the flux multiplier by adding an extra term in Eq. (17). In particular, the factor $\langle F(M, z) \rangle$ has to be replaced by $\langle F(M, z) \rangle (1 + B(M, z))$, where $B(M, z)$ is called the “boost factor”.²⁰

The subhalo population is characterized by a subhalo mass function:

$$\frac{dn_{\text{sub}}}{dM}(m_{\text{sub}}) \propto \left(\frac{m_{\text{sub}}}{M_{\text{host}}} \right)^{-\alpha}, \quad (20)$$

extending down to M_{min} . The slope of the subhalo mass function has been measured in high-resolution N -body simulations, ranging between -1.9 and -2 [332, 271]. These values are also in line with theoretical expectations from the Press-Schechter theory of structure formation [333, 334, 335]. It has been noted, though, that several effects may prevent the subhalo mass function to reach the lowest subhalo masses, since processes such as tidal disruption, accretion or merging may be particularly efficient and deplete the low-mass tail of the mass function. It is difficult to estimate the survival probability of these small subhalos, while it remains computationally very expensive to simulate and keep track of such processes with the resolution needed. Although the properties of low-mass DM subhalos are expected to follow those of the more massive counterparts, the abundance and distribution of DM substructures below the resolution of current simulations remain uncertain. The internal properties of subhalos are also subject to debate. We still lack a comprehensive understanding of the subhalo concentration, even if subhalos have been shown to exhibit larger $c_{\Delta}(M)$ than halos of the same mass [336, 271, 337, 338]. Similarly to the case of main halos, the assumptions made on $c_{\Delta}(M)$ and on the abundance of low-mass subhalos have a large impact on the amplitude of the subhalo boost factor. Overall, under the most extreme scenarios (corresponding to blind power-law extrapolations of $c_{\Delta}(M)$), the presence of subhalos can increase the total cosmological annihilation signal

²⁰This definition of the boost factor is particularly convenient for the computation of the flux multiplier and of the cosmological DM signal. We warn the reader, though, that alternative definitions of $B(M, z)$ can be found in the literature.

by more than one order of magnitude [48, 62, 217, 339].

As an alternative to the Halo Model described above, the Power Spectrum approach has been recently introduced to compute the flux multiplier [340, 264]. In this new framework, $\zeta(z)$ can be calculated by means of the non-linear matter power spectrum P_{NL} , i.e. the Fourier transform of the two-point correlation function of the matter density field, as follows:

$$\zeta(z) \equiv \langle \delta^2(z) \rangle = \int^{k_{\max}} \frac{dk}{k} \frac{k^3 P_{NL}(k, z)}{2\pi^2}, \quad (21)$$

where $k_{\max}(z)$ is a maximal scale that can be related to M_{\min} in the Halo Model formalism.²¹ The main benefit of the Power Spectrum approach relies on the fact that only one single quantity is needed for the calculation of $\zeta(z)$, i.e. P_{NL} in Eq. (21). P_{NL} can be measured directly in N -body cosmological simulations using only a matter density map and it does not rely on the concept of DM halos. It is, thus, also independent on the complex issue of halo finding and on the uncertainties associated with it [341].²² This is, indeed, what the authors of Ref. [264] did, guided by the results of the Millennium-I and Millennium-II simulations [284, 343]. Yet, as in the Halo Model approach, current N -body simulations do not reach the highest k values needed in Eq. (21) and, thus, extrapolations beyond the simulation resolution are again required.²³ Note, however, that only P_{NL} is extrapolated in this case, as opposed to the Halo Model approach that relies on the knowledge of several quantities in the low-mass regime. This is indeed the reason why the authors in Ref. [64] adopted the Power Spectrum approach to obtain a realistic estimate of the uncertainty on $\zeta(z)$, even if their fiducial flux multiplier is computed within the Halo Model framework. Furthermore, within the PS approach, it is possible to motivate in a realistic way both the choice of k_{\max} and the way the extrapolation is performed. Note also that, by construction, the Power Spectrum approach naturally includes the contribution of substructures down to length scales $\sim \pi/k_{\max}$, while in the Halo Model the description of substructures requires additional knowledge, often leading to further debatable extrapolations and uncertainties.²⁴

A comparison between the Power Spectrum and Halo Model approaches is performed in Refs. [264, 344, 64]. Results from Refs. [264, 64] are reproduced in Fig. 10. In the left panel, the red bands indicate the predictions for $\zeta(z)$ (multiplied by factors depending on redshift) obtained by means of the Power Spectrum method for different choices of k_{\max} . For each value of k_{\max} adopted, the corresponding band accounts for different ways of extrapolating P_{NL} beyond the resolution of the Millennium simulations. The predictions for the Halo Model (gray band) refer to a $M_{\min} = 10^{-6} M_{\odot}/h$ and have been obtained following Refs. [56, 58]. In the right panel of Fig. 10, the predictions of the

²¹The exact relation between k_{\max} and M_{\min} is not trivial, as discussed in detail in Refs. [264, 64].

²²In Refs. [342, 331], the authors introduce the concept of particle phase space average density, an estimate of the coarse-grained phase-space density of DM structures. Interestingly, they show in Ref. [331] how this observable can be used to determine the DM-induced emission of MW-like halos. The particle phase space average density can be directly computed directly from N -body simulations' raw data and, therefore, the formalism shares some similarities with the Power Spectrum approach, introduced here to estimate the cosmological DM signal.

²³At redshift zero, for instance, the maximum k values resolved in current large-scale structure simulations are typically of the order of few hundreds, while k_{\max} may take values up to 10^6 .

²⁴We remind the reader that Eq. (21) only determines the cosmological DM signal. Any gamma-ray emission associated with the halo of the MW and its subhalos is not accounted for by the Power Spectrum model and, thus, needs to be added by hand (see further discussion at the end of this section).

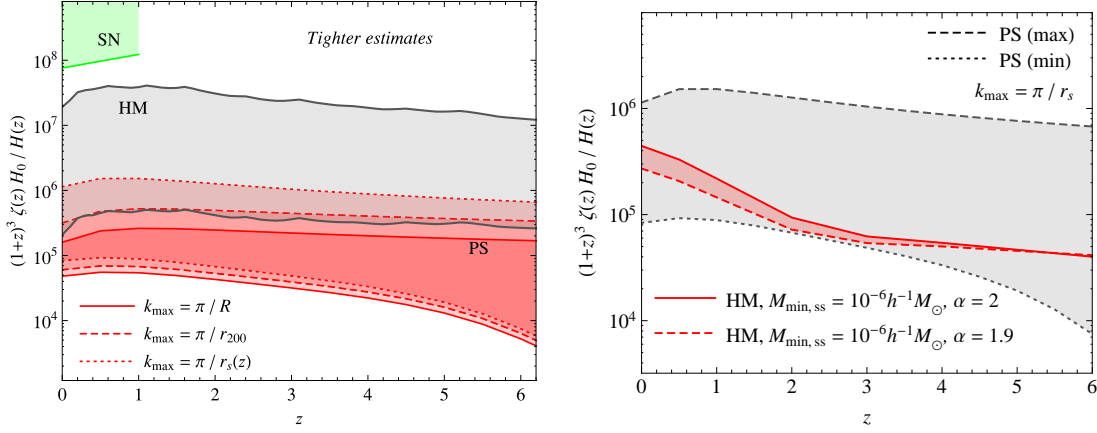


Figure 10: Comparison of the Halo Model and Power Spectrum approaches for the calculation of the flux multiplier. The Halo Model makes use of Eq. (18) while the Power Spectrum formalism adopts Eq. (21). *Left*: Power Spectrum predictions are shown in red. The different bands correspond to different prescriptions to derive the cut-off scale k_{\max} from the size of the DM halo with mass M_{\min} . The width of the bands accounts for different extrapolation schemes up to k_{\max} . The Halo Model predictions (gray band) are obtained following Refs. [56] and [58]. Figure taken from Ref. [264]. *Right*: Predictions according to the Power Spectrum approach (gray) and the Halo Model (red). The Halo Model formalism follows what done in Ref. [64] for two possible subhalo mass functions. The gray band corresponds to a particular choice of k_{\max} in the Power Spectrum approach, for different ways (labeled as “PS (max)” and “PS (min)” in the figure) to extend P_{NL} beyond the resolution of the simulations. For both panels, a value of $M_{\min} = 10^{-6} M_{\odot}/h$ is adopted in the Halo Model formalism. Figure taken from Ref. [64].

Power Spectrum approach (for a specific value of k_{\max}) are given by the gray band. The width of the band corresponds to two different prescriptions to perform the extrapolation (labeled “PS (min)” and “PS (max)” in the figure). On the other hand, the red band reproduces the results of the Halo Model in Ref. [64] for $M_{\min} = 10^{-6} M_{\odot}/h$ and two values of the slope for the subhalo mass function. Remarkably, the two methods agree well in their predictions for $\zeta(z)$, within uncertainties. This is so despite the caveats mentioned above and the intrinsic differences of the two formalisms.

From Sec. 2.2 we know that gamma-ray emission of astrophysical origin is able to explain a significant fraction, if not all, of the DGRB, therefore leaving very little room for a potential DM contribution (see also Fig. 9). Moreover, the gamma-ray energy spectrum expected from DM annihilations is generally slightly curved, with a cut-off at the mass of the DM particle and the possibility of spectral features like bumps or lines. On the other hand, the DGRB detected by the *Fermi* LAT exhibits a power-law spectrum at low energies and a cut-off compatible with EBL attenuation at higher energies (see Sec. 2.1). This suggests, again, that DM annihilations cannot provide a dominant contribution to the DGRB. Thus, the DGRB can be used to set limits on the intensity of the DM-induced emission. These are usually translated into upper limits in the $(m_{\chi}, \langle\sigma v\rangle)$ plane, identifying the region that, given a model for the abundance and properties of DM halos and subhalos, is excluded as it overproduces the measured DGRB.

Most of the works following this idea employ the Halo Model approach to predict the cosmological DM annihilation signal. Given the large number of parameters involved in the Halo Model framework, as well as the large uncertainties associated with some of them, it is very hard to perform a detailed, one-to-one comparison among the different DM limits available in the literature. In particular, predictions obtained by different

groups differ mainly due to different assumptions on $c_\Delta(M, z)$ and M_{\min} . In addition, some works also consider the Galactic DM signal. Differences can be further amplified by the various statistical prescriptions employed to compute the upper limits. Yet, we believe that a comparison among the limits in the literature is useful, as it showcases the potential of searching for DM in the DGRB compared to other indirect DM probes. Fig. 11 summarizes some of the upper limits available.²⁵ They all refer to annihilations entirely into b quarks. Note that the limits obtained by assuming a power-law $c_\Delta(M)$ below the mass resolution of N -body simulations are among the most constraining in Fig. 11 (see, e.g., the gray dashed line from Ref. [217]). However, as argued above, power-law $c_\Delta(M)$ are not well motivated, putting the corresponding limits into question.

Two approaches are possible when deriving DM limits from the DGRB measurement. In the first one it is required that the DM signal does not overshoot the measured DGRB at a particular confidence level, typically 2 or 3σ . See, e.g., Refs. [365, 59, 366, 60, 62, 335, 339]. This leads to *conservative* and robust upper limits on the DM annihilation cross section, shown by the green lines in Fig. 11. Alternatively, one or more astrophysical contributions to the DGRB can be modeled and included in the analysis. The DM component is, then, required not to overshoot the fraction of the DGRB not already accounted for by astrophysics. These limits are more constraining than the previous ones [58, 367, 61, 109, 248, 217]. Nevertheless, since the exact contribution from astrophysical sources is not known, it must be noted that they are subject to larger uncertainties.

The most recent constraints on annihilating DM comes from Ref. [64] and are shown by black lines in Fig. 11. The “conservative limit” (solid black line) is obtained without including any modeling of astrophysical contributors to the DGRB. These limits exclude annihilation cross sections a factor of ~ 3 lower than the thermal value of $3 \times 10^{-26} \text{cm}^3 \text{s}^{-1}$ for a mass of 10 GeV, while, for $m_\chi \geq 1 \text{TeV}$, the upper limit is around $5 \times 10^{-24} \text{cm}^3 \text{s}^{-1}$. Ref. [64] also shows that an improvement of one order of magnitude (a factor ~ 2) for DM masses of the GeV scale (around 30 TeV) is possible when *i*) the cumulative astrophysical contribution to the DGRB is modeled as a power-law in energy with an exponential cut-off and *ii*) slope and position of the cut-off are fixed to the best-fit values to the DGRB data in Ref. [9]. Note that this approach (referred to as “sensitivity reach” and denoted by the dashed black line in Fig. 11) does not account for any uncertainty in the description of the astrophysical emission. A more realistic scenario is the one of Ref. [25], where the authors estimate the unresolved astrophysical emitters using the most up-to-date information from resolved sources or from other frequencies (see Sec. 2.2). A renormalization factor \mathcal{A} is included in front of the total astrophysical contribution to account for possible fluctuations in its intensity. The limit of $\langle \sigma v \rangle$ (solid blue line in Fig. 11) is then obtained by profiling over \mathcal{A} . This results in an improvement of a factor of ~ 3 for $m_\chi = 10 \text{GeV}$, with respect to the conservative limits of Ref. [64]. A negligible improvement is expected at masses larger than 10 TeV, where the limits are determined by the Galactic DM signal.

Similar results have recently been obtained in Ref. [65], which also employs a model for the astrophysical components to the DGRB. The different statistical analysis performed in Ref. [65] suggests that a description of the DGRB of Ref. [9] in terms of unresolved astrophysical sources *and* gamma rays from DM annihilations in the MW

²⁵We only consider limits derived from the two measurements of the DGRB performed by the *Fermi* LAT [8, 9]. Older works based on earlier DGRB measurements can be found, e.g., in Refs. [345, 346, 347, 48, 49, 348, 349, 350, 50, 351, 51, 52, 352, 353, 354, 355, 356, 274, 357, 358, 55, 359, 321, 360, 361, 362, 363, 56, 364].

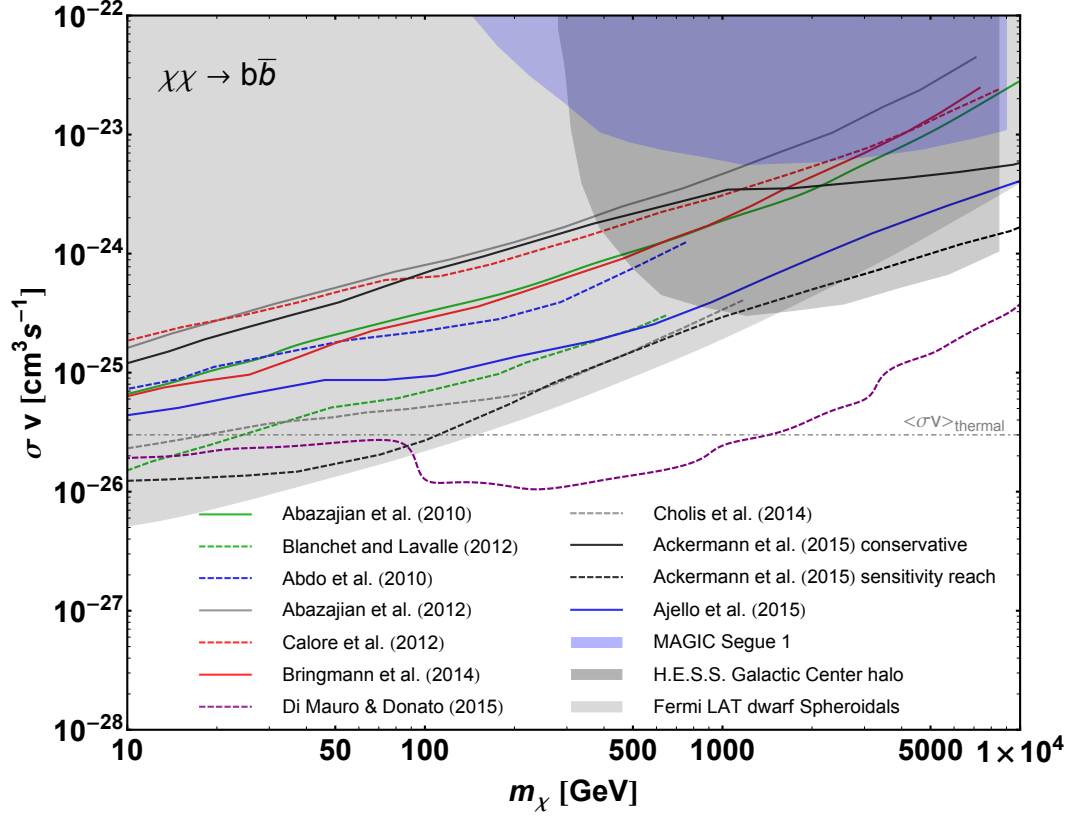


Figure 11: Upper limits obtained by considering the DGRB energy spectrum measured in Refs. [8, 9]. Annihilations into b quarks are assumed. The regions above the colored lines are excluded because the cumulative DM-induced emission would overproduce the DGRB. Different lines correspond to different assumptions for the properties of DM halos (especially for low halo masses) and different methods to compute the upper limits. The solid green line is taken from Fig. 2 of Ref. [365] while the dashed green line is from Fig. 8 of Ref. [335] (lower bound of the band relative to $\alpha_m = 2$ for the emission from the Galactic Poles). The dashed blue line is taken from Fig. 5 of Ref. [58] (conservative limits for model MSII-Sub1) and the solid gray one from Fig. 2 of Ref. [367]. The solid and dashed red lines are taken from Fig. 3 of Ref. [61] (limits labeled “Fermi EGB”) and from Fig. 5 of Ref. [248] (panel labeled “best-fit background”), respectively. The dashed gray line is from Fig. 15 of Ref. [217] (default substructures’ model). The black lines correspond to the predictions obtained in Ref. [64] by means of the Halo Model (reference scenario). The solid blue line is taken from Fig. 4 of Ref. [25], while the dashed purple one is from Fig. 4 of Ref. [65]. The blue region indicates the portion of the $(m_\chi, \langle\sigma v\rangle)$ plane already excluded by the observation of the Segue 1 dwarf Spheroidal galaxy performed by the MAGIC telescopes (see Fig. 6 of Ref. [368]). The dark gray region is excluded by the analysis performed by the H.E.S.S. telescopes in Ref. [369] from the so-called “Galactic Center halo” (see their Fig. 4 for an Einasto DM density profile). Finally, the light gray region indicates the DM candidates not compatible with the combined analysis of 15 dwarf Spheroidal galaxies by the *Fermi* LAT [370]. A comparison between the *Fermi* LAT DGRB and the DM-induced signal can also be found in Refs. [366, 59, 60, 109, 62, 339]. The dash-dotted horizontal line marks the value of the thermally averaged annihilation cross section.

halo provides a better fit, compared to a purely astrophysical interpretation with no DM. Such a hint of a DM signal in the DGRB suggests a DM particle with a mass of $\sim 10 - 20$ GeV (for annihilation into b quarks), depending on the model adopted for the diffuse Galactic foreground.²⁶

Indeed, some of the limits shown in Fig. 11 have been obtained assuming that DM annihilations in the MW halo also contribute to the DGRB [58, 365, 367, 59, 366, 61, 109, 62, 335, 339, 248, 217]. Note that, as mentioned in Sec. 2.1, the DGRB is obtained from the normalization of the isotropic template in the multi-component fit to the gamma-ray data at high Galactic latitudes. Thus, when a Galactic DM signal is included, it is implicitly assumed that the DM signal is sufficiently isotropic in this particular region of the sky.

Two distinct components contribute to the Galactic DM signal. The first accounts for the *smooth* DM distribution of the host DM halo of the MW, while the second one comes from the population of Galactic subhalos. The former depends on the DM density profile assumed for the MW main halo. This is uncertain in the innermost parts of the Galaxy, but for $|b| > 20^\circ$, i.e. more than 3 kpc from the Galactic Center, N -body simulations roughly agree. The signal from this smooth component peaks towards the Galactic Center and, between $b = 20^\circ$ and 90° , typical variations are of a factor of ~ 16 [64]. Thus, even outside the Galactic plane the signal is largely anisotropic and, therefore, this component cannot be described by an isotropic template as the DGRB. Indeed, the presence of an emission with such a well-defined morphology may impact the procedure used in Ref. [9] to measure the DGRB energy spectrum. This was tested in Ref. [64], where the authors re-derived the DGRB including an additional template for the smooth Galactic DM signal. They found that this signal can be degenerate with other diffuse Galactic emissions, especially the one from IC. They also checked the impact that the new template would have on the upper limits on $\langle\sigma v\rangle$. The result suggests that, at least for DM candidates not excluded by the conservative limits in Ref. [64], this additional Galactic DM template has only a moderate effect.

The second contribution to the Galactic DM signal comes from the subhalos of the MW: the brightest or closest of them may potentially give rise to bright spots in the gamma-ray sky. However, none of the unassociated sources in the 2FGL catalog has been robustly interpreted as a DM subhalo [371, 372]. The overall subhalo population is expected to give rise to a diffuse smooth emission [274, 53, 55, 359]. Its morphology depends on the abundance and distribution of subhalos in the Galaxy. A general prediction is that the cumulative emission of subhalos is more extended (thus more isotropic) than that of the main halo. More specifically, factors between 0.1 and 2 are quoted in Ref. [64] for the variation of the signal of Galactic substructures between $b = 20^\circ$ and 90° . These small variations motivate the authors of Ref. [64] to assume this component as isotropic and, thus, to include it when setting their DM limits. Its impact can be quite significant since Galactic subhalos can boost the Galactic DM signal by a factor of 3 to 15, depending on the slope of the subhalo mass function [280].

We end this section by comparing the upper limits on the annihilation cross section derived in Ref. [64] to the results of other indirect searches for DM. In particular, in Fig. 11, the shaded regions indicate which portion of the parameter space has been already excluded by these other probes. The blue region is derived from the observation of the Segue 1 dwarf Spheroidal galaxy by the MAGIC telescopes [368], while the dark

²⁶A similar indication of a DM component to the DGRB was also reported in Refs. [348, 357] based on the EGRET measurement of the DGRB in Ref. [7].

gray region indicates the portion of the $(m_\chi, \langle\sigma v\rangle)$ space not compatible with the analysis of H.E.S.S. data from the so-called “Galactic Center halo” [369]. Finally, the light gray area is excluded by the non-detection of gamma rays from the observation of 15 dwarf Spheroidal galaxies with the *Fermi* LAT [370]. Note that the conservative upper limits derived in Ref. [64] (solid black line) are always inside the area already excluded, while the most stringent *sensitivity reach* (dashed black line) provides the strongest constraints on $\langle\sigma v\rangle$ for DM masses up to 1 TeV, above which the limit from H.E.S.S. becomes more stringent.

2.3.2. The case of decaying Dark Matter

Decaying particles can be a viable DM candidates if their decay lifetime is larger than the age of the Universe [373, 374, 375]. As in the previous section, we will not discuss here the models that can accommodate such particles or the mechanisms that guarantee long lifetimes. We simply consider generic WIMPs that decay emitting gamma-ray photons.

In contrast to the case of annihilating DM, the gamma-ray signal expected from decaying DM particles is linearly proportional to the DM density. For instance, the contribution of the MW halo (at a certain energy E_0 and towards the direction ψ) can be written as follows:

$$\frac{d\phi}{dE_0 d\Omega} = \frac{1}{4\pi} \frac{1}{\tau m_\chi} \int ds \rho_{\text{MW}}[r(s, \psi)] \sum_i B_i \left. \frac{dN^i}{dE} \right|_{E=E_0} \quad (22)$$

where τ is the DM particle lifetime, ρ_{MW} the DM density profile of the MW halo and s is the line-of-sight variable pointing towards the direction of observation. In the case of prompt emission, the s -wave annihilation of 2 non-relativistic DM particles with a mass m_χ is equivalent to the decay of a s -wave state with mass $2m_\chi$ and integer spin [376]. Under those assumptions, the photon yield dN^i/dE in Eq. (22) can be determined from the same quantity in Eq. (15). A decaying DM candidate can also produce gamma rays through semileptonic channels (provided that it is characterized by a semi-integer spin) or through a three-body decays [255]. Mono-chromatic lines are also a typical signature of a vast class of decaying DM candidates [377, 378, 379, 374, 380], while the so-called “box-shaped” spectra have been recently introduced in Ref. [381]. Finally, secondary gamma rays can also be produced when primary leptons from DM decay interact via bremsstrahlung with the interstellar medium of the Galaxy or via IC off its radiation fields [382].

Given the linear dependence on the DM density in Eq. (22), the gamma-ray signal expected from the smooth MW DM halo has a different morphology, compared to the case of annihilating DM. For a decaying particle, the emission is now more isotropic and, thus, there exists a better motivation to include it among the contributors to the DGRB. Note also that, on the case of decaying DM, the emission of a DM halo is proportional to the its total mass. This means that DM substructures are not expected to boost significantly the predicted DM signal. Therefore, for a specific DM candidate, the main uncertainty affecting the emission in Eq. (22) comes from the unknown DM density profile of the MW halo.²⁷ Remarkably, this translates into a considerably smaller uncertainty on the intensity of the DM-induced emission compared to the case of annihilating DM.

²⁷When considering secondary emission, one should also add the uncertainty associated with our imperfect knowledge of the propagation of charged particles in the MW [382].

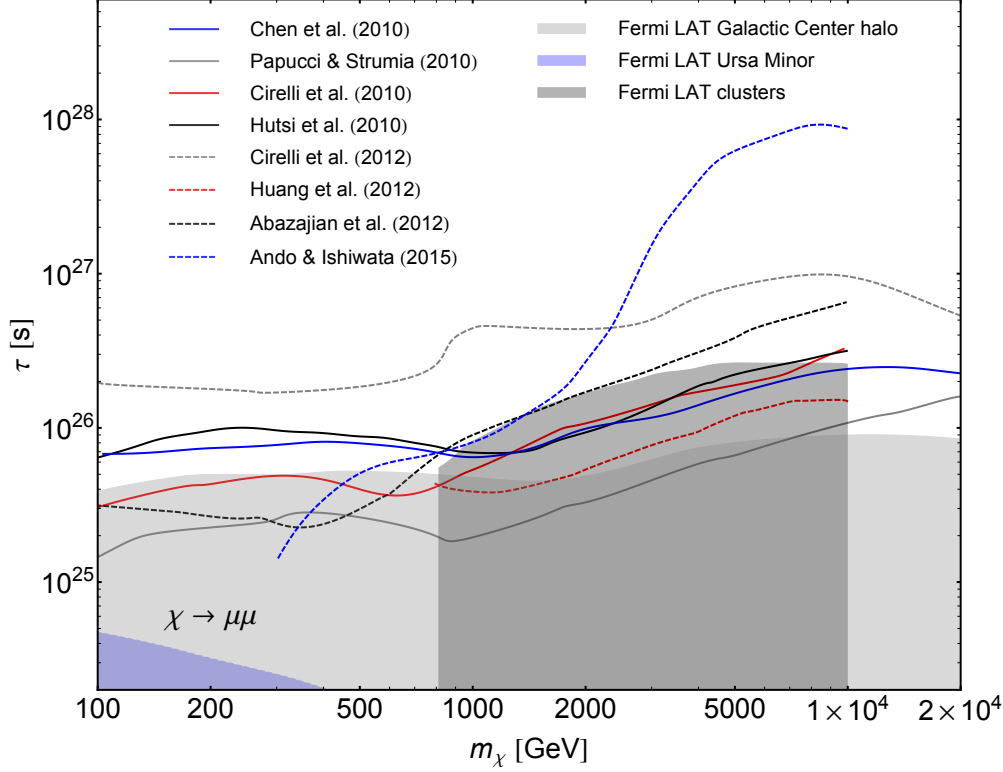


Figure 12: Lower limits obtained by considering the DGRB energy spectrum measured in Ref. [8]. Decays into $\mu^+\mu^-$ are assumed. The regions below the colored lines are excluded because the cumulative DM-induced emission would overproduce the DGRB. Different lines correspond to different assumptions for the properties of DM halos and different methods to compute the lower limits. The solid blue line is taken from Fig. 3 of Ref. [383], while the solid gray one is from Fig. 8 of Ref. [384] (NFW DM density profile). The solid red and solid black lines are taken from Fig. 4 of Ref. [385] and from Fig. 6 of Ref. [59] (NFW DM density profile), respectively. The dashed gray line is from Fig. 2 of Ref. [386] (DM signal and power-law background) and the dashed red one from Fig. 4 of Ref. [380]. The dashed black line is taken from Fig. 4 of Ref. [367]. The dashed blue line comes from Fig. 3 of Ref. [387] (for model A of the Galactic foreground). The blue region indicates the portion of the (m_χ, τ) plane already excluded by the observation of the Ursa Minor dwarf Spheroidal galaxy performed by the *Fermi* LAT (see Fig. 3 of Ref. [388], for the case of no IC emission). The dark gray region is excluded by the analysis performed in Ref. [380] combining *Fermi* LAT data from the position of 8 galaxy clusters (see their Fig. 4). Finally, the light gray region indicates the DM candidates not compatible with the observation of the so-called “Galactic Center halo” performed by the *Fermi* LAT in Ref. [389] (see their Fig. 5 for a NFW DM density profile).

The cosmological signal for a decaying DM candidate is written as follows:

$$\frac{d\phi}{dE_0 d\Omega} = \frac{c}{4\pi} \frac{\Omega_{\text{DM}} \rho_c}{\tau m_{\text{DM}}} \int dz \frac{e^{-\tau_{\text{EBL}}(E_0, z)}}{H(z)} \frac{dN}{dE} \Big|_{E=E_0(1+z)}. \quad (23)$$

There is no need of including the flux multiplier since the average emission depends on the total amount of DM, accounted for by Ω_{DM} . This eliminates any dependence on M_{min} or on the shape of $c_{\Delta}(M, z)$ and it translates into more robust predictions.²⁸

Many works have used the DGRB to derive constraints on the nature of decaying DM candidates. Refs. [390, 391, 392, 377, 378, 393, 394, 374] consider the DGRB measured by EGRET in Refs. [6, 7], while Refs. [386, 385, 383, 380, 59, 367, 387] rely on the DGRB measurements by the *Fermi* LAT. Results are summarized in Fig. 12, which collects lower limits on τ as a function of m_{χ} . The regions below the lines in Fig. 12 are excluded since the corresponding DM particle (for a specific decay channel) produces a gamma-ray emission which is not compatible with the DGRB data. The scatter among the different lines in the figure is due both to the different statistical techniques used to derive the limits and to the different modeling adopted for the DM-induced emission. It should be noted that all lines are obtained by assuming that the DM-induced emission is the only component of the DGRB. The only exceptions are the dashed gray line from Refs. [386] and the dashed blue one from Ref. [387], in which the authors also model the astrophysical component of the DGRB. Both the Galactic and cosmological signals are considered when deriving all lower limits in Fig. 12, but the ones given by the solid gray and dashed blue lines, which correspond to Ref. [384] and Ref. [387], respectively. In these two cases, limits refer to the cosmological DM component only. Other predictions for the contribution of decaying DM to the DGRB can be found in Refs. [395, 396, 62, 397].

The most constraining lower limit in Fig. 12 comes from Ref. [386] (dashed gray line) below ~ 2 TeV, and from Ref. [387] (dashed blue line) for larger DM masses. Decay lifetimes as large as 2×10^{26} s are excluded for DM masses below ~ 500 GeV, while the limit goes up to 10^{28} s for $m_{\chi} \sim 10$ TeV. Note that the results of Ref. [387] are obtained from the most recent *Fermi* LAT measurement of the DGRB reported in Ref. [9]. The authors also shows how the lower limit changes depending on the model employed to describe the diffuse Galactic foreground. Furthermore, the lower limit at large DM masses is found to vary by up to a factor of a few for different ways of parametrizing the astrophysical component of the DGRB and its uncertainty.

Compared to the limits derived from other DM targets, the dashed gray and dashed blue lines in Fig. 12 represent the most constraining information available on τ . In particular, in Fig. 12 we show the regions excluded by three different analyses performed with *Fermi* LAT data, namely the observation of *i*) the Segue 1 dwarf Spheroidal galaxy [388] (blue region), *ii*) 8 galaxy clusters [380] (in dark gray) and *iii*) the “Galactic Center halo” [389] (in light gray).

3. The angular power spectrum of anisotropies

In this section we move away from the study of the all-sky average of the DGRB, focusing on what can be learnt from its spatial fluctuations. Note that, following the

²⁸Even if one rewrites Eq. (23) in terms of the Halo Model formalism, the result of integrating the HMF times the number of gamma rays expected from a DM halo of mass M will be quite insensitive to the value adopted for M_{min} [62].

procedure outlined in Sec. 2.1 and used in Ref. [9], the DGRB should be isotropic by construction. Yet, the template fitting is not sensitive to moderate small-scale anisotropies in the emission.²⁹ A well-established strategy to quantify the amount of spatial fluctuations is the anisotropy APS. Traditionally employed for the study of the CMB [254], the technique consists in decomposing a 2-dimensional map $I(\mathbf{n})$ in spherical harmonics $Y_{\ell,m}(\mathbf{n})$: $I(\mathbf{n}) = \sum_{\ell,m} a_{\ell,m} Y_{\ell,m}(\mathbf{n})$. The APS C_ℓ is, then, computed as follows:

$$C_\ell = \frac{\sum_{|m| \leq \ell} |a_{\ell,m}|^2}{2\ell + 1}. \quad (24)$$

A measurement of the APS of the DGRB provides information on its composition that is complementary to the study of its intensity energy spectrum. In Sec. 3.1 we summarize the measurement of the DGRB anisotropies performed by the *Fermi* LAT in Ref. [66]. Then, in Sec. 3.2, we describe how such a measurement can be used to constrain the DGRB contributors.³⁰

3.1. The *Fermi* LAT measurement of gamma-ray anisotropies

The measurement performed by the *Fermi* LAT Collaboration in Ref. [66] is currently the only observational data available on the APS of the DGRB. 22 months of data are analyzed between 1 and 50 GeV, divided in 4 energy bins. Gamma rays are binned into a HEALPix map³¹ [402] with $N_{\text{side}} = 512$. The count maps are divided by the exposure of the instrument in order to obtain gamma-ray intensity maps. This is required in order to eliminate any spurious spatial fluctuations due to the non-uniform exposure of *Fermi* LAT.

Two definitions of the APS are used in Ref. [66]. The so-called *intensity* APS C_ℓ is obtained from Eq. (24), while the *fluctuation* APS C_ℓ^{fluct} comes from the decomposition of the *relative* fluctuations $I(\mathbf{n})/\langle I \rangle$, where $\langle I \rangle$ is the all-sky average intensity. The two definitions are related by $C_\ell^{\text{fluct}} = C_\ell / \langle I \rangle^2$. Note that the fluctuation APS is a dimensionless quantity, while C_ℓ inherits the units of the intensity map (squared).

Contrary to what is done in Ref. [9] (see Sec. 2.1), no template fitting is employed in Ref. [66] to isolate the DGRB. Nevertheless, a mask is applied, screening the regions in the sky where the emission is dominated by the diffuse Galactic foreground or by the resolved point sources. The mask covers the strip with $|b| < 30^\circ$ around the Galactic plane and a 2° -radius circle around each source in the 1FGL catalog. The contamination of the Galactic foreground is not completely removed by the use of the mask, but the residual Galactic emission only induces large-scale features that contribute to the APS at small multipoles. That is why only multipoles larger than 105 are considered in Ref. [66].

The mask may alter the shape and normalization of the APS. Following Ref. [403], the APS is corrected for the effect of the mask simply by dividing C_ℓ by the fraction of

²⁹Moreover, as we will see in Sec. 3.1, the measurement of the DGRB anisotropies performed in Ref. [66] does not rely on the template fitting used in Ref. [9].

³⁰Other observables have been used to quantify the anisotropies in the DGRB: Refs. [107, 398, 399] consider the 2-point correlation function in real space, while Ref. [400] relies on the nearest-neighbor statistics. Ref. [401] compares the number of “isolated” gamma-ray events with the “empty regions” in the sky. In this section, we focus only on the APS since it is the most commonly used technique.

³¹<http://healpix.jpl.nasa.gov/index.shtml>

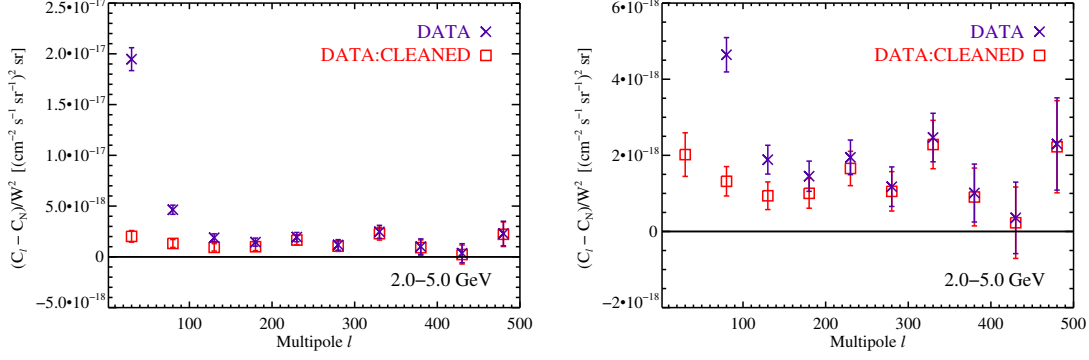


Figure 13: Intensity APS of the data before (purple crosses) and after (red boxes) the removal of the diffuse Galactic foreground. The signal region is defined between $\ell = 155$ and 504. The large increase in the intensity APS with no foreground subtraction (purple crosses) at $\ell < 155$ is likely attributable to contaminations from the Galactic foreground emission. The right panel is an expanded version of the left panel and it focuses on the high-multipole angular power. Taken from Ref. [66].

unmasked sky, f_{sky} . Therefore, the APS estimator considered in Ref. [66] is

$$C_\ell = \frac{C_\ell^{\text{raw}}/f_{\text{sky}} - C_N}{(W_\ell^{\text{beam}})^2}, \quad (25)$$

where C_ℓ^{raw} is the intensity APS computed directly from the masked intensity maps. C_N is the so-called *photon noise*, i.e. $C_N = \langle I \rangle^2 4\pi f_{\text{sky}}/N_\gamma$, where N_γ is the total number of events detected outside the mask. Finally, the factor W_ℓ^{beam} corrects for the smearing induced by the Point Spread Function (PSF) of the telescope (see Ref. [66] for a definition of W_ℓ^{beam}). The effect of the PSF becomes too extreme for angular scales beyond $\ell = 504$ so that, in Ref. [66], no data are considered for multipoles larger than $\ell = 504$.

Fig. 13 shows the APS for gamma rays between 1.99 and 5.0 GeV. The data points show the weighted average of the APS inside bins in multipoles with $\Delta\ell = 50$. The purple crosses correspond to the APS estimator C_ℓ of Eq. (25) derived from the intensity maps. On the other hand, the empty red boxes indicate the APS measured from the residual maps obtained after the subtraction of a model for the diffuse Galactic foreground. The error bars are computed following Ref. [404].³²

The measured APS is different from zero in the signal region, i.e. $155 \leq \ell \leq 504$. The (unbinned) APS is fitted with a power law $(\ell/155)^n$ in order to determine any dependence of the APS on ℓ . It is found that the $n = 0$ case is compatible with the best fit at 95% confidence level for all energy bins. This means that the measured APS is compatible with being Poissonian, i.e. independent of ℓ . The significance of the detection is 6.5 (7.2) between 1.04 and 1.99 GeV (between 1.99 and 5.0 GeV), while it decreases to 4.1 and 2.7 in the two remaining bins at higher energies.

The fluctuation APS of a population of sources depends on the energy only if their spatial clustering is itself energy-dependent or if they are characterized by significantly different energy spectra. On the other hand, their intensity APS scales with the energy as $\langle I \rangle^2$. When computing the APS of an emission that is the sum of different components

³²More recently, Ref. [405] presented an alternative method to estimate the error on C_ℓ , developed specifically for scenarios like the DGRB, where the emission is affected by limited statistics.

(as in the case of the DGRB), it may be interesting to study how the APS of the total emission C_ℓ^{total} depends on the spectra of the individual components C_ℓ^i . By construction, the intensity APS is an additive quantity:³³

$$C_\ell^{\text{total}} = \sum C_\ell^i, \quad (26)$$

while the fluctuation APS follows the following summation rule:

$$C_\ell^{\text{fluct, total}} = \sum f_i^2 C_\ell^{\text{fluct, } i} \quad (27)$$

where f_i is the fraction of the emission associated with the i -th contribution, with respect to the total, i.e. $f_i = \langle I_i \rangle / \langle I^{\text{total}} \rangle$.

Assuming that the components have an energy-independent $C_\ell^{\text{fluct, } i}$, any energy dependence in $C_\ell^{\text{fluct, total}}$ must arise from the f_i -factors in Eq. (27). Indeed, Ref. [359] proves that detecting an energy modulation in the fluctuation APS of the DGRB may indicate that the emission is the sum of more components (see also Refs. [407, 408]). In that case, the behavior of the *intensity* APS as a function of energy would follow the energy spectrum of the dominant component. Thus, studying if (and how) fluctuation and intensity APS depend on the energy may be crucial to unravel the composition of the DGRB.

Fig. 14 shows the Poissonian C_P measured in Ref. [66] in the 4 energy bins³⁴. The left panel proves that the fluctuation APS does not depend on the energy.³⁵ On the other hand, the right panel shows that C_P decreases with energy as $C_P \propto E^{-(4.79 \pm 0.13)}$. This result suggests that the *Fermi* LAT APS is produced by one single population of unclustered sources with an energy spectrum proportional to $\propto E^{-2.40}$. In the next section we will see that unresolved blazars fits this description.

After the publication of the *Fermi* LAT APS measurement, Ref. [409] pointed out that the *Fermi* LAT Collaboration used 22 months of data to measure the APS, but masked only the contribution of the point-like sources in the 1FGL (relative to an exposure of only 11 months). Thus, the emission considered in Ref. [66] will probably be contaminated by the contribution of sources that, being not bright enough to be included in the 1FGL, could have been detected in the larger dataset of Ref. [66].

3.2. Deducing the nature of the Diffuse Gamma-Ray Background from its anisotropies

We start this section by summarizing the technique used to estimate the APS of a generic class of sources. The discussion will, then, focus on the gamma-ray emitters considered in Secs. 2.2 and 2.3. We will finally show how the comparison of the model predictions to the APS signal detected by the *Fermi* LAT in Ref. [66] can be used to constrain the contribution of different populations to the DGRB.

As done at the beginning of Sec. 2.2, the formalism proposed here assumes that the sources are characterized by a generic parameter Y . However, Eq. (1) only determines

³³In Eqs. (26) and (27) we are neglecting, for simplicity, possible cross-correlation terms between different components. Under the hypothesis that gamma-ray sources trace the same LSS of the Universe, these cross-correlation terms can contribute significantly to the total APS C_ℓ^{total} and, thus, should be taken into account [52, 145, 339, 73, 406, 74].

³⁴Since, as commented before, the APS is compatible with being constant in multipole, the whole APS can be completely characterized by just one number, that we refer to as C_P .

³⁵However, the large error bars and the fact that only 4 energy bins are available do not allow to exclude large-scale modulations or very localized peaks.

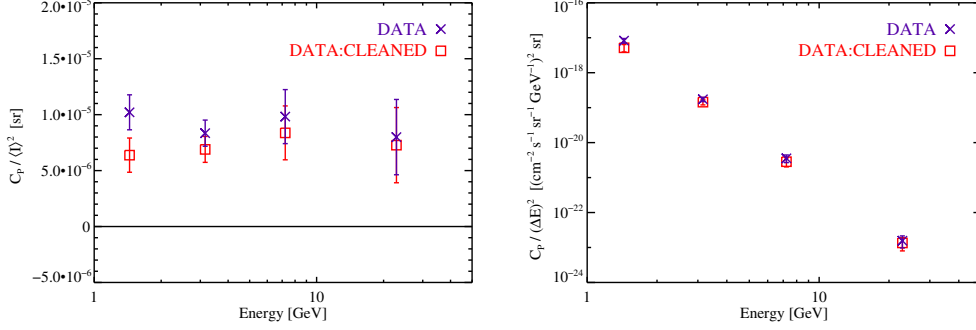


Figure 14: Anisotropy energy spectra of the data (purple crosses) and of the Galactic-foreground-cleaned data (red boxes). *Left*: Fluctuation anisotropy energy spectrum. *Right*: Differential intensity anisotropy energy spectrum. Taken from Ref. [66].

the all-sky average gamma-ray emission associated with population X , referred to here as $\langle I_X \rangle$ to underline that it is obtained by integrating over all the possible pointings in the sky. The emission $I_X(\mathbf{n})$ from direction \mathbf{n} can be written as follows [51, 107, 406]:

$$I_X(\mathbf{n}) = \int d\chi g_X(\chi, \mathbf{n}) W_X(\chi), \quad (28)$$

where $\chi = \chi(z)$ is the comoving distance relative to redshift z . $W_X(\chi)$ is the so-called *window function* and it gathers all the quantities that, in the definition of $I_X(\mathbf{n})$, do not depend on the direction of observation. In particular, $W_X(\chi)$ may depend on the energy at which I_X is computed. The factor $g_X(\chi, \mathbf{n})$ is called the “source field” and it describes how I_X changes from point to point in the sky. It encodes the dependence on the abundance and distribution of the sources. The averaged source field, $\langle g_X \rangle$, can be used to write $\langle I_X \rangle$ as $\int d\chi \langle g_X(\chi) \rangle W_X(\chi)$. The average source field depends only on the abundance of sources and it can be written as:³⁶

$$\langle g_X(\chi) \rangle = \int_{Y_{\min}}^{Y_{\max}} dY \frac{dN}{dV dY}(\chi, Y). \quad (29)$$

The $a_{\ell, m}^{\text{fluct}, X}$ coefficients of the fluctuation APS of population X can be computed decomposing the *relative* intensity fluctuations $I_X(\mathbf{n})/\langle I_X \rangle$ in spherical harmonics, as follows:

$$a_{\ell, m}^{\text{fluct}, X} = \frac{1}{\langle I_X \rangle} \int d\Omega_{\mathbf{n}} I_X(\mathbf{n}) Y_{\ell, m}^*(\mathbf{n}), \quad (30)$$

where $d\Omega_{\mathbf{n}}$ indicates the angular integration. Now, from Eq. (28)

$$\begin{aligned} a_{\ell, m}^{\text{fluct}, X} &= \frac{1}{\langle I_X \rangle} \int d\Omega_{\mathbf{n}} \int d\chi g_X(\chi, \mathbf{n}) W_X(\chi) Y_{\ell, m}^*(\mathbf{n}) \\ &= \frac{1}{\langle I_X \rangle} \int d\Omega_{\mathbf{n}} \int d\chi f_X(\chi, \mathbf{n}) \langle g_X(\chi) \rangle W_X(\chi), \end{aligned} \quad (31)$$

where $f_X(\chi, \mathbf{n}) = g_X(\chi, \mathbf{n})/\langle g_X \rangle$. The fluctuation APS is obtained from the average of

³⁶Compared to Eq. (1), we are neglecting the dependence on the spectral shape Γ .

$|a_{\ell,m}^{\text{fluct},X}|^2$ with the same multipole ℓ , see Eq. (24). It can be shown [51, 406] that it is equivalent to:

$$C_\ell^{\text{fluct},X} = \frac{1}{\langle I_X \rangle^2} \int \frac{d\chi}{\chi^2} \langle g_X(\chi) \rangle^2 W_X^2(\chi) P_X \left(k = \frac{\ell}{\chi}, \chi \right), \quad (32)$$

where $P_X(k, \chi)$ is the 3-dimensional power spectrum of the field $f_X(\chi, \mathbf{n})$:

$$\langle \tilde{f}_X(\chi, \mathbf{k}) \tilde{f}_X(\chi, \mathbf{k}') \rangle = (2\pi)^3 \delta^3(\mathbf{k} + \mathbf{k}') P_X(k, \chi), \quad (33)$$

and \tilde{f}_X indicates the Fourier transform of the field f_X . Eq. (32) makes use of the so-called Limber approximation [410, 411], valid for $\ell \gg 1$. This is indeed the regime of interest here since the *Fermi* LAT APS measurement is robust only for $\ell \geq 155$.

The hypothesis of working with a collection of unresolved sources allows the decomposition of the 3-dimensional power spectrum P_X into a 1-halo term and a 2-halo term, P_{1h} and P_{2h} , respectively. This helps in the interpretation of P_X and it allows to express it easily in the context of the Halo Model. The 1-halo term accounts for the correlation between two points located within the same source, while P_{2h} describes the correlation between points that reside in different objects and, thus, it depends on the spatial clustering of the sources. Within the Halo Model formalism, 1-halo and 2-halo terms can be written, respectively, as follows [51, 52, 406]:

$$P_{1h}(k, z) = \int_{Y_{\min}(z)}^{Y_{\max}(z)} dY \frac{dN}{dV dY}(Y, z) \left(\frac{\tilde{u}(k|Y, z)}{\langle g_X \rangle} \right)^2 \quad (34)$$

and

$$P_{2h}(k, z) = \left[\int_{Y_{\min}(z)}^{Y_{\max}(z)} dY \frac{dN}{dV dY}(Y, z) b_X(Y, z) \frac{\tilde{u}(k|Y, z)}{\langle g_X \rangle} \right]^2 P^{\text{lin}}(k, z). \quad (35)$$

The factor $\tilde{u}(k|Y, z)$ is the Fourier transform of the radial brightness profile of a source characterized by parameter Y at a distance z . Astrophysical sources are normally considered to be point-like, i.e. intrinsically smaller than the PSF of the telescope at any energy. This implies that \tilde{u} is proportional to the source gamma-ray flux S , without any dependence on k . In that case, the 1-halo power spectrum becomes Poissonian and it depends only on the abundance of sources. In fact, taking $Y = S$, Eq. (34) can be re-written as follows:

$$P_{1h}^{\text{Poissonian}} = \int_{S_{\min}(z)}^{S_{\max}(z)} dS \frac{dN}{dV dS}(S, z) \left(\frac{S}{\langle g_X \rangle} \right)^2. \quad (36)$$

On the other hand, the 2-halo term in Eq. (35) is obtained under the hypothesis that the fluctuations in the source distribution traces the fluctuations in the matter field, except for a bias factor $b_X(Y, z)$. That is the reason to include the linear power spectrum of matter fluctuations P^{lin} in Eq. (35). Thus, even for point-like sources, the 2-halo term inherits a dependence on k .

The balance between the 1-halo and 2-halo terms determines the shape of $P_X(k, \chi)$ and of C_ℓ through Eq. (32). For a population of point-like sources that are very bright but scarce in number, $P_{1h}^{\text{Poissonian}}$ usually dominates and it is difficult (if not impossible) to use the APS to extract information on their clustering. On the other hand, if the point-like emitters are very abundant, $P_{1h}^{\text{Poissonian}}$ is smaller, allowing for some sensitivity to the 2-halo term. On the other hand, if the sources appear extended, the 1-halo is no

longer Poissonian and it is suppressed above a certain scale associated with the typical size of the sources [51, 107, 406].

Following the formalism presented above, Refs. [52, 107] compute the APS of unresolved blazars. Blazars are characterized in Refs. [52, 107] by their gamma-ray luminosity ($Y \equiv L_\gamma$) which is assumed to correlate with the X-ray luminosity L_X , see Sec. 2.2.1. The free parameters in the model are fitted to reproduce the abundance of sources detected by EGRET. Ref. [107] finds that the APS of unresolved blazars is within reach of the *Fermi* LAT and that it is dominated by the Poissonian 1-halo term for multipoles larger than a few. Similar results are obtained in Ref. [52].

Ref. [67] revises the predictions for the APS of unresolved blazars by modeling the differential source count distribution dN/dS as done in Ref. [18]. Eq. (36) is used to derive the *intensity* APS from dN/dS :

$$C_P = \int_0^{S_{\text{thr}}} \frac{dN}{dS} S^2 dS, \quad (37)$$

where S_{thr} is the flux sensitivity threshold for point-like sources. dN/dS is assumed to be a broken power law, tuned to reproduce the measured abundance of blazars. Interestingly, the best-fit dN/dS corresponds to a model in which unresolved blazars exhibit an APS that is consistent with the value measured by the *Fermi* LAT in Ref. [66]. This suggests that blazars *alone* are able to explain the whole APS signal. The same best-fit model predicts that unresolved blazars can account only for $\sim 30\%$ of the DGRB intensity reported by the *Fermi* LAT in Ref. [8] between 1 and 10 GeV.

The authors of Ref. [68] employ a more detailed model of the blazar population, based on the correlation between L_γ and L_X and on a parametrization of their SED (see Ref. [19] and Sec. 2.2.1). They confirm the existence of a scenario in which blazars fit *at the same time* the *Fermi* LAT dN/dS and the measured APS. In this case, unresolved AGNs account for at most 4.3% of the DGRB intensity in Ref. [8] (in any energy bin). The constraints obtained in Refs. [67, 68] on the contribution of unresolved blazars to the DGRB intensity showcase how informative and complementary the study of gamma-ray anisotropies can be for the reconstruction of the composition of the DGRB.

The most recent estimate of the APS of blazars can be found in Ref. [63], where the authors consider three distinct AGN subclasses: *i*) FSRQs, *ii*) HSP BL Lacs and *iii*) a combination of LSP and ISP BL Lacs (see Sec. 2.2.1). Their Poissonian intensity APS is computed separately, according to Eq. (37). The dN/dS is taken from Ref. [22] for FSRQs and from Ref. [24] for the two classes of BL Lacs. They conclude that, as found previously, unresolved blazars can explain the whole APS signal, see Fig. 15. HSP BL Lacs are responsible for the largest fraction of the measured intensity APS: between 1 and 2 GeV, they account for $34.5^{+9.5}_{-9.4}\%$ of the total APS signal and the fraction increases to $105^{+49}_{-30}\%$ above 10 GeV.

Ref. [63] also provides the first estimate of APS associated to MAGNs. It is computed from Eq. (37), assuming that the 2-halo term can be neglected. The properties of MAGNs are inferred from a modeling of the sources at radio frequencies, via the $L_\gamma - L_{\text{r,core}}$ relation discussed in Sec. 2.2.2. Unresolved MAGNs are found to contribute to approximately 10% of the *Fermi* LAT APS (6.1% between 1 and 2 GeV and 16.7% above 10 GeV).

The APS of unresolved SFGs is computed in Ref. [145]. SFGs are described assuming that their luminosity is proportional to the product of their SFR and of gas mass. The model is tuned to reproduce the properties of the MW. A power law with an index of

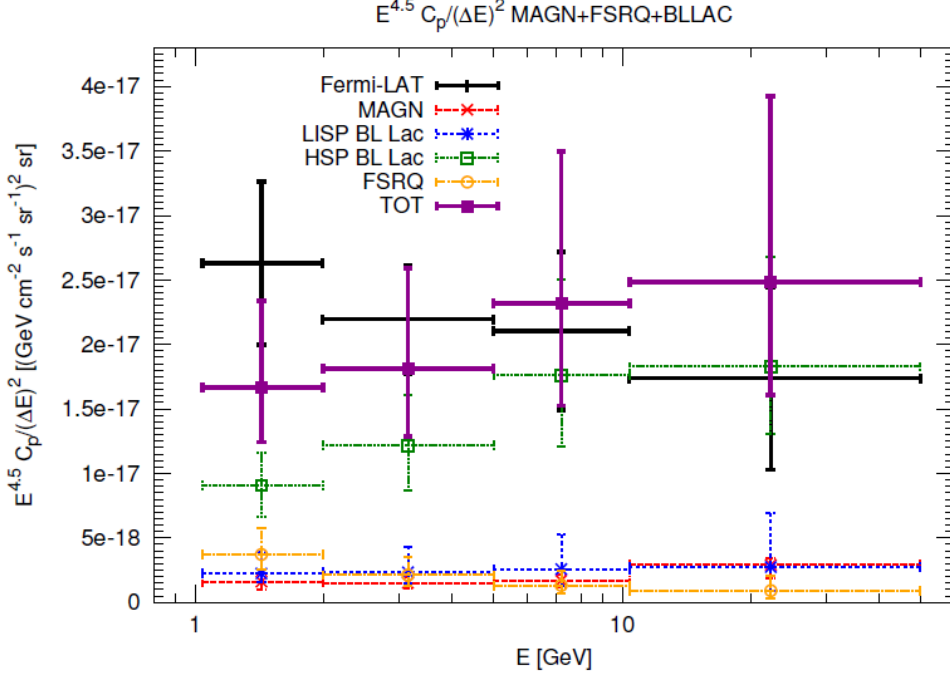


Figure 15: The angular power $C_P(E)$ in units of $E^{4.5} C_P (\Delta E)^{-2}$ for MAGNs (red long-dashed points), a class of sources combining BL Lacs LSPs and BL Lacs ISPs (blue short-dashed), HSP BL Lacs (green dotted), FSRQs (yellow dot-dashed) and the total (violet solid) of all radio-loud AGNs. The APS measurement by the *Fermi* LAT Collaboration is also shown (black solid points). Taken from Ref. [63].

2.7 is assumed in Ref. [145] as an universal energy spectrum (see Sec. 2.2.3). The APS is computed from Eqs. (34) and (35) assuming a bias factor of 1.11, independent of redshift and luminosity [412] (see also Ref. [399]). Contrary to the case of blazars or MAGNs, the APS of SFGs is not dominated by the Poissonian 1-halo term, at least below multipoles of few hundreds. As commented before, this is expected from a population of dim but very abundant sources. Thus, the signal may be used to constrain the clustering of SFGs. Unfortunately, the signal is overall too faint to contribute significantly to the APS detected by the *Fermi* LAT.

Refs. [37] and [38] performed Monte Carlo simulations of the APS signal expected from unresolved MSPs. Sources are modeled combining radio and gamma-ray data (see Sec. 2.2.4). The results of the two references differ from each other, due to the different models employed for the description of the MSPs: Ref. [38] assumes that the APS of MSPs is Poissonian and it finds that MSPs are responsible for no more than 1% of the APS measured by the *Fermi* LAT, while a larger fraction is allowed in the reference model considered by Ref. [37].

Among the other astrophysical components considered in Sec. 2.2.5, we mention that the clustering of Type Ia supernovae is considered in Ref. [413]: the authors find that unresolved supernovae can exhibit a moderately large APS but the emission peaks in the MeV energy range. Refs. [414, 209, 415, 202, 416, 107, 39] study the case of galaxy clusters. In particular, the model in Ref. [39] is tested against radio data and it proves that the intensity APS associated to galaxy clusters is expected to be two orders of magnitude lower than the APS measurement by the *Fermi* LAT.

Turning to the case of gamma-ray emission induced by DM, the study of its angular anisotropies has also been traditionally considered as a very powerful strategy to sin-

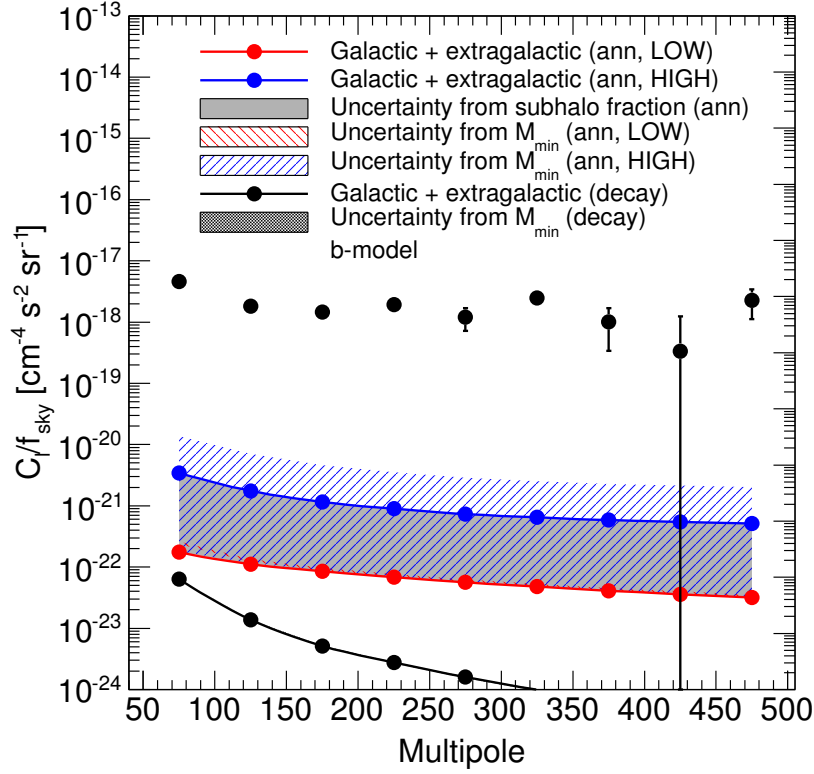


Figure 16: Total intensity APS of the gamma-ray emission from DM annihilation (color lines) or decay (black line) in extragalactic and galactic (sub)halos. The blue and red lines correspond to the LOW and HIGH subhalo boosts, respectively, so that the filled gray area between them corresponds to the uncertainty due to the subhalo boost, for a fixed value of M_{\min} . The red (blue) shaded area around the red (blue) solid line indicates the uncertainty in changing the value of M_{\min} from 10^{12} to $1 M_{\odot}/h$, for the LOW (HIGH) case. The red-shaded area is very thin and difficult to see. The solid black line shows the prediction for a decaying DM candidate. The observational data points with error bars refer to the measurement of the APS between 2 and 5 GeV as given in Ref. [66]. The predictions refer to a DM particle with a mass of 200 GeV, an annihilation cross section of $3 \times 10^{-26} \text{ cm}^3 \text{ s}^{-1}$ and annihilations entirely into b quarks (for annihilating DM) and to a mass of 2 TeV, a decay lifetime of $2 \times 10^{27} \text{ s}$ and decaying entirely into b quarks (for decaying DM). Taken from Ref. [62].

gle out the DM component of the DGRB [417]. Refs. [51, 52] adopt the Halo Model approach to determine the 1-halo and 2-halo terms from Eqs. (34) and (35), modeling the fluctuations in the gamma-ray emission produced by DM in extragalactic halos and subhalos. In Ref. [51] the authors neglect the contribution of subhalos, which is included in Ref. [52] assuming that the number of subhalos hosted by a halo with mass M scales with M . Their results suggest that, depending on the value of M_{\min} , the DM-induced *fluctuation* APS can be within reach of the *Fermi* LAT and that it can be larger than the APS expected for unresolved blazars.³⁷ Similar results are obtained also in Ref. [356], where only the 2-halo term is considered and modeled from N -body simulation data.

The analytic formalism of Refs. [51, 52] is extended to the case of Galactic DM in Ref. [54]. The DM halo of the MW is responsible only for large-scale anisotropies. On

³⁷The formalism was extended to include p -wave annihilations in Ref. [257].

the other hand, the emission induced by Galactic subhalos can exhibit an APS that is even larger than the one from extragalactic DM structures. Results are tested in Ref. [54] against different parametrizations of the Galactic subhalo population.³⁸

Galactic and extragalactic DM signals are considered at the same time in Ref. [339]. For multipoles larger than few tens, the APS of the extragalactic component is dominated by the 1-halo term, which depends mainly on the amount of subhalos. In the fiducial model of Ref. [339], their luminosity is described by a power-law extrapolation of the $c_{\Delta}(z, M)$ relation. As discussed in Sec. 2.3.1, this probably leads to an overestimation of the DM signal, which is, anyway, much smaller than the measured intensity APS. The latter can be used to derive upper limits on the annihilation cross section, excluding the region in the $(m_{\chi}, \langle\sigma v\rangle)$ plane associated with too large anisotropies.³⁹ The upper limits obtained in Ref. [339] exclude cross sections larger than $10^{-25}\text{cm}^3\text{s}^{-1}$ ($5 \times 10^{-24}\text{cm}^3\text{s}^{-1}$) for a DM mass of 10 GeV (1 TeV), see the solid red line in Fig. 17. Similar results are obtained in Ref. [75].

Refs. [53, 55, 359] follows an alternative approach for the study of the anisotropies induced by Galactic DM subhalos. Instead of computing the APS analytically like in Refs. [51, 52, 54, 356, 339], Refs. [53, 359] simulate sky-maps of the gamma-ray emission expected from mock realizations of DM subhalos in the MW. The APS is, then, computed by means of the HEALPix package (see also Ref. [419]). In Ref. [366] the results of Ref. [53] on the APS of Galactic subhalos are combined with the predictions in Ref. [356] for the anisotropies of extragalactic DM to determine the sensitivity of *Fermi* LAT to the detection of a DM component in the DGRB through its APS.

Similarly, Ref. [55] employs a *hybrid approach* (inspired by Ref. [274]) in which Galactic DM subhalos are simulated only inside a sphere of radius r_{max} centered on the observer. The value of r_{max} is related to the distance beyond which subhalos become point-like. It is assumed that subhalos located further than r_{max} cumulatively generate a smooth emission. This is equivalent to assume that APS generated by subhalos beyond r_{max} is dominated by the 2-halo term.

Semi-analytic hybrid methods are used also in Refs. [56, 62] to compute the anisotropies in the emission of extragalactic DM structures. In this case, the distribution and properties of extragalactic (sub)halos with a mass larger than the mass resolution of the Millennium-II N -body simulation [343] are taken directly from the halo catalogs of the simulation. Mock sky-maps are generated by replicating the Millennium-II simulation box until it covers the region within $z \sim 2$.⁴⁰ DM halos less massive than the resolution of Millennium-II are included assuming that they share the same clustering of those immediately above the mass resolution [56, 343]. Subhalos of extragalactic DM clumps are also accounted for considering multiple scenarios for their abundance and internal properties. Ref. [62] completes the prediction by modeling also the Galactic signal. The

³⁸Ref. [54] and the majority of the references mentioned in this section do not consider the effect of baryons on the clustering of DM and, thus, on its anisotropy pattern. One exception is Ref. [418], which computes the APS expected by the so-called DM “mini-spikes”, i.e. DM overdensities induced by the presence of Intermediate-Mass Black Holes. The authors find that this scenario can lead to a significant increase in the amplitude of the DM-induced APS.

³⁹We note that, in general, the intensity APS associated with DM scales quadratically on $\langle\sigma v\rangle$. The study of anisotropies is, therefore, quite sensitive to a DM signal. Whether the upper limits on $\langle\sigma v\rangle$ derived from the *Fermi* LAT APS are more constraining than those from the DGRB intensity energy spectrum, will depend on the amplitude of the intrinsic fluctuations in the DM-induced gamma-ray emission. See also Fig. 17.

⁴⁰Beyond this distance, at the energies considered, the gamma-ray flux is almost entirely attenuated by the interaction with the EBL.

all-sky DM maps produced in Ref. [62] represent complete and accurate templates of the total DM-induced gamma-ray emission.

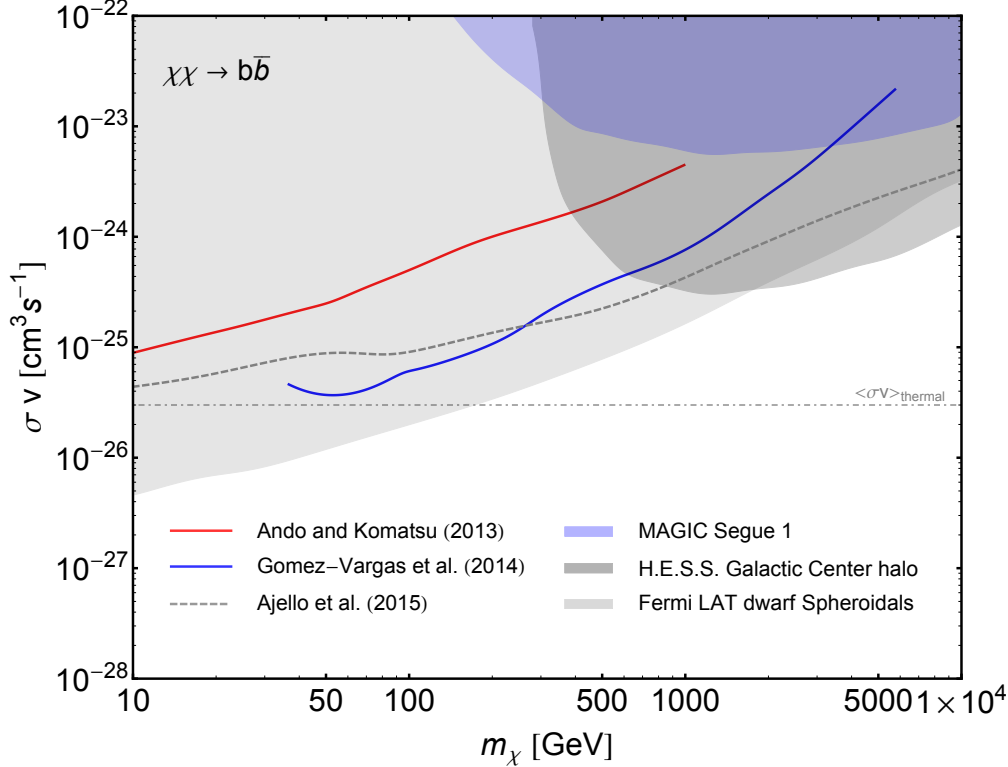


Figure 17: Upper limits obtained by considering the DGRB APS measured in Ref. [66]. The regions above the solid red and blue lines are excluded because the cumulative DM-induced emission would overproduce the APS of the DGRB. The solid red line is taken from Ref. [339] while the solid blue one is from Ref. [420]. The dashed gray line shows the upper limits on $\langle\sigma v\rangle$ obtained by requiring that the DM-induced emission does not overproduce the DGRB emission measured in Ref. [9]. The limit is obtained in Ref. [25] by modeling the astrophysical DGRB contributors. The blue region indicates the region already excluded by the observation of the Segue 1 dwarf Spheroidal galaxy performed by the MAGIC telescope [368]. The dark gray region is excluded by the analysis performed by the H.E.S.S. telescope in Ref. [369] on the so-called “Galactic Center halo” region (assuming an Einasto DM density profile). The light gray region indicates the DM candidates not compatible with the combined analysis of *Fermi* LAT data from 15 dwarf Spheroidal galaxies [370]. The dash-dotted line marks the thermal annihilation cross section.

As in Sec. 2.3.1, the main sources of uncertainties in the DM-induced APS are the value of M_{\min} and the subhalo boost factor. Extreme scenarios are identified in Ref. [62] for both M_{\min} and the subhalo boost factor, bracketing their theoretical uncertainties. The effect of their variability on the intensity APS sums up to approximately two orders of magnitude, as it can be seen in Fig. 16. The red and blue lines show the intensity APS for two different prescriptions of the subhalo boost, labeled “LOW” and “HIGH”. The blue line is obtained following the prescription of Ref. [276], which employs power-law extrapolations for low-mass halos. On the contrary, the red line makes use of the model by Ref. [327], extended in Ref. [329]. The blue-shaded region shows the effect of changing M_{\min} on the HIGH scenario.⁴¹ The black data points indicate the *Fermi* LAT

⁴¹Changing M_{\min} has no effect on the red line (LOW case), see Ref. [62] for details.

APS measurement between 2 and 5 GeV. As in Ref. [339], the DM-induced emission is found to contribute only marginally to the measured APS.

In Ref. [420] the predictions of the HIGH case (blue line) are, then, used to derive upper limits on the DM annihilation cross section, shown as a solid blue line in Fig. 17. The upper limit reaches values as low as $3 \times 10^{-26} \text{cm}^3 \text{s}^{-1}$ for $m_\chi = 50 \text{ GeV}$, while going to $10^{-23} \text{cm}^3 \text{s}^{-1}$ if the mass approaches the TeV scale. Fig. 17 also summarizes other constraints on $\langle \sigma v \rangle$ available in the literature. In particular, we plot the limit from the analysis of Ref. [25] of the DGRB intensity energy spectrum (dashed gray lines). The shaded regions indicate the areas already excluded by other indirect searches of DM, i.e. the observation of Segue 1 with MAGIC (blue), of the Galactic Center halo region with H.E.S.S. (dark gray) and the *Fermi* LAT combined analysis of dwarf Spheroidals (light gray). Fig. 17 proves that the study of the anisotropies of the DGRB can produce competitive upper limits on $\langle \sigma v \rangle$, but probably not as strong as those induced by the DGRB energy spectrum.

Ref. [62] also estimates the APS associated with a decaying DM candidate. In this case, as found also by Ref. [57], the predictions are subject to less theoretical uncertainties than for an annihilating DM candidate. In fact, the signal is less affected by the value of M_{min} and there is no subhalo boost (see also Sec. 2.3.2). Yet, in decaying DM scenarios, DM halos yield a more extended emission. This is particularly true for Galactic subhalos which are still close enough not to be point-like. Thus, the APS is expected to decrease rapidly at high multipoles being, therefore, hard to detect. See, e.g., the black line in Fig. 16.

4. The photon count distribution

Another powerful statistic tool to constrain the nature of the DGRB is provided by the photon count Probability Distribution Function (PDF). This technique can be used when the emission is represented by a pixelated sky-map. The photon count PDF is, then, built from the number of pixels n_k in which k photons are detected. The study of the photon count PDF is commonly used in radio and X-ray astronomy for the analysis of diffuse emissions, in particular when trying to estimate the contribution of faint unresolved sources. It can also be used at gamma-ray frequencies to single out different components in the DGRB, even if they are subdominant. Indeed, different PDFs are expected for different populations of gamma-ray emitters: bright but rare sources generate pixels with a large (or moderately large) number of photons, i.e. n_k will be significantly different from zero even at large k . On the other hand, a population of faint but numerous sources is normally associated with a Poissonian PDF. Intrinsically diffuse emissions also correspond to Poissonian PDFs.

Ref. [69] measures the PDF directly from 11 months of *Fermi* LAT data between 1 and 300 GeV. The data are binned into a HEALPix map with $N_{\text{side}} = 32$, corresponding to a binsize of approximately 0.4° . A region of 30° around the Galactic plane is masked, while point sources are not masked. The observed PDF is represented as red data points in Fig. 18. A model based on the so-called *generating functions* is developed to interpret the data. If p_k is the probability of finding k photons in a certain pixel (i.e. $p_k = n_k / N_{\text{pixels}}$, where N_{pixels} is the total number of pixels considered in the analysis), the corresponding generating function $P(t)$ is defined as

$$P(t) = \sum_{k=0}^{\infty} p_k t^k. \quad (38)$$

Viceversa, the probabilities p_k can be derived from $P(t)$ as the coefficients in front of each term in the power-law expansion of $P(t)$. The generating function of an emission composed by multiple components is the product of the generating functions of the single components [421]. In particular, the model considered in Ref. [69] consists of 3 terms:

- point sources, both resolved and unresolved. The corresponding generating function is $P(t) = \exp[\sum_{m=1}^{\infty} (x_m t^m - x_m)]$, where x_m is the average number of sources emitting exactly m photons in a pixel. The set of $\{x_m\}$ can be derived from the differential source count distribution dN/dS . In Ref. [69], dN/dS is taken to be a broken power law [18], leaving its 4 parameters free.
- the diffuse Galactic foreground, whose emission, in each pixel, is interpreted as a collection of sources that emit exactly 1 photon. The number of those sources is proportional to the intensity of the foreground in that pixel. Its generating function $P(t, i)$ depends on the particular pixel i considered and it can be written as $P(t, i) = \exp(x_{\text{diff}}^i t - x_{\text{diff}}^i)$, where x_{diff}^i is the number of photons of foreground emission in the i -th pixel. In Ref. [69], the intensity and morphology of the foreground are derived from the *Fermi* LAT data itself.
- an isotropic component, included to represent the emission associated to faint abundant sources. As for the Galactic foreground, this term is modeled as a collection of x_{iso} sources emitting exactly 1 photon and its generating function is $P(t) = \exp(x_{\text{iso}} t - x_{\text{iso}})$, for all the pixels. The quantity x_{iso} is left free in the fit.

The model is fitted to the photon count PDF in Fig. 18 in order to determine the free parameters, i.e. those characterizing dN/dS and the normalization of the isotropic component. The best-fit dN/dS is compatible with what found in Ref. [18]. The analysis of the PDF is different and complementary to Ref. [18] but it succeeds in reconstructing the properties of a population of non-Poissonian blazar-like sources. By integrating the best-fit dN/dS obtained in Ref. [69] below the sensitivity of the *Fermi* LAT, unresolved blazars are found to account for $\sim 23\%$ of the DGRB reported in Ref. [8] above 1 GeV. We remark that this result is consistent with the independent estimation obtained in Ref. [18]. Similar results are also obtained in Ref. [364] using 5 years of simulated *Fermi* LAT data and a pixel size of 0.25° .

Predictions for the PDF are available not only for blazars: Ref. [36] computed the PDF expected from unresolved MSPs finding that their PDF is highly non-Poissonian.

In the case of DM-induced emission, the shape of the PDF is expected to depend on which DM structures are considered. Ref. [422] computes the probability $P(F)$ of detecting a certain flux F due to Galactic DM subhalos in a generic pixel. The probability depends on the modeling of the subhalo population and, in particular, on the value of M_{min} . It can be written as follows (see the Appendix of Ref. [422] for a detailed derivation):

$$P(F) = \mathcal{F}^{-1}\{\exp[\mu(\mathcal{F}\{P_1(F)\} - 1)]\}, \quad (39)$$

where $\mathcal{F}\{f(x)\}$ indicates the Fourier transform of $f(x)$ and \mathcal{F}^{-1} its inverse. The quantity μ is the average number of sources expected inside one pixel and $P_1(F)$ is the probability of having exactly one source emitting the flux F . The DGRB model in Ref. [422] also includes a background component with a Poissonian PDF. The authors prove that there exists a region in their parameter space in which Galactic DM subhalos are faint enough to escape detection as individual sources after 5 years of *Fermi* LAT data, but bright enough to be detected by studying the photon count PDF.

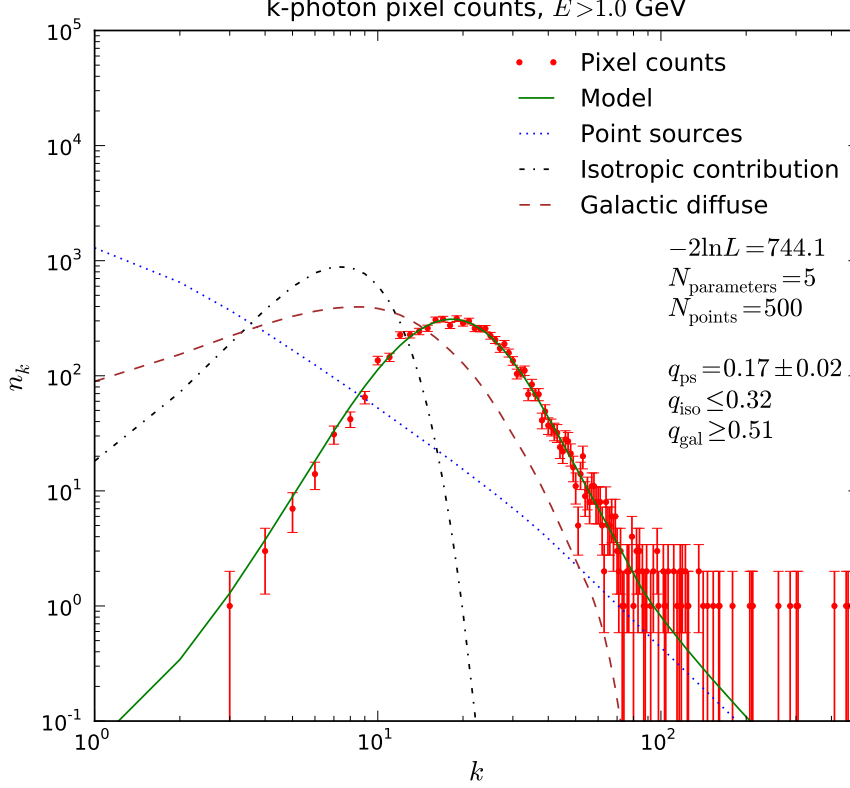


Figure 18: n_k is the number of pixels with k photons. The red dots correspond to the pixel counts derived from the data of the *Fermi* LAT, the error bars are equal to $\sqrt{n_k}$. The model devised to interpret the data considers three classes of sources: *i*) AGN-like point-like objects (blue dotted line), *ii*) isotropic Poisson contribution (brown dashed line) and *iii*) anisotropic Galactic diffuse emission (black dash-dotted line). Note that the photon count PDF for the total (solid black line) on this plot is not the sum of the components, but the corresponding generating function of the PDF is the product of the generating functions of the three contributions. $N_{\text{parameters}}$ is the number of parameters used in the fit. q_{ps} , q_{iso} and q_{gal} are the relative contributions of the point sources, of the isotropic and of the Galactic foreground, respectively. N_{points} is the number of points in the x -axis employed in the fit and the log-likelihood of the best-fit is indicated in the legend. Taken from Ref. [69].

Ref. [423] also studies the possibility of separating the emission associated with Galactic DM subhalos from the diffuse Galactic foreground and from an isotropic background (both characterized by a Poissonian PDF). The authors choose some benchmark models for the description of the DM-induced emission and of the Poissonian backgrounds. After building the PDFs of the different components, they use them to generate mock sky-maps of the expected gamma-ray emission. This mimics a real observation and it allows to estimate the sensitivity of a PDF analysis to the DM signal. The mock photon count PDF is compared to model predictions in order to determine the free parameters in the model, as done in Ref. [69]. This relies on a *a priori* knowledge of the shape of the PDF for the different components in the model. Ref. [423] proves that, in an idealized case without background, the reconstructed intensity of the DM-induced emission depends significantly on the assumed shape of the PDF. Employing the wrong PDF would lead to biased reconstruction of the intensity of the DM component. However, when the Poissonian backgrounds are included, Ref. [423] finds that an unbiased reconstruction

(within statistical uncertainties) can be obtained independently of the shape of the PDF.

Ref. [424] considered the gamma-ray emission of extragalactic DM halos and subhalos, instead. The authors derive $P_1(F)$ analytically, relying on the halo model, and they show how its shape changes when using three different prescriptions for the subhalo boost. Then, they compute $P(F)$ by means of the central limit theorem below a reference flux F_\star , and through MC simulations above that. The resulting flux distribution $P(E)$ exhibits two regimes: below $5 \times 10^{-12} \text{cm}^{-2} \text{s}^{-1} \text{GeV}^{-1} \text{sr}^{-1}$ it follows a Gaussian distribution, while it is a power law for larger fluxes.⁴² The latter is the case when a few bright DM structures dominate the flux distribution. Ref. [424] also developed a model for the $P(F)$ of the astrophysical components of the DGRB: for a fiducial subhalo boost model inspired by Ref. [280], the authors of Ref. [424] show that a measurement of $\{p_k\}$ after 5 years of *Fermi* LAT data can lead to a detection of a DM signal, provided that the annihilation cross section is, at least, twice the thermal value, for a DM mass of 85 GeV and annihilations into b quarks.

5. The cross-correlation with independent probes

The most recent development in our understanding of the composition of the DGRB has focused on the study of its cross-correlation with other observables. For instance, the fraction of the DGRB that originates from extragalactic objects (whether astrophysical sources or DM halos) traces the LSS of the Universe, up to a maximal redshift that depends on the EBL attenuation. Thus, a certain level of cross-correlation is expected with any LSS tracer, e.g. the distribution of resolved galaxies [399, 73, 74, 70] or the gravitational lensing effect of cosmic shear [72, 71, 75]. These are new and independent observables that can complement the information inferred from the DGRB energy spectrum (see Sec. 2) or from its auto-correlation APS (see Sec. 3). Also, note that the gamma-ray sky-maps analyzed in Ref. [66] to measure the auto-correlation APS are noise dominated. Thus, even if it was still possible to report a significant auto-correlation signal by subtracting the photon noise, one may expect the cross-correlation with other signal-dominated quantities to be, in principle, very informative.

In the following sections, we present the formalism proposed to predict the cross-correlation of the DGRB with LSS tracers. We also summarize the data currently available. Sec. 5.1 focuses on the cross-correlation with galaxy catalogs, while in Sec. 5.2 we discuss the case of the cosmic shear. Sec. 5.3 presents the results of the cross-correlation of the DGRB with other observables.

5.1. The cross-correlation with galaxy catalogs

Ref. [399] was the first work that measured the 2-point correlation function of the *Fermi* LAT DGRB with 4 galaxy surveys, namely: *i*) the Sloan Digital Sky Survey (SDSS) Data Release 6 of optically-selected quasars from Ref. [425], *ii*) the IR galaxies of the 2 Micron All-Sky Survey (2MASS) Extended Source Catalog from Ref. [426], *iii*) the radio sources from the NRAO VLA Sky Survey (NVSS) [427] and *iv*) the luminous red galaxies in SDSS Data Release 8 from Ref. [428]. The authors of Ref. [399] analyzed 21 months of *Fermi* LAT data but no significant cross-correlation was observed. More recently, Ref. [70] have updated the analysis using 60 months of data and exploring also the cross-correlation with the main galaxy sample of SDSS Data Release 8 from Ref. [429]. The region with $|b| < 30^\circ$ around the Galactic plane was masked out, as well

⁴²The gamma-ray flux is computed at 1 GeV.

as the 1-degree region around the point sources in the 3FGL catalog. Both the Large and Small Magellanic Clouds were also left out of the analysis, together with the Fermi Bubbles and of the so-called Loop-I. A model for the diffuse Galactic foreground was subtracted from the sky maps. The residuals of the gamma-ray maps and the distribution of galaxies in the catalogs were re-binned into HEALPix maps with $N_{\text{side}} = 512$.

The authors computed both the cross-correlation APS and the 2-point correlation functions⁴³ using the PolSpice package⁴⁴. The signal region was defined between 0.1 and 100 degrees for the 2-point correlation function and between multipoles of 10 and 1000 for the cross-correlation APS. Three different energy thresholds were considered for the gamma rays, including all events above *i*) 500 MeV, *ii*) 1 GeV or *iii*) 10 GeV. The authors in Ref. [70] also validated their results against changes in the mask and in the model adopted for the diffuse Galactic foreground. They also tested their analysis pipeline on a simulated sky map with no signal.

The 2-point correlation functions are shown in Fig. 19 for the 5 different catalogs: a cross-correlation signal is evident up to few degrees for all the catalogs apart from the SDSS luminous red galaxies (rightmost central panel). The significance of these detections is 4.5σ for the SDSS quasars, 3.6σ for the 2MASS catalog, 3σ for the SDSS main galaxies and as large as 10σ in the case of NVSS. These numbers refer to the energy threshold that maximizes the detection significance, i.e. 500 MeV for the case of the SDSS quasars and 1 GeV otherwise. These are also the thresholds considered in the different panels of Fig. 19. The case of the cross-correlation with NVSS deserves some additional comments: the authors of Ref. [70] noticed that, for that catalog, the cross-correlation signal exhibits an angular extension that is consistent with the PSF of *Fermi* LAT. In particular, it decreases as the energy threshold increases. This suggests a different origin for the NVSS signal with respect to the one observed with the other catalogs. They also noted that a 1-halo component to the signal (see Sec. 3.2) would manifest itself as a Dirac delta at $\theta = 0$ degrees, smeared up to the angular size of the *Fermi* LAT PSF. Such a 1-halo term would be present, for example, if some of the galaxies in NVSS emitted also in the gamma-ray band as well. Indeed, NVSS galaxies are standard candidates to be gamma-ray emitters and this catalog is routinely searched for counterparts of gamma-ray sources [115, 2]. With all these considerations in mind, the authors of Ref. [70] concluded that the 2-point correlation function with NVSS is probably contaminated by a 1-halo term and it does trace the LSS.

In Ref. [70], the measured correlation functions are compared with the predictions obtained if the DGRB were contributed *entirely* by only one class of astrophysical sources. These theoretical predictions are included in Fig. 19 as colored lines. In particular, the dashed red line stands for FSRQs, modeled as in the luminosity-dependent density evolution scheme of Ref. [22], while the solid black is for BL Lacs, following the results of Ref. [23], see Sec. 2.2.1. The dot-dashed lines denote the case of SFGs, considering two different models: *i*) the gamma-ray emission of SFGs is assumed to follow the cosmic SFR, as in Ref. [31], and *ii*) the gamma-ray luminosity is related to the IR one through the $L_\gamma - L_{\text{IR}}$ relation obtained in Ref. [33] (see Sec. 2.2.3). The two scenarios are represented by the blue and green dot-dashed lines, respectively. Finally, we note that MAGNs are not included in the analysis of Ref. [70] as their emission is showed to be very similar (and, therefore, degenerate) with the contribution of SFGs. MAGNs,

⁴³We note that the two are related by a Fourier transform and they contain the same information. However, they probe different scales with different efficiency and, thus, it is interesting to consider both.

⁴⁴<http://www2.iap.fr/users/hivon/software/PolSpice/>

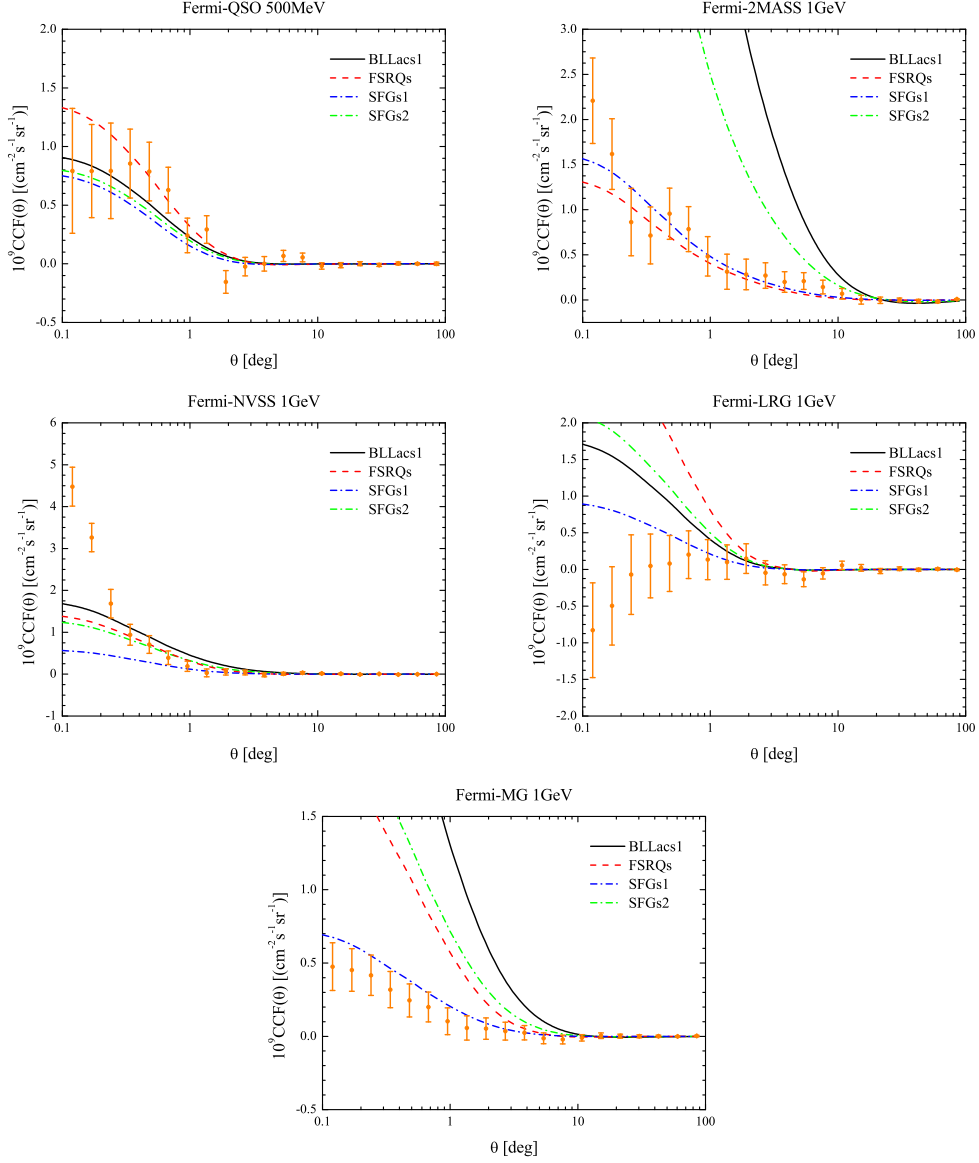


Figure 19: *Upper left*: 2-point cross-correlation function (orange data points) estimated from the SDSS Data Release 6 optically-selected quasars and the DGRB obtained from 60 months of *Fermi* LAT data at $|b| > 30^\circ$ and for $E > 500$ MeV. Errors bars represent the diagonal elements of the covariance matrix. Model predictions for different classes of sources are represented by continuous curves: FSRQs (red dashed), BL Lacs (black solid), two models of SFGs (blue and green dot-dashed). All predictions are obtained assuming that each source class contributes 100% of the DGRB intensity and they do not represent fits to the data. *Upper right*: same as in the previous panel but for the cross-correlation with the 2MASS Source Extended Catalog and for energies ≥ 1 GeV. The other panels show the same as in the previous panel but for the NVSS catalog (medium left), luminous red galaxies in the SDSS Data Release 8 (medium right) and the main galaxy sample in the SDSS Data Release 8 (bottom). Note the different scale in the plots. Taken from Ref. [70].

however, are explicitly included in the follow-up analysis of Ref. [430].

The 2-point correlation functions are, then, computed assuming that the fluctuations in the gamma-ray maps and in the galaxy distributions from the catalogs both trace the LSS matter density fluctuations (provide that the so-called *bias factor* is considered). This allows for the correlation functions to be determined in terms of the non-linear power spectrum of matter fluctuations, which can be obtained, e.g., by means of the public CAMB code [431] or Halofit routine [432].

We note that the cross-correlation expected from the classes of astrophysical sources mentioned above (colored lines in Fig. 19) is indeed different from zero at small angles, as in the observed signal. Whether the amplitude of the predicted correlation functions is in agreement with the data or not depends on the redshift overlap between the gamma-ray emitters and the sources in the catalogs. In particular, optically-selected quasars and sources in the NVSS catalog have a quite broad redshift distribution, extending to $z \sim 3-4$. Thus, a large cross-correlation is expected with the emission from unresolved SFGs (modeled as in Ref. [31]), whose redshift distribution peaks at $z \sim 2-3$. On the other hand, the luminous red galaxies and the objects in the 2MASS catalog probe the local Universe (respectively, from $z \sim 0.8$ and $z \sim 0.3$, and down to the present time) and they are characterized by narrower redshift distributions. Both are expected to correlate mainly with BL Lacs. Indeed, by considering several galaxy catalogs with different redshift distributions, one can effectively probe different redshift ranges, developing a full tomographic approach. Specifically, in Ref. [70], the authors build a model of the DGRB that includes FSRQs, BL Lacs and SFGs, leaving the normalization of the different components free to vary when fitting the cross-correlation data in Fig. 19. Ref. [70] shows that including the cross-correlation with SDSS quasars is crucial in deriving a lower bound on the contribution of SFGs.⁴⁵ These are, indeed, found to be the dominant component in the DGRB, with blazars accounting for, at most 10% of the total DGRB measured by *Fermi* LAT in Ref. [9] (at 1σ level). Also, depending on which description is assumed for the SFGs, the best-fit model to the cross-correlation data in Fig. 19 can account for only 70% or 20% of the total DGRB intensity.

The cross-correlation with galaxy catalogs can also be used to constrain the DM component of the DGRB. This possibility was studied in Refs. [73, 74], where the authors considered the 2MASS Redshift Survey [433] and the 2MASS Extended Source Catalog from Ref. [426]. These two catalogs are chosen against others because they trace the matter distribution in the local Universe and, therefore, they are expected to correlate with any potential DM-induced gamma-ray signal. The 2MASS Redshift Survey extends to $z \sim 0.1$, while the 2MASS Extended Source Catalog peaks at $z = 0.072$ and does not contain galaxies beyond $z \sim 0.4$. The *Fermi* LAT has detected most of the blazars in this volume, down to a very low sensitivity. Thus, unresolved blazars are not expected to exhibit a large cross-correlation with catalogs of the local Universe.⁴⁶ This means that the cross-correlation APS will be potentially very sensitive to other DGRB contributors, emitting mainly at low redshift as, e.g., SFGs or DM.

In Refs. [73, 74], galaxies are described by means of the so-called Occupation Distribution (HOD) model. This framework postulates that each source is embedded into a DM halo of mass M and that the abundance and distribution of galaxies are related to the properties of the host DM halos. The HOD model is a phenomenological formalism,

⁴⁵Note that this lower bound is found only if SFGs are modeled according to Ref. [31].

⁴⁶In other words, the window function of unresolved blazars does not overlap significantly with that of the 2MASS catalogs considered above.

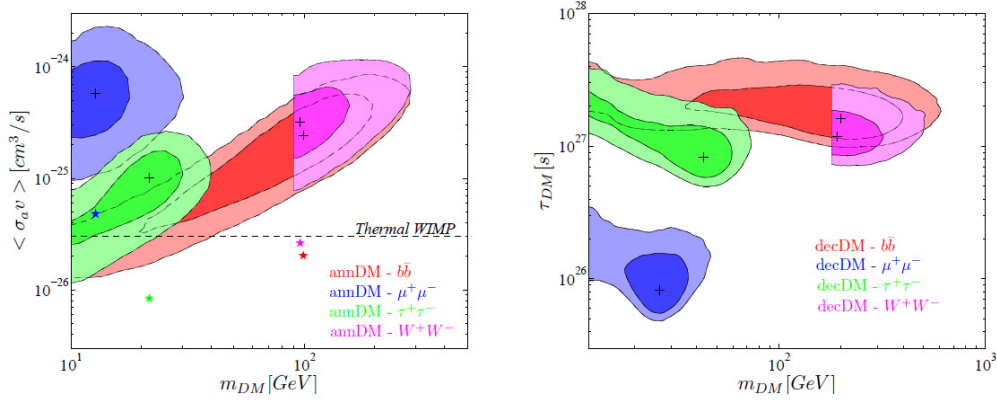


Figure 20: *Left:* 1σ and 2σ allowed regions for the DM annihilation rate versus DM mass, for different gamma-ray production channels and assuming the “LOW” substructure scheme in Ref. [62]. Crosses indicate the best-fit models. In the “HIGH” scenario of Ref. [62], regions remain similar in shape but they shift downward by a factor of ~ 12 (star symbols). *Right:* The same but for decaying DM, showing the DM particle lifetime as a function of its mass. Taken from Ref. [436].

based on results from N -body simulations and on semi-analytical descriptions of DM halos and galaxy formation [434, 201, 435]. Under this formalism, Ref. [73] shows that DM dominates the cross-correlation with the 2MASS Redshift Survey and that 5 years of *Fermi* LAT data should be able to distinguish a DM scenario from one with purely a astrophysical sources. Ref. [74] also computes the upper limit that it would be possible to derive on $\langle \sigma v \rangle$ if the cross-correlation were found compatible with an astrophysical interpretation. These results, however, largely depend on the model adopted for low-mass DM halos and subhalos. In the most optimistic scenario, the cross-correlation will be able to exclude thermal cross sections for DM masses up to almost 1 TeV.

These predictions were tested against actual data in Ref. [436], where the authors explained the measured cross-correlation signal with the 2MASS Extended Source Catalog in Ref. [70] in terms of DM. They found that a WIMP DM particle with a mass in the range between 10 and 100 GeV (depending on the annihilation channel) and a thermal cross section can reproduce both the shape and intensity of the measured cross correlation. This is also the case for decaying DM candidates, for a similar range in DM mass and a decay lifetime between 5×10^{25} and 5×10^{27} s. The colored contours in Fig. 20 show the the regions in the $(m_\chi, \langle \sigma v \rangle)$ and (m_χ, τ) parameter spaces that are compatible with the cross-correlation found with 2MASS. The figure also shows how, for an annihilating DM candidate, a different assumption for the subhalo boost can shift the preferred contours by more than one order of magnitude.

In addition, Ref. [436] used the measured cross-correlation to derive upper limits on $\langle \sigma v \rangle$, by requiring that the DM-induced correlation function do not to over-produce the data. This allowed Ref. [436] to exclude thermal annihilation cross sections for DM masses below 100 GeV (in the case of annihilations into b quarks and a “LOW” subhalo boost model inspired by Ref. [62]). This makes the cross-correlation with *local* galaxy catalogs the strongest observable up to date to constrain a potential DM contribution to the DGRB, compared to the DGRB energy spectrum reported in Ref. [9] or the auto-correlation APS in Ref. [66].

Astrophysical and DM-induced emissions are considered at the same time in Ref. [430]: the authors define a model of the DGRB that includes FSRQs, BL Lacs, SFGs, MAGNs

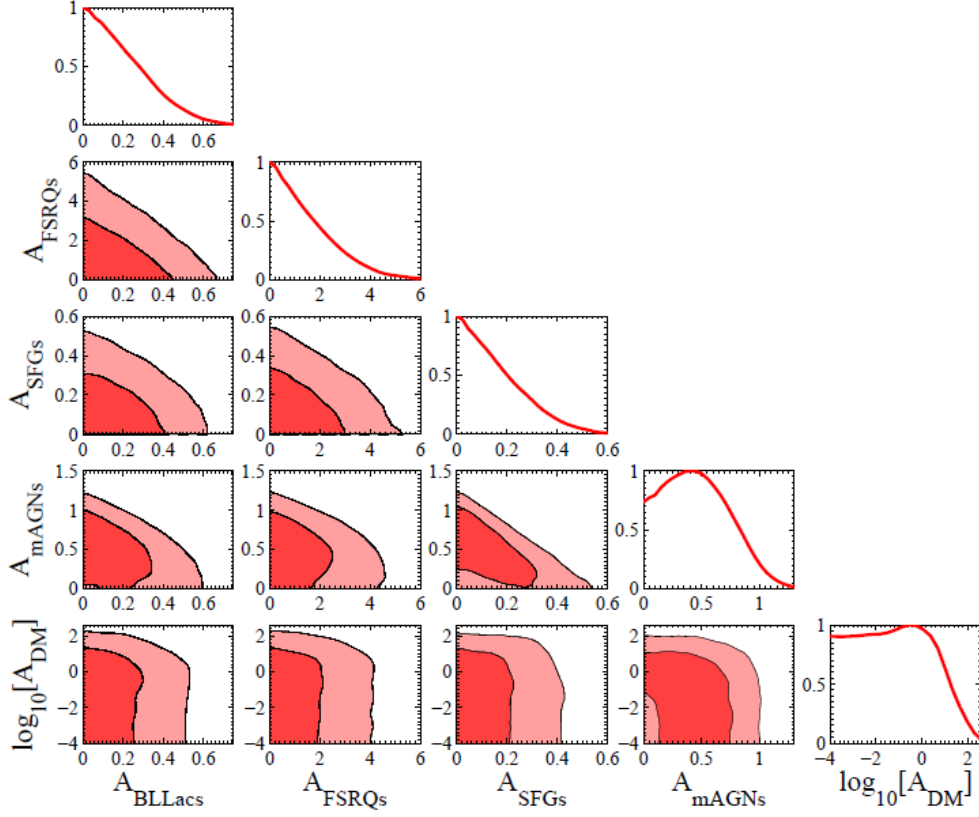


Figure 21: Posterior probability distributions for the normalization of the component to the DGRB due to FSRQs (A_{FSRQs}), BL Lacs (A_{BLLacs}), SFGs (A_{SFGs}), MAGNs (A_{mAGNs}) and annihilating DM (A_{rmDM}). These parameters are defined with respect to a fiducial model introduced in Ref. [430]. Panels along the diagonal show the marginalized 1-dimensional probability distribution for each parameters. All the others indicate the 1σ (darker, innermost) and 2σ (lighter, outermost) confidence level contours in the probability distributions of the different combinations of parameters. The full model contains a total of 11 free parameters, but only the 5 mentioned above are shown in this figure. Taken from Ref. [430].

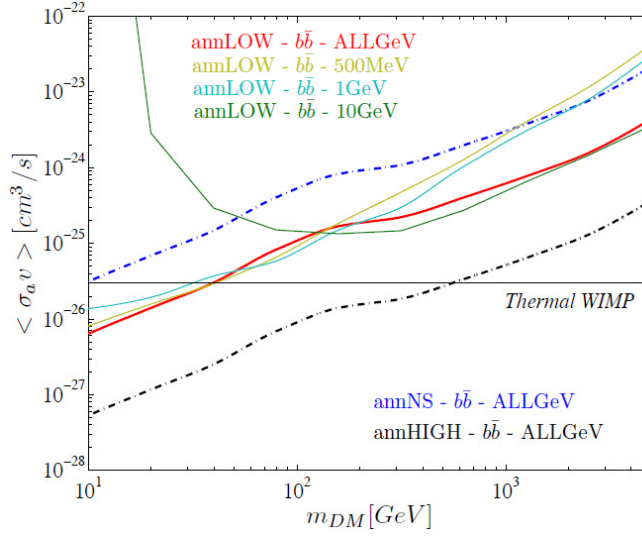


Figure 22: 95% confidence limit upper bounds on the DM annihilation rate $\langle \sigma v \rangle$ as a function of the DM mass, for the “LOW” substructures model of Ref. [62] and the reference NVSS-10 $A_{1h}^k \neq 0$ fit (see Ref. [430] for details). Solid lines refer to the $b\bar{b}$ annihilation channel: the red line refers to the analysis that combines information from all the three energy bins under consideration (i.e. $E > 0.5, 1$ and 10 GeV), while the other three lines refer to the analysis performed on a single energy bin (as stated in the figure label). The upper dot-dashed blue line refers to the “NS” substructure model, where halos do not have substructures and $M_{\min} = 10^7 M_{\odot}$. The lower dot-dashed black line, instead, represents the “HIGH” substructure model, inspired by Ref. [62]. Taken from Ref. [430].

(parametrized according to Refs. [22, 23, 161, 29], respectively) and annihilating DM. The galaxy catalogs are described following the HOM formalism. The normalizations of the emission of the 4 mentioned astrophysical source classes are left free in the model, as well as the DM mass and annihilation cross section. 5 additional parameters are included, one for each class of gamma-ray emitters, accounting for possible 1-halo terms in the 2-point correlation functions. The model is, then, used to fit the measured cross-correlation reported in Ref. [70]. As expected, the posterior probability distribution function for the intensity of the 1-halo term points towards a value different than zero, in the case of the cross-correlation with NVSS. The distributions are compatible with zero for the other catalogs.

Fig. 21 summarizes the probability distributions of the remaining 5 free parameters (excluding m_{χ}). An examination of this figure makes evident that the interpretation of the cross-correlation data is affected by significant degeneracies: there is a mild indication of a peak in the probability distribution of the normalizations of MAGNs (A_{mAGNs} in Fig. 21) and of the DM component (A_{DM} , proportional to $\langle \sigma v \rangle$), but, otherwise, the data effectively just enforce upper limits on the other parameters. The degeneracy is particularly visible between A_{mAGNs} and A_{DM} in the fourth panel of the bottom row of Fig. 21. Nevertheless, the measured cross correlations are still able to provide stringent upper limit on the DM component, as it can be seen in Fig. 22. The regions above the solid lines are excluded as they would over-produce the 2-point correlation functions measured above 500 MeV (yellow line), 1 GeV (cyan line), 10 GeV (green). The red solid line indicates the upper limit obtained from the combined analysis of the data sets for the three mentioned energy thresholds. These results are all obtained by adopting the assume a “LOW” subhalo boost. Note that, even for such a moderate description of

low-mass DM structures, the inferred DM limits are more stringent than those obtained in Ref. [64] by studying the DGRB intensity or those derived from the DGRB auto-correlation APS in Ref. [420].⁴⁷ In the case that a “HIGH” subhalo boost were adopted instead, the upper limit on the DM annihilation cross section would improve by roughly one order of magnitude (dash-dotted black line in Fig. 22). On the contrary, in an overly conservative scenario in which no substructures are present below $M_{\min} = 10^7 M_{\odot}$, the exclusion worsen by a factor $\sim 4 - 5$ (blue dash-dotted line).

As already hinted at in Ref. [70], the authors of Ref. [430] noted that the models that provide a good fit to the cross-correlation data fall short of accounting for the intensity of the DGRB: above 1 GeV, in the most likely scenario, the model is able to explain only $\sim 30\%$ of the DGRB intensity measured by *Fermi* LAT in Ref. [9]. Note, though, that multiple reasons can be invoked to explain this apparent discrepancy, e.g. uncertainties in the modeling of the Galactic diffuse foreground when performing the measurement of the DGRB intensity, and/or uncertainties in the model predictions. Another possibility is the presence of a Galactic component in the DGRB that, therefore, does not correlate with the LSS. In this regard, Galactic DM would be a plausible and interesting candidate (see, e.g., Ref. [64] for further discussion on this issue).

5.2. The cross-correlation with cosmic shear

Another tracer of LSS is the gravitational lensing effect of cosmic shear. Due to lensing, the light emitted by distant sources is distorted while it propagates towards us by the presence of intervening matter. In the weak lensing regime, the effect is very small and it is directly related to the distribution of matter at large scale. The signal, referred to as *cosmic shear*, is expected to cross-correlate with the gamma-ray emission since the same structures responsible for light bending are also those producing the gamma-ray emission, either because they emit light themselves (through DM annihilation or decay) or because they host the astrophysical emitters.

The gravitational distortion can be evaluated on the null-geodesic of the unlensed photon. It can be decomposed into the so-called convergence κ and shear γ [437, 438]. In the flat-sky approximation (i.e. small distortion angles), κ and γ share the same APS and, for convenience, we focus only on the former from now on. The convergence κ is a direct estimator of the fluctuations in the Newtonian potential of the LSS, integrated along the line of sight. κ can be estimated via a statistical analysis of the correlations in the ellipticities of the images of galaxies. Thanks to Poissons equation, which links the gravitational potential to the matter distribution, the intensity of the cosmic shear signal $I_{\kappa}(\mathbf{n})$ from a direction \mathbf{n} can be written as follows:

$$I_{\kappa}(\mathbf{n}) = \int d\chi g_{\kappa}(\mathbf{n}, \chi) W_{\kappa}(\chi). \quad (40)$$

The decomposition of $I_{\kappa}(\mathbf{n})$ resembles the way we expressed the gamma-ray emission in Eq. (28): the source field $g_{\kappa}(\mathbf{n}, \chi)$ indicates directly the distribution of matter and it is modulated by the window function. The product of the average source field $\langle g_{\kappa}(\chi) \rangle$ and the window function can be expressed as follows:

$$\langle g_{\kappa}(\chi) \rangle W_{\kappa}(\chi) = \frac{3}{2} H_0^2 \Omega_m [1 + z(\chi)] \chi \int_{\chi}^{\infty} d\chi' \frac{\chi' - \chi}{\chi'} \frac{dN_g(\chi')}{d\chi'}, \quad (41)$$

⁴⁷These limits are sensitive to the way the 1-halo terms are implemented. See Ref. [430] for details.

where $dN_g/d\chi'$ is the redshift distribution of the background galaxies, normalized to 1 over the observed redshift range.

As done in Sec. 3, the gamma-ray emission associated with a certain population X is written in terms of its window function $W_X(\chi)$ and of the source field $g_X(\chi, \mathbf{n})$ as $I_X(\mathbf{n}) = \int d\chi g_X(\chi, \mathbf{n}) W_X(\chi)$. The average source field $\langle g_X(\chi) \rangle$ depends on the abundance of sources as a function of their Y -parameter and of redshift (see Eq. (29)). Similarly to Eq. (32), the cross-correlation APS between the gamma-ray emission produced by population X and the cosmic shear can be written as [406, 74]:

$$C_\ell^{X,\kappa} = \frac{1}{\langle \mathcal{I}_X \rangle \langle \mathcal{I}_\kappa \rangle} \int \frac{d\chi}{\chi^2} \langle g_X(\chi) \rangle \langle g_\kappa(\chi) \rangle W_X(\chi) W_\kappa(\chi) P_{X,\kappa} \left(k = \frac{\ell}{\chi}, \chi \right). \quad (42)$$

The 3-dimensional cross-correlation power spectrum $P_{X,\kappa}$ can be split into the following 1-halo and 2-halo terms:

$$P_{1h}(k, z) = \int_{M_{\min}}^{M_{\max}} dM \frac{dn}{dM} \tilde{u}(k|M) \frac{\tilde{u}_X(k|Y(M))}{\langle g_X(\chi) \rangle}, \quad (43)$$

$$P_{2h}(k, z) = \left[\int_{M_{\min}}^{M_{\max}} dM \frac{dn}{dM} b_h(M) \tilde{u}(k|M) \right] \left[\int_{Y_{\min}}^{Y_{\max}} dY \frac{dN}{dY} b_X(Y) \frac{\tilde{u}_X(k|Y)}{\langle g_X(\chi) \rangle} \right] P_{\text{lin}}(k, z). \quad (44)$$

The quantity $\tilde{u}(k|M)$ is the Fourier transform of the radial density profile of a DM halo with mass M , while $\tilde{u}_X(k|Y(M))$ is the Fourier transform of the gamma-ray surface brightness profile of the source characterized by parameter Y . Note that these equations depend on the $Y(M)$ relation that links the Y -parameter to the mass of the host DM halo. For astrophysical sources, Y is usually taken to be the gamma-ray luminosity L_γ . Ref. [75] determines the $L_\gamma(M)$ empirically for the case of blazars, SFGs and MAGNs, making use of correlations between different source properties or of the results of semi-analytical models. However, the $L_\gamma(M)$ remains very uncertain for all the source classes considered in Ref. [75]. Its uncertainty can become an issue when estimating the cross-correlation APS $C_\ell^{X,\kappa}$. However, in the case of astrophysical sources, $C_\ell^{X,\kappa}$ is dominated by the 2-halo term (at least up to multipoles as large as few hundreds), while the $L_\gamma(M)$ relation mainly affects the 1-halo term.⁴⁸ The uncertainty on $C_\ell^{X,\kappa}$ generated by the variability of $L_\gamma(M)$ can be seen in the left panel of Fig. 23. The different solid lines show the expected cross-correlation APS for different classes of astrophysical sources (red for blazars, orange for SFGs and pink for MAGNs), while dashed lines indicate how the cross-correlation APS changes for two extreme scenarios bracketing our lack of knowledge on $M(L_\gamma)$. The uncertainty bands are within a factor of 2 from the solid lines, at least at high multipoles. They increase in size at smaller angular scales (i.e. large ℓ), since the APS becomes more sensitive to the 1-halo term.

The left panel of Fig. 23 also demonstrates that the expected cross-correlation between cross-correlation and the emission of unresolved blazars is more than 2 orders of magnitude smaller than the one with the other classes of astrophysical sources in Ref. [75], i.e. SFGs and MAGNs. As commented in the previous section, this is because the *Fermi* LAT has detected most of the blazars populating the volume probed by cosmic shear (i.e. $z \lesssim 2$ [75]) and, thus, the window functions $W_{\text{blazars}}(\chi)$ and $W_\kappa(\chi)$ do not

⁴⁸The $L_\gamma(M)$ relation enters in the computation of the 2-halo term only through the bias factor, $b_X(Y(M))$, which is, generally, of $\mathcal{O}(1)$.

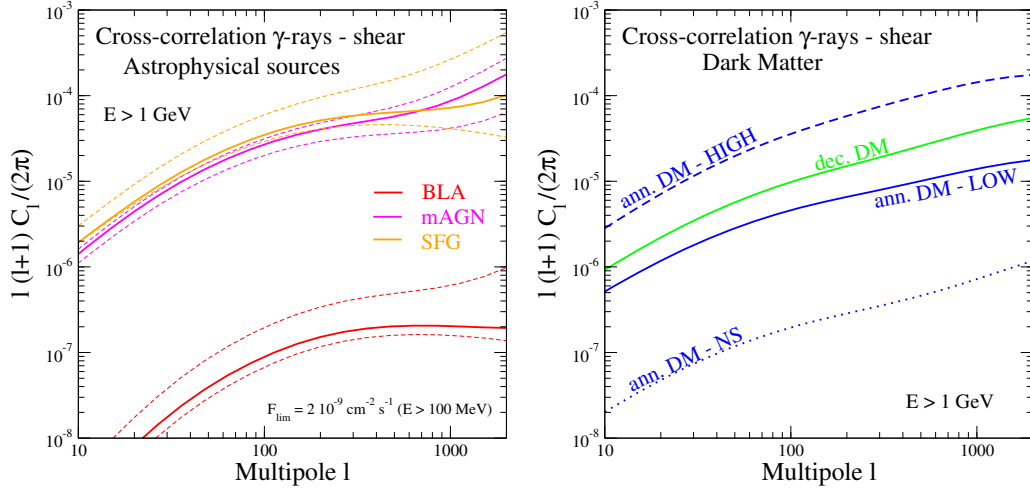


Figure 23: *Left*: Cross-correlation APS between cosmic shear and gamma rays from blazars (red), MAGNs (pink), and SFGs (orange). Among the curves with the same color, different lines correspond to different choices for the $L_\gamma(M)$ relation: solid lines represent the fiducial models considered in Ref. [75], while dashed ones indicate extreme scenarios assumed to bracket the uncertainty on $L_\gamma(M)$. *Right*: Cross-correlation APS between cosmic shear and DM-induced gamma-ray emission. Blue lines correspond to an annihilating DM candidate and the green one to a decaying DM candidate. The different blue lines represent different scenarios for low-mass DM (sub)halos (see Ref. [75] for details). The mass of the DM particle is taken to be 100 GeV (200 GeV) in the case of annihilating (decaying) DM. The annihilation cross section is fixed at $3 \times 10^{-26} \text{ cm}^3 \text{ s}^{-1}$ and the decay lifetime at $3 \times 10^{27} \text{ s}$. Annihilations and decays entirely into $b\bar{b}$ are assumed. Taken from Ref. [75].

overlap significantly. On the other hand, only a limited number of MAGNs and SFGs have been observed by the *Fermi* LAT (see also Secs. 2.2.2 and 2.2.3), so that the emission of their unresolved counterparts is still characterized by a notable cross-correlation with the lensing signal.

The right panel of Fig. 23 shows the expected cross-correlation APS with the gamma-ray emission produced by annihilating DM (blue lines) or decaying DM (green line). Different blue lines corresponds to different models for the description of low-mass DM halos. As seen in the previous sections, this uncertainty can have a significant impact on the properties of the DM-induced emission. Ref. [75] estimates that different description of the DM (sub)halos below the mass resolution of N -body simulations can lead to an uncertainty as large as a factor of 100 on the expected cross-correlation APS.⁴⁹ In the most optimistic scenario considered in Ref. [75], the cross-correlation APS from annihilating DM is of the same order of that expected from astrophysical sources. This demonstrates how effective this observable can be for the detection of the DM component in the DGRB.

Ref. [75] estimates that the measurement of the cross-correlation between the data of the Dark Energy Survey [439] and those of the *Fermi* LAT (after 5 years of operation) has the potential to detect an annihilating DM particle with an annihilation cross section smaller than the thermal value of $3 \times 10^{-26} \text{ cm}^3 \text{ s}^{-1}$ for DM masses up to 300 GeV (for

⁴⁹Note, however, that the “NS” model (dotted blue line in Fig. 23) is probably underestimating the signal from DM since it assumes no contribution from DM subhalos and a quite large $M_{\text{min}} = 10^7 M_\odot$. On the other hand, the “HIGH” scenario (dashed blue line) is based on power-law extrapolations from Ref. [276] and, thus, it likely overestimates the DM signal (see Sec. 2.3).

annihilations into b quarks). The result refers to a very optimistic subhalo boost and the predicted signal decreases by a factor of ~ 10 in the case of a more realistic description of DM subhalos (see right panel of Fig. 23). Prospects improve significantly with the inclusion of data from the forthcoming Euclid mission (expected for 2020) [440, 441]. Indeed, the cross correlation of Euclid data with those of a hypothetical future gamma-ray telescope with improved performances with respect to the *Fermi* LAT⁵⁰ has the potential to detect a DM component for DM masses up to the TeV scale (assuming a thermal annihilation cross section and an optimistic subhalo boost).

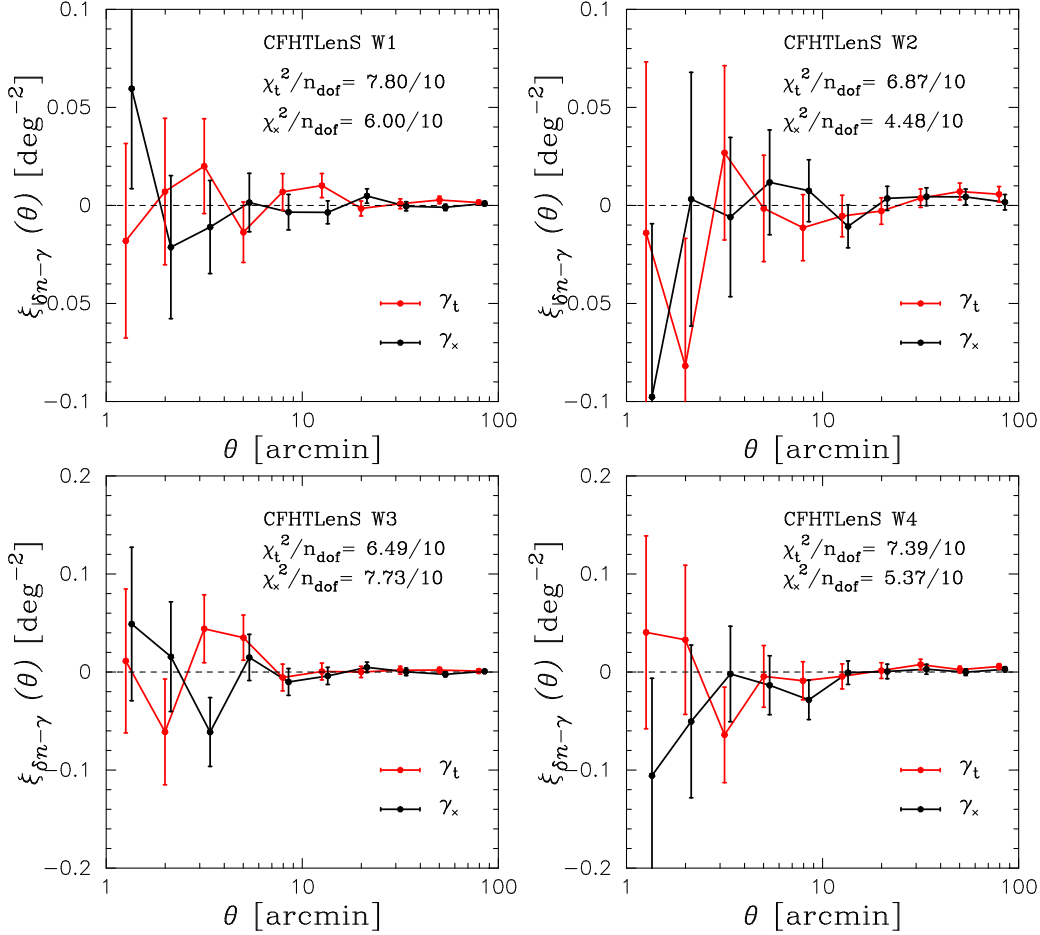


Figure 24: The cross-correlation signal of cosmic shear and the DGRB. The 4 panels corresponds to the 4 sky-patches W1-W4 covered by CFHTLenS. Red points show the results obtained using tangential shear (indicated as γ_t), while black points are for a component of the shear (γ_x in the legends) rotated by 45° with respect to γ_t . The error bars indicate the standard deviation, estimated from 500 randomized shear catalogs. The χ^2 quantifies the significance of the signal with respect to the statistical error. Taken from Ref. [71].

Such an optimal prospect for a DM detection is possible thanks to the “tomographic

⁵⁰This improved version the *Fermi* LAT is described by a wide energy range, i.e. from 300 MeV to 1 TeV. It is also assumed to achieve ~ 2.5 times more exposure (defined in Ref. [75] as the product of the effective area and the observation time) than 5 years of *Fermi* LAT data and to drastically improve the angular resolution to a value of 0.027° over the whole energy range. Its field of view is similar to that of the *Fermi* LAT.

spectral approach” employed in Ref. [75], which combines spectral information with the study of the dependence of $C_\ell^{X,\kappa}$ on redshift (i.e. tomography). Such a technique provides an excellent sensitivity to DM-induced emission, even if the intensity or auto-correlation APS of such a component are only subdominant.

The first (and, to date, only) measurement of the cross-correlation between DGRB and cosmic shear is performed in Ref. [71]. The authors make use of the data of CFHTLenS from Ref. [442]. The survey detected more than 5 million galaxies in 4 patches, covering an area of 154 square degrees. The corresponding shear signal is correlated in Ref. [71] with 65 months of *Fermi* LAT data from the same region in the sky. Only photons between 1 and 500 GeV are considered in the analysis. A model for the diffuse Galactic foreground (determined in Ref. [71] from the gamma-ray data) is subtracted from the total gamma-ray emission and 2FGL sources are masked, before computing the cross-correlation.

The estimator considered in Ref. [71] for the 2-point correlation function is

$$\xi(\vartheta) = \frac{\sum_{ij} n_i^\gamma(\phi_i) w_j \epsilon_j(\phi_i + \vartheta_j)}{(1 + K(\vartheta)) \sum_{i,j} w_j}, \quad (45)$$

where n_i^γ is the number of gamma rays in the pixel centered on direction ϕ_i , and ϵ_j is the shear-induced tangential ellipticity in pixel $\phi_j = \phi_i + \vartheta_j$. The factors w_j and $K(\vartheta)$ depend on the precision in the estimation of ϵ_j (see Refs. [443, 71]) and the sum runs over all the pairs of pixels available. Fig. 24 shows the 2-point cross-correlation function (binned in 10 logarithmic bins with $\Delta \log_{10} \vartheta = 0.2$) for the 4 CFHTLenS sky patches. The measured 2-point correlation function using Eq. (45) are showed in red, while the black points are obtained from another shear component rotated by 45° with respect to the tangential one. In the case of a perfect measurement of the shape of the galaxies and of no intrinsic alignment, there should be no cross-correlation with this rotated data set. Thus, the black points in Fig. 24 represent a control sample with no cross-correlation. Note that black and red points in Fig. 24 are compatible with each other within errors, proving that no significant cross-correlation is present between CFHTLenS and *Fermi* LAT. This result can be translated into an upper limit on the DM annihilation cross section as a function of its mass. Ref. [71] excludes cross sections as low as the thermal value of $3 \times 10^{-26} \text{cm}^3 \text{s}^{-1}$ for DM masses smaller than ~ 10 GeV (in the case of annihilation into $\tau^+ \tau^-$ and of the optimistic subhalo boost model of Ref. [276]).

5.3. The cross-correlation with other tracers

In addition to galaxy catalogs and cosmic shear, it is also possible to consider other observables that trace the LSS of the Universe. Below, we highlight some of these studies.

Ref. [399] cross-correlates the DGRB inferred from the first 21 months of *Fermi* LAT data with the CMB measured by WMAP7 [444]. Such a measurement has the potential to probe the properties of dark energy through the detection of the so-called integrated Sachs-Wolfe effect [445]. This arises when the LSS gravitational potential changes with time during a cosmic era dominated by dark energy, as, e.g., in the local Universe. Additional anisotropies are induced in the CMB, which are expected to correlate with the LSS and, thus, potentially with the DGRB. In Ref. [399], the 2-point correlation function is computed, similarly to what was done for galaxy catalogs in Sec. 5.1. Their

results are compatible with a null detection, due to the large statistical errors.⁵¹ Overall, Ref. [399] shows that the goal of detecting the integrated Sachs-Wolfe effect by cross-correlating the DGRB with the CMB is not unrealistic, but beyond the reach of the limited gamma-ray sample considered in Ref. [399].

More recently, Ref. [446] computed, for the first time, the cross-correlation of the DGRB with the so-called “lensing potential” of the CMB: the gravitational lensing induced by LSS imprints some distortions on the anisotropy pattern of the CMB, in such a way that the radiation detected by the Planck satellite [447] today is not exactly the one emitted at recombination. A statistical analysis of the non-Gaussianity of the CMB allows to reconstruct the lensing potential responsible for such perturbations [448, 449, 450]. The first all-sky map of the CMB lensing potential has been recently reported by the Planck collaboration [451]. The signal is mainly contributed by structures at $z \sim 2$ and it exhibits an auto-correlation APS that peaks at $\ell \sim 20 - 30$.

Ref. [446] cross-correlates the sky-map of the CMB lensing potential with 68 months of *Fermi* LAT data, after having removed the diffuse Galactic emission. Six energy bins are considered, between 700 MeV and 300 GeV. The region at $|b| < 25^\circ$ along the Galactic plane and a 1° -circle around each source in the 2FGL are masked, together with the *baseline* 70% Galactic mask from Ref. [451]. The signal region is defined between $\ell = 40$ and 400. A detection with a significance of 3.2σ is reported in the low-multipole region ($\ell < 160$). No signal is present above $\ell = 160$ (see data points in Fig. 25). The signal at low multipoles is compared to the predicted cross-correlation between the lensing potential and the gamma-ray emission from 4 classes of unresolved sources, namely FSRQs, BL Lacs, SFGs and MAGNs. The LF of these populations are fixed to the best-fit models from Refs. [22, 23, 29, 164, 33] (see Secs. 2.2.1, 2.2.2 and 2.2.3). The combined emission of these 4 source classes (solid black line in Fig. 25) reproduces fairly well the experimental data. More precisely, BL Lacs, SFGs and MAGNs (red, orange and green lines in Fig. 25, respectively) contribute more or less in equal parts to the cross-correlation signal, while FSRQs (blue line) are subdominant. This model also provides a good fit to the DGRB energy spectrum and auto-correlation APS.

6. The science of the Diffuse Gamma-Ray Background

In this review we have summarized the current knowledge on the Diffuse Gamma-Ray Background (DGRB). The DGRB is what remains in the gamma-ray sky after the subtraction of the diffuse Galactic foreground and of the resolved sources. It is interpreted as the cumulative emission of the objects that are not bright enough to be detected individually.

Since its first detection in 1972 by the OSO-3 satellite [1], this emission has been deeply investigated in an attempt to understand its composition. The *Fermi* LAT satellite, in operation since 2008, has greatly improved our understanding of the DGRB. This emission is measured as an isotropic template in a multi-component fit to the *Fermi* LAT data. The fit also includes a model for the resolved sources and for the diffuse Galactic foreground. The most recent measurement of the DGRB energy spectrum is reported in Ref. [9] and it covers almost 4 orders of magnitude in energy, from 100 MeV to 820 GeV. Our imperfect knowledge of the Galactic foregrounds represents the main source

⁵¹The lack of a significant detection is compatible with the expectation if the DGRB is composed by unresolved sources (parametrized as in Ref. [399]).

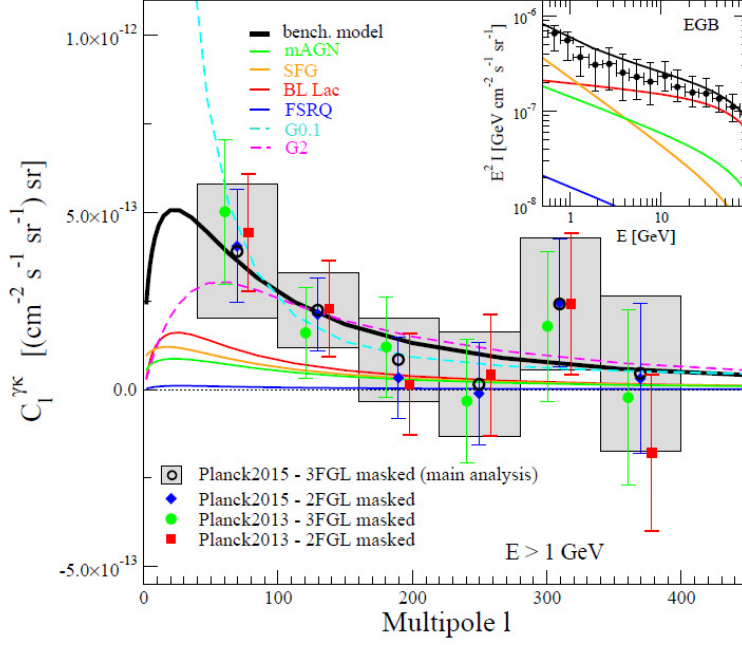


Figure 25: Cross-correlation APS $C_l^{\gamma\kappa}$ between the DGRB and the CMB lensing potential, as a function of the multipole ℓ , for gamma-ray energies $E > 1$ GeV. The measurement is averaged (linearly in terms of $\ell C_l^{\gamma\kappa}$) in multipole bins of $\Delta\ell = 60$, starting at $\ell = 40$. Points report the minimum-variance combination of the measurement in the individual energy bins (assuming a spectrum $\propto E^{-2.4}$), as described in Ref. [446]. Four different analyses are shown. They arise from the combination of two lensing maps (from the 2013 and 2015 release of Planck data) and two gamma-ray point-source masks (masking sources in 2FGL or 3FGL). The benchmark theoretical model, shown in black, is the sum of the contributions from BL Lacs (red), FSRQs (blue), MAGNs (magenta) and SFGs (orange), multiplied by a normalization factor $A^{\kappa\gamma} = 1.35$. Two generic models (labeled “G0.1” and “G2”) with Gaussian window functions are also shown. The peak of the Gaussian is at $z_0 = 0.1$ ($z_0 = 2$), with a dispersion $\sigma_z = 0.1$ ($\sigma_z = 0.5$) for G0.1 (G2). In the inset, the intensity energy spectrum is shown for the *Fermi* LAT measurement (black data point, labeled “EGB”) and for the model predictions. Taken from Ref. [446].

of uncertainty in the analysis and it induces a systematic error on the DGRB intensity of $\sim 15 - 30\%$, depending on the energy range considered.

Before the *Fermi* LAT, the energy spectrum was the only source of information available on the DGRB. However, the scenario drastically changed in 2012 when, for the first time, the *Fermi* LAT measured also the angular power spectrum (APS) of anisotropies in the DGRB [66]. The emission was found to exhibit a Poissonian APS in the multipole range between $\ell = 155$ and 504, with a significance as large as 7.2σ between 1.99 and 5.0 GeV. This signal is independent of energy between 1 and 50 GeV.

Recently, cross-correlations of the DGRB with different data sets have also revealed to be a powerful tool to unveil the composition of the DGRB. Ref. [70] reported a significant cross-correlation of the DGRB with 4 out of the 5 galaxy catalogs considered, namely the optically-selected quasars of the Sloan Digital Sky Survey (SDSS) Data Release 6 in Ref. [425], the IR galaxies of the 2 Micron All-Sky Survey (2MASS) Extended Source Catalog from Ref. [426], the main galaxy sample of SDSS Data Release 8 from Ref. [429] and the radio sources from the NRAO VLA Sky Survey (NVSS) [427]. These cross-correlation signals, obtained after the analysis of 60 months of *Fermi* LAT data, are localized at small angles (below few degrees) with significances that range between 3σ (in the case of SDSS Data Release 8 main galaxies) and more than 10σ (for the

NVSS catalog), for gamma-ray energies above 1 GeV. The cross-correlation with NVSS, however, is most likely contaminated by a 1-halo term not related to the Large Scale Structure (LSS) of the Universe.

In Ref. [71], the authors measured, for the first time, the cross-correlation of the DGRB with the cosmic shear induced by the gravitational lensing detected in the Canada-France-Hawaii Telescope Lensing Survey (CFHTLenS) [442]. Their results are compatible with a null cross-correlation signal in the angular range between 1 and 100 arcmin. Ref. [71] proves, though, that measuring the cross-correlation with the cosmic shear signal is not an unrealistic goal. Indeed, more promising results are expected from the cross-correlation between the DGRB and the data expected from the Dark Energy Survey (DES) or from Euclid [75]. Finally, Ref. [446] reported a 3.2σ detection of the cross-correlation between the DGRB and the lensing potential of the CMB measured by the Planck Collaboration [451]. The signal is localized in the multipole region between $\ell = 40$ and 160, for gamma-ray energies between 700 MeV and 300 GeV.

The increased amount of observational data on the DGRB has allowed significant progress in the modeling of its composition. The DGRB is interpreted as the cumulative emission of unresolved sources, e.g. blazars, misaligned Active Galactic Nuclei (MAGNs), star-forming galaxies (SFGs) and MilliSecond Pulsars (MSPs). It, therefore, represents a reservoir of invaluable information on these astrophysical sources as it may be the only way to study the emission of objects that are too faint to be detected individually. In particular, the DGRB can potentially determine the faint end of the luminosity function of the aforementioned populations, i.e. a goal that would be quite difficult, if not impossible, to achieve otherwise.

Before the *Fermi* LAT, the predictions for the contribution of unresolved blazars to the DGRB were affected by large uncertainties [94, 10, 11, 12, 13, 15, 30, 16]. Nowadays, the wealth of new information on the DGRB, combined with the population studies of resolved blazars performed by the *Fermi* LAT Collaboration, have established that this source class cannot account for more than $(20 \pm 4)\%$ of the DGRB in the energy range between 0.1 and 100 GeV [25]. The subclass of blazars responsible for the bulk of the blazar contribution varies depending on the energies considered. Indeed, Refs. [23, 24, 25] showed that unresolved high-synchrotron-peaked BL Lacs can explain the whole DGRB at energies above ~ 100 GeV. At lower energies, astrophysical populations other than blazars are required. Yet, the modeling of these other gamma-ray emitters, such as namely MAGNs, SFGs and MSPs, is not as robust as that of blazars. This is caused by difficulty in performing reliable population studies with the limited sample of resolved sources currently available in the gamma-ray range. Generally, it is useful to assume a correlation between luminosities at different wavelengths (i.e. gamma-ray with radio frequencies [28, 29] in the case of MAGNs, or gamma rays and infra-red light [33] for SFGs).

The overall picture indicates that the 4 classes of astrophysical sources mentioned above are enough to explain the totality of the DGRB energy spectrum measured in Ref. [9] (see Fig. 9). As for the APS of DGRB anisotropies, Refs. [67, 68, 63] prove that unresolved blazars alone (more specifically, high-synchrotron-peak BL Lacs) can account for the whole APS reported in Ref. [66]. These two important results can be reconciled by the fact that the blazar component is produced by a relatively small number of bright but unresolved objects and, thus, it gives rise to significant anisotropies. On the contrary, the other source classes produce fairly isotropic cumulative emission, as their members are more numerous and fainter.

The picture gets more complicated, though, when considering also the measured

cross-correlation with LSS tracers: the sum of unresolved blazars, MAGNs and SFGs provides a good fit to the cross-correlation APS detected between the DGRB and the CMB lensing potential [446]. It is also compatible with the lack of significant cross-correlation with the CFHTLenS cosmic shear [71]. However, Ref. [430] finds that the model that best fits the two-point correlation functions measured in Ref. [70] with 5 galaxy catalogs can only account for $\sim 30\%$ of the DGRB intensity reported in Ref. [9]. It is still unclear if such a limitation of the astrophysical interpretation of the DGRB can be alleviated by a more sophisticated modeling of its components. Also, it will be interesting to verify whether a similar scenario will be confirmed by new surveys or by more complete data releases of the catalogs currently employed. Alternatively, one will be forced to supplement the model with another component, which does not correlate with the LSS, such as gamma-ray emission associated with the DM halo of the MW or with its DM substructures.

Quantifying the contribution of known astrophysical populations automatically constrains the intensity of other potential contributors to the DGRB. We briefly presented, among others, the case of clusters of galaxies, Type Ia supernovae and of Ultra-High-Energy Cosmic Rays interacting with background radiation. However, the most studied scenario is that of a potential gamma-ray emission from Dark Matter (DM) annihilation or decay. Since no DM signal has been undoubtedly detected in the gamma-ray sky so far, it is expected that most of this hypothetical gamma-ray emission will contribute to the DGRB. Searching for DM in the DGRB has the advantage that the DM-induced component is sourced by the emission coming from *all* DM halos and subhalos around us. It will, thus, depend on the ensemble-averaged properties of the DM halo population, which can be inferred from N -body cosmological simulations [452, 343, 267, 453, 454] or predicted by the theory of structure formation [200, 201]. This is intrinsically different from the observation of a specific target, e.g. the Galactic Center or a dwarf Spheroidal satellite galaxy. Indeed, each of these targets could be very peculiar and deviate considerably from the ensemble average, potentially hamper the interpretation of any data. Another benefit of using the DGRB to search for DM is that a potential DM signal contributing to the DGRB would be sensitive to the process of assembly of DM halos and their subsequent evolution. This kind of information would be difficult (if not impossible) to extract by observing individual targets in the sky. In this regard, the DGRB may be the only cosmological non-gravitational probe of DM. In addition, it represents a fundamental source of complementary information in the study of any claimed DM signal.

The intensity of this DM-induced cosmological emission depends on the properties of the DM particle, e.g. its mass, annihilation cross section or decay lifetime. Also, it rests on the abundance and properties of DM structures. Our understanding of DM (sub)halos heavily relies on the results of N -body cosmological simulations. Yet, as of today, even the simulations with the highest resolution are far from resolving the whole DM halo hierarchy down to the predicted M_{\min} . The properties of low-mass DM structures, thus, need to be inferred by extrapolating the characteristics of their more massive counterparts, that are well resolved in the simulations. Heuristic power-law extrapolations, which predict very bright low-mass DM halos, have been commonly used in the literature [274, 56, 275, 276, 339, 217]. However, recent high-resolution simulations of the smallest DM halos [277, 279] suggest that those extrapolations are not well motivated, favoring, instead, models that yield a more moderate DM-induced gamma-ray emission from low-mass structures [267, 280, 281]. Overall, this results in a DM-induced cosmological signal which is substantially weaker than the one obtained

when assuming power-law extrapolations. Also, and perhaps even more importantly, the improved knowledge provided by Refs. [267, 280, 281] on the structural properties of the smallest DM halos has considerably reduced the theoretical uncertainty associated with the DM contribution to the DGRB down to a factor of ~ 20 [64].

Not unexpectedly, the measured DGRB energy spectrum can be used to constrain the intensity of the DM-induced emission and, thus, to derive upper (lower) limits on the annihilation cross section (decay lifetime). Figs. 11 and 12 summarize some of these results. For annihilating DM, the so-called “sensitivity-reach” limits derived in Ref. [64] from their fiducial Halo Model exclude thermal annihilation cross sections of $3 \times 10^{-26} \text{cm}^2 \text{s}^{-1}$ for masses below ~ 100 GeV in the case of annihilations into b quarks. When compared to other indirect searches for DM, the upper limits inferred from the DGRB represent the strongest constraints on $\langle \sigma v \rangle$ currently available, for DM masses below ~ 1 TeV. A more conservative statistical analysis would increase the upper limits by a factor of ~ 10 .⁵² In the case of decaying DM, the lower limits on τ obtained in Ref. [386] from the DGRB measurement in Ref. [8] exclude decay lifetimes smaller than $\sim 3 \times 10^{27}$ s for $m_\chi \lesssim 2$ TeV and decays into $\mu^+ \mu^-$. At larger masses, the strongest lower limit comes from Ref. [387], which excludes lifetimes as large as 10^{28} s. When compared to other searches of decaying DM, these limits represent the most constraining information available on τ , up to DM masses of 20 TeV.

A similar strategy can be used when comparing the APS measured in Ref. [66] to the predicted anisotropies in the DM-induced emission. Nevertheless, the latter turns out to be quite isotropic [56, 62, 339] and, thus, the corresponding upper limits, although competitive with other indirect DM searches, are less stringent than those inferred from the DGRB [339, 420]. The cross-correlation with galaxy catalogs and with cosmic shear are also very promising strategies to constrain (or even to detect) a potential DM signal in the DGRB [73, 74, 72, 75]. This is possible mainly thanks to the fact that both cross-correlations are particularly sensitive to the way the matter is distributed in the local Universe and, in particular, to the most massive DM halos. We remind that unresolved blazars, the main contributors to the auto-correlation APS, do not populate neither the local volume nor the largest DM halo masses. A model of the DGRB including both astrophysical sources and annihilating DM is used in Ref. [430] to describe measurement of the 2-point correlation function reported in Ref. [70]. The analysis excludes DM candidates with annihilation cross sections larger than the thermal value for masses below 40 GeV, for annihilations into b quarks and a moderate value of the subhalo boost. When assuming the same value of the subhalo boost, the obtained upper limit is currently the strongest one among all those derived from DGRB data, including measurements of the DGRB intensity and of the auto-correlation APS.

The energy spectrum, auto-correlation and cross-correlation APS of the DGRB are sensitive to different characteristics of the sources contributing to the emission. Considering *at the same time* all three observables provide a very powerful handle to reconstruct the composition of the DGRB. Needless to say, such an ambitious goal requires ample data sets, including information from wavelengths other than the gamma-ray energy range. Fortunately, a great wealth of new observational information is expected in the near future: the *Fermi* LAT will continue gathering data until, at least, 2016. The Cherenkov Telescope Array (CTA), expected to be in operation by 2020, will improve by a factor ~ 10 the sensitivity of current Cherenkov telescopes in the energy range be-

⁵²Note also that both the fiducial sensitivity-reach limits and the more conservative ones in Ref. [64] are affected by an uncertainty of a factor of ~ 3 .

tween a few dozens of GeV and a few dozens of TeV. Its complementarity with respect to the *Fermi* LAT will allow an improved precision in the determination of the DGRB energy spectrum in the sub-TeV energy range, as well as the extension of the measurement beyond the TeV. In addition, CTA will perform the first survey of a significant portion of the sky at these very-high energies [455, 456]. Combined with the *Fermi* LAT data gathered since Ref. [66], it will be possible to extend the data on the auto-correlation APS to higher energies and to decrease the size of the bins in energy. On the other hand, the cross-correlation of the DGRB with LSS tracers will hugely benefit for the imminent release of the data gathered by the DES [439] during its first year of operation. The near future will also see the advent of the next generation of galaxy catalogs, e.g. the extended Baryon Oscillation Spectroscopy Survey (eBOSS)⁵³ and the Dark Energy Spectroscopic Instrument (DESI, formerly BigBoSS) [457]. On a longer scale, Euclid will offer weak lensing measurements with unprecedented precision after 2020 [440].

The increased observational data available on the DGRB will also be accompanied by significant progress in the modeling of its contributors. Improving our understanding of the emission of blazars, SFGs and MAGNs will alleviate the degeneracies currently affecting our interpretation and will reduce the uncertainty associated with each component. A fully multi-wavelength approach is required to achieve such a goal: in the X-ray band the Nuclear Spectroscopic Telescope Array (NuSTAR) [458] has been recently launched and ASTRO-H [459, 460] will follow within this year (2015). Infra-red data from Herschel and the Wide-field Infrared Survey Explorer (WISE)⁵⁴ are already public and the James Webb Space Telescope (JWST)⁵⁵ is expected to be launched in 2018. Regular observation in radio has started with Low-Frequency Array (LOFAR)⁵⁶, a pathfinder for the Square Kilometer Array (SKA)⁵⁷ planned for 2020.

We end the review by noting that the IceCube Collaboration has recently reported the detection of the first extraterrestrial neutrinos [461, 462, 463]. The 37 observed neutrino events represent an excess over the atmospheric background extending to the PeV scale, with a significance of more than 5σ [463]. Even if the origin of these neutrinos is not clearly established yet (see Refs. [464, 465] and references therein), a possibility is that they originate from a diffuse neutrino flux similar to the DGRB.⁵⁸ If this interpretation was confirmed, many of the techniques discussed in this review could also be adopted to investigate this diffuse neutrino flux. Indeed, many of the sources contributing to the DGRB are expected to emit neutrinos as well [466, 467, 468, 469]. This implies that any constraint on their neutrino emission would indirectly constrain also their contribution to the DGRB (and viceversa). The development of a fully multi-messenger approach is certainly a very tantalizing possibility that has been already considered, e.g., in Refs. [470, 471, 472, 207, 473, 161].

In conclusion, the DGRB is a fundamental component of the gamma-ray sky, whose exact composition still remains unveiled. The recent rapid growth of available data on the DGRB (mostly thanks to the outstanding performance of the *Fermi* LAT) has triggered an increased attention from the scientific community. Astrophysicists and astroparticle physicists aim at reconstructing the composition of the DGRB to infer

⁵³<https://www.sdss3.org/future/eboss.php>

⁵⁴<http://wise.ssl.berkeley.edu/>

⁵⁵<http://www.jwst.nasa.gov/>

⁵⁶<http://www.lofar.org/>

⁵⁷<http://www.skatelescope.org/>

⁵⁸To stress the similarity with the DGRB, we propose to call this neutrino emission, the Diffuse Neutrino Background (DNB).

novel information on the sources contributing to the emission, especially in their low-luminosity regime. New data sets are already available (or will be soon) which can provide a significant progress to the common goal of dissecting the true nature of the DGRB. By summarizing where we stand on our current understanding of this emission, with this review we hope to have offered a useful reference to those who will analyze and interpret the data to come, as well as to help finding new avenues and opportunities for further research.

7. Acknowledgments

MF gratefully acknowledges support of the Leverhulme Trust. MASC is Wenner-Gren Fellow and acknowledges the support of the Wenner-Gren foundation to develop his research. We also acknowledge the project MultiDark CSD2009-00064. We thank M. Ajello, S. Ando, K. Bechtol, M. Di Mauro, A. M. Green, G. Zaharijas and J. Zavala for useful comments on the manuscript.

References

- [1] W. L. Kraushaar, G. W. Clark, G. P. Garmire, L. V. Borken R., T. Thorson, High-Energy Cosmic Gamma-Ray Observations from the OSO-3 Satellite, *Astrophys. J.* 177 (1972) 341.
- [2] F. Acero, et al., Fermi Large Area Telescope Third Source Catalog, *Astrophys.J.Suppl.* 218. [arXiv:1501.02003](#).
- [3] J. Lande, M. Ackermann, A. Allafort, J. Ballet, K. Bechtol, et al., Search for Spatially Extended Fermi-LAT Sources Using Two Years of Data, *Astrophys.J.* 756 (2012) 5. [arXiv:1207.0027](#), [doi:10.1088/0004-637X/756/1/5](#).
- [4] M. Ackermann, et al., The Spectrum and Morphology of the Fermi Bubbles, *Astrophys.J.* [arXiv:1407.7905](#), [doi:10.1088/0004-637X/793/1/64](#).
- [5] C. E. Fichtel, et al., High-energy gamma-ray results from the second small astronomy satellite, *Astrophys.J.* 198 (1975) 163–182.
- [6] P. Sreekumar, et al., EGRET observations of the extragalactic gamma-ray emission, *Astrophys.J.* 494 (1998) 523–534. [arXiv:astro-ph/9709257](#), [doi:10.1086/305222](#).
- [7] A. Strong, I. Moskalenko, O. Reimer, A new determination of the extragalactic diffuse gamma-ray background from egret data, *Astrophys.J.* 613 (2004) 956–961. [arXiv:astro-ph/0405441](#), [doi:10.1086/423196](#).
- [8] A. Abdo, et al., The Spectrum of the Isotropic Diffuse Gamma-Ray Emission Derived From First-Year Fermi Large Area Telescope Data, *Phys.Rev.Lett.* 104 (2010) 101101. [arXiv:1002.3603](#), [doi:10.1103/PhysRevLett.104.101101](#).
- [9] M. Ackermann, et al., The spectrum of isotropic diffuse gamma-ray emission between 100 MeV and 820 GeV, *Astrophys.J.* 799 (1) (2015) 86. [arXiv:1410.3696](#), [doi:10.1088/0004-637X/799/1/86](#).
- [10] F. Stecker, M. Salamon, M. Malkan, The High-energy diffuse cosmic gamma-ray background radiation from blazars, *Astrophys.J.* 410 (1993) L71–L74.

- [11] F. Stecker, M. Salamon, The Gamma-ray background from blazars: A New look, *Astrophys.J.* 464 (1996) 600–605. [arXiv:astro-ph/9601120](#), [doi:10.1086/177348](#).
- [12] A. Muecke, M. Pohl, On the contribution of unresolved blazars to the extragalactic gamma-ray background, *ASP Conf.Ser.* 159 (1998) 217. [arXiv:astro-ph/9807297](#).
- [13] T. Narumoto, T. Totani, Gamma-ray luminosity function of blazars and the cosmic gamma-ray background: evidence for the luminosity dependent density evolution, *Astrophys.J.* 643 (2006) 81–91. [arXiv:astro-ph/0602178](#), [doi:10.1086/502708](#).
- [14] C. D. Dermer, The Extragalactic Gamma Ray Background, *AIP Conf.Proc.* 921 (2007) 122–126. [arXiv:0704.2888](#), [doi:10.1063/1.2757282](#).
- [15] V. Pavlidou, T. M. Venters, The Spectral Shape of the Gamma-ray Background from Blazars, *Astrophys.J.* 673 (2008) 114–118. [arXiv:0710.0002](#), [doi:10.1086/523956](#).
- [16] Y. Inoue, T. Totani, The Blazar Sequence and the Cosmic Gamma-Ray Background Radiation in the Fermi Era, *Astrophys.J.* 702 (2009) 523–536. [arXiv:0810.3580](#), [doi:10.1088/0004-637X/702/1/523](#), [doi:10.1088/0004-637X/728/1/73](#).
- [17] M. Ajello, L. Costamante, R. Sambruna, N. Gehrels, J. Chiang, et al., The Evolution of Swift/BAT blazars and the origin of the MeV background, *Astrophys.J.* 699 (2009) 603–625. [arXiv:0905.0472](#), [doi:10.1088/0004-637X/699/1/603](#).
- [18] A. Abdo, et al., The Fermi-LAT high-latitude Survey: Source Count Distributions and the Origin of the Extragalactic Diffuse Background, *Astrophys.J.* 720 (2010) 435–453. [arXiv:1003.0895](#), [doi:10.1088/0004-637X/720/1/435](#).
- [19] K. N. Abazajian, S. Blanchet, P. Harding, The contribution of Blazars to the Extragalactic Diffuse Gamma-ray Background and Their Future Spatial Resolution, *Phys.Rev. D* 84 (2011) 103007. [arXiv:1012.1247](#), [doi:10.1103/PhysRevD.84.103007](#).
- [20] F. W. Stecker, T. M. Venters, Components of the Extragalactic Gamma Ray Background, *Astrophys.J.* 736 (2011) 40. [arXiv:1012.3678](#), [doi:10.1088/0004-637X/736/1/40](#).
- [21] J. Singal, V. Petrosian, M. Ajello, Flux and Photon Spectral Index Distributions of Fermi-LAT Blazars And Contribution To The Extragalactic Gamma-ray Background, *Astrophys.J.* 753 (2012) 45. [arXiv:1106.3111](#).
- [22] M. Ajello, M. Shaw, R. Romani, C. Dermer, L. Costamante, et al., The Luminosity Function of Fermi-detected Flat-Spectrum Radio Quasars, *Astrophys.J.* 751 (2012) 108. [arXiv:1110.3787](#), [doi:10.1088/0004-637X/751/2/108](#).
- [23] M. Ajello, R. Romani, D. Gasparrini, M. Shaw, J. Bolmer, et al., The Cosmic Evolution of Fermi BL Lacertae Objects, *Astrophys.J.* 780 (2014) 73. [arXiv:1310.0006](#), [doi:10.1088/0004-637X/780/1/73](#).
- [24] M. Di Mauro, F. Donato, G. Lamanna, D. Sanchez, P. Serpico, Diffuse γ -ray emission from unresolved BL Lac objects, *Astrophys.J.* 786 (2014) 129. [arXiv:1311.5708](#), [doi:10.1088/0004-637X/786/2/129](#).

- [25] M. Ajello, D. Gasparrini, M. Snchez-Conde, G. Zaharijas, M. Gustafsson, et al., The Origin of the Extragalactic Gamma-Ray Background and Implications for Dark-Matter Annihilation, *Astrophys.J.* 800 (2) (2015) L27. [arXiv:1501.05301](#), [doi:10.1088/2041-8205/800/2/L27](#).
- [26] L. Stawarz, T. Kneiske, J. Kataoka, Kiloparsec-scale jets in FR I radio galaxies and the gamma-ray background, *Astrophys.J.* 637 (2006) 693–698. [arXiv:astro-ph/0507316](#), [doi:10.1086/498084](#).
- [27] F. Massaro, M. Ajello, Fueling lobes of radio galaxies: statistical particle acceleration and the extragalactic gamma-ray background, *Astrophys.J.* 729 (2011) L12. [arXiv:1102.0774](#).
- [28] Y. Inoue, Contribution of the Gamma-ray Loud Radio Galaxies Core Emissions to the Cosmic MeV and GeV Gamma-Ray Background Radiation, *Astrophys.J.* 733 (2011) 66. [arXiv:1103.3946](#), [doi:10.1088/0004-637X/733/1/66](#).
- [29] M. Di Mauro, F. Calore, F. Donato, M. Ajello, L. Latronico, Diffuse γ -ray emission from misaligned active galactic nuclei, *Astrophys.J.* 780 (2014) 161. [arXiv:1304.0908](#), [doi:10.1088/0004-637X/780/2/161](#).
- [30] D. Bhattacharya, P. Sreekumar, R. Mukherjee, Contribution from unresolved discrete sources to the Extragalactic Gamma-Ray Background (EGRB), *Res.Astron.Astrophys.* 9 (2009) 1205–1214. [arXiv:0907.1741](#), [doi:10.1088/1674-4527/9/11/004](#).
- [31] B. D. Fields, V. Pavlidou, T. Prodanovic, Cosmic Gamma-Ray Background from Star-Forming Galaxies, *Astrophys.J.* 722 (2010) L199. [arXiv:1003.3647](#).
- [32] R. Makiya, T. Totani, M. Kobayashi, Contribution from Star-Forming Galaxies to the Cosmic Gamma-Ray Background Radiation, *Astrophys.J.* 728 (2011) 158. [arXiv:1005.1390](#), [doi:10.1088/0004-637X/728/2/158](#).
- [33] M. Ackermann, et al., GeV Observations of Star-forming Galaxies with *Fermi* LAT, *Astrophys.J.* 755 (2012) 164. [arXiv:1206.1346](#), [doi:10.1088/0004-637X/755/2/164](#).
- [34] B. C. Lacki, S. Horiuchi, J. F. Beacom, The Star-Forming Galaxy Contribution to the Cosmic MeV and GeV Gamma-Ray Background, *Astrophys.J.* 747 (2012) 2. [arXiv:1206.0772](#).
- [35] N. Chakraborty, B. D. Fields, Inverse Compton Contribution to the Star-Forming Extragalactic Gamma-Ray Background, *Astrophys.J.* 773 (2013) 104. [arXiv:1206.0770](#), [doi:10.1088/0004-637X/773/2/104](#).
- [36] C.-A. Faucher-Giguere, A. Loeb, The Pulsar Contribution to the Gamma-Ray Background, *JCAP* 1001 (2010) 005. [arXiv:0904.3102](#), [doi:10.1088/1475-7516/2010/01/005](#).
- [37] J. M. Siegal-Gaskins, R. Reesman, V. Pavlidou, S. Profumo, T. P. Walker, Anisotropies in the gamma-ray sky from millisecond pulsars, *Mon.Not.Roy.Astron.Soc.* 415 (2011) 1074S. [arXiv:1011.5501](#).

- [38] F. Calore, M. Di Mauro, F. Donato, F. Donato, Diffuse gamma-ray emission from galactic pulsars, *Astrophys.J.* 796 (2014) 1. [arXiv:1406.2706](#), [doi:10.1088/0004-637X/796/1/14](#).
- [39] F. Zandanel, I. Tamborra, S. Gabici, S. Ando, High-energy gamma-ray and neutrino backgrounds from clusters of galaxies and radio constraints, *Astron.Astrophys.* 578 (2015) A32. [arXiv:1410.8697](#), [doi:10.1051/0004-6361/201425249](#).
- [40] S. Horiuchi, J. F. Beacom, Revealing Type Ia supernova physics with cosmic rates and nuclear gamma rays, *Astrophys.J.* 723 (2010) 329–341. [arXiv:1006.5751](#), [doi:10.1088/0004-637X/723/1/329](#).
- [41] A. Lien, B. D. Fields, The Diffuse Gamma-ray Background from Type Ia Supernovae, *Astrophys.J.* 747 (2012) 120. [arXiv:1201.3447](#), [doi:10.1088/0004-637X/747/2/120](#).
- [42] O. E. Kalashev, D. V. Semikoz, G. Sigl, Ultra-High Energy Cosmic Rays and the GeV-TeV Diffuse Gamma-Ray Flux, *Phys.Rev.* D79 (2009) 063005. [arXiv:0704.2463](#), [doi:10.1103/PhysRevD.79.063005](#).
- [43] M. Ahlers, J. Salvado, Cosmogenic gamma-rays and the composition of cosmic rays, *Phys.Rev.* D84 (2011) 085019. [arXiv:1105.5113](#), [doi:10.1103/PhysRevD.84.085019](#).
- [44] G. Bertone, D. Hooper, J. Silk, Particle dark matter: Evidence, candidates and constraints, *Phys.Rept.* 405 (2005) 279–390. [arXiv:hep-ph/0404175](#), [doi:10.1016/j.physrep.2004.08.031](#).
- [45] M. Cirelli, G. Corcella, A. Hektor, G. Hutsi, M. Kadastik, et al., PPPC 4 DM ID: A Poor Particle Physicist Cookbook for Dark Matter Indirect Detection, *JCAP* 1103 (2011) 051. [arXiv:1012.4515](#), [doi:10.1088/1475-7516/2011/03/051](#).
- [46] A. Ibarra, Indirect dark matter detection, *Acta Phys.Polon.* B43 (2012) 2199–2224. [doi:10.5506/APhysPolB.43.2199](#).
- [47] T. Bringmann, C. Weniger, Gamma Ray Signals from Dark Matter: Concepts, Status and Prospects, *Phys.Dark Univ.* 1 (2012) 194–217. [arXiv:1208.5481](#), [doi:10.1016/j.dark.2012.10.005](#).
- [48] P. Ullio, L. Bergstrom, J. Edsjo, C. G. Lacey, Cosmological dark matter annihilations into gamma-rays - a closer look, *Phys.Rev.* D66 (2002) 123502. [arXiv:astro-ph/0207125](#), [doi:10.1103/PhysRevD.66.123502](#).
- [49] J. E. Taylor, J. Silk, The Clumpiness of cold dark matter: Implications for the annihilation signal, *Mon.Not.Roy.Astron.Soc.* 339 (2003) 505. [arXiv:astro-ph/0207299](#), [doi:10.1046/j.1365-8711.2003.06201.x](#).
- [50] S. Ando, Can dark matter annihilation dominate the extragalactic gamma-ray background?, *Phys.Rev.Lett.* 94 (2005) 171303. [arXiv:astro-ph/0503006](#), [doi:10.1103/PhysRevLett.94.171303](#).
- [51] S. Ando, E. Komatsu, Anisotropy of the cosmic gamma-ray background from dark matter annihilation, *Phys.Rev.* D73 (2006) 023521. [arXiv:astro-ph/0512217](#), [doi:10.1103/PhysRevD.73.023521](#).

- [52] S. Ando, E. Komatsu, T. Narumoto, T. Totani, Dark matter annihilation or unresolved astrophysical sources? Anisotropy probe of the origin of cosmic gamma-ray background, Phys.Rev. D75 (2007) 063519. [arXiv:astro-ph/0612467](#), [doi:10.1103/PhysRevD.75.063519](#).
- [53] J. M. Siegal-Gaskins, Revealing dark matter substructure with anisotropies in the diffuse gamma-ray background, JCAP 0810 (2008) 040. [arXiv:0807.1328](#), [doi:10.1088/1475-7516/2008/10/040](#).
- [54] S. Ando, Gamma-ray background anisotropy from galactic dark matter substructure, Phys.Rev. D80 (2009) 023520. [arXiv:0903.4685](#), [doi:10.1103/PhysRevD.80.023520](#).
- [55] M. Fornasa, L. Pieri, G. Bertone, E. Branchini, Anisotropy probe of galactic and extra-galactic Dark Matter annihilations, Phys.Rev. D80 (2009) 023518. [arXiv:0901.2921](#), [doi:10.1103/PhysRevD.80.023518](#).
- [56] J. Zavala, V. Springel, M. Boylan-Kolchin, Extragalactic gamma-ray background radiation from dark matter annihilation, Mon.Not.Roy.Astron.Soc. 405 (2010) 593. [arXiv:0908.2428](#).
- [57] A. Ibarra, D. Tran, C. Weniger, Detecting Gamma-Ray Anisotropies from Decaying Dark Matter: Prospects for Fermi LAT, Phys.Rev. D81 (2010) 023529. [arXiv:0909.3514](#), [doi:10.1103/PhysRevD.81.023529](#).
- [58] A. Abdo, et al., Constraints on Cosmological Dark Matter Annihilation from the Fermi-LAT Isotropic Diffuse Gamma-Ray Measurement, JCAP 1004 (2010) 014. [arXiv:1002.4415](#), [doi:10.1088/1475-7516/2010/04/014](#).
- [59] G. Hutsi, A. Hektor, M. Raidal, Implications of the Fermi-LAT diffuse gamma-ray measurements on annihilating or decaying Dark Matter, JCAP 1007 (2010) 008. [arXiv:1004.2036](#), [doi:10.1088/1475-7516/2010/07/008](#).
- [60] J. Zavala, M. Vogelsberger, T. R. Slatyer, A. Loeb, V. Springel, The cosmic X-ray and gamma-ray background from dark matter annihilation, Phys.Rev. D83 (2011) 123513. [arXiv:1103.0776](#), [doi:10.1103/PhysRevD.83.123513](#).
- [61] F. Calore, V. De Romeri, F. Donato, Conservative upper limits on WIMP annihilation cross section from Fermi-LAT gamma-rays, Phys.Rev. D85 (2012) 023004, 10 pages, 6 figures Version updated, as sent to PRD. [arXiv:1105.4230](#), [doi:10.1103/PhysRevD.85.023004](#).
- [62] M. Fornasa, J. Zavala, M. A. Sanchez-Conde, J. M. Siegal-Gaskins, T. Delahaye, et al., Characterization of Dark-Matter-induced anisotropies in the diffuse gamma-ray background, MNRAS, 429, 1529. [arXiv:1207.0502](#), [doi:10.1093/mnras/sts444](#).
- [63] M. Di Mauro, A. Cuoco, F. Donato, J. M. Siegal-Gaskins, Fermi-LAT */gamma-ray* anisotropy and intensity explained by unresolved Radio-Loud Active Galactic Nuclei, JCAP 1411 (11) (2014) 021. [arXiv:1407.3275](#), [doi:10.1088/1475-7516/2014/11/021](#).

- [64] M. Ackermann, et al., Limits on Dark Matter Annihilation Signals from the Fermi LAT 4-year Measurement of the Isotropic Gamma-Ray Background [arXiv:1501.05464](#).
- [65] M. Di Mauro, F. Donato, Composition of the Fermi-LAT isotropic gamma-ray background intensity: Emission from extragalactic point sources and dark matter annihilations, *Phys.Rev. D* 91 (2015) 123001. [arXiv:1501.05316](#).
- [66] M. Ackermann, et al., Anisotropies in the diffuse gamma-ray background measured by the Fermi LAT, *Phys.Rev. D* 85 (2012) 083007. [arXiv:1202.2856](#).
- [67] A. Cuoco, E. Komatsu, J. Siegal-Gaskins, Joint anisotropy and source count constraints on the contribution of blazars to the diffuse gamma-ray background, *Phys.Rev. D* 86 (2012) 063004. [arXiv:1202.5309](#), [doi:10.1103/PhysRevD.86.063004](#).
- [68] J. P. Harding, K. N. Abazajian, Models of the Contribution of Blazars to the Anisotropy of the Extragalactic Diffuse Gamma-ray Background, *JCAP* 1211 (2012) 026. [arXiv:1206.4734](#), [doi:10.1088/1475-7516/2012/11/026](#).
- [69] D. Malyshev, D. W. Hogg, Statistics of gamma-ray point sources below the Fermi detection limit, *Astrophys.J.* 738 (2011) 181. [arXiv:1104.0010](#), [doi:10.1088/0004-637X/738/2/181](#).
- [70] J.-Q. Xia, A. Cuoco, E. Branchini, M. Viel, Tomography of the Fermi-lat γ -ray Diffuse Extragalactic Signal via Cross Correlations With Galaxy Catalogs, *Astrophys.J.Suppl.* 217 (1) (2015) 15. [arXiv:1503.05918](#), [doi:10.1088/0067-0049/217/1/15](#).
- [71] M. Shirasaki, S. Horiuchi, N. Yoshida, Cross-Correlation of Cosmic Shear and Extragalactic Gamma-ray Background: Constraints on the Dark Matter Annihilation Cross-Section, *Phys.Rev. D* 90 (6) (2014) 063502. [arXiv:1404.5503](#), [doi:10.1103/PhysRevD.90.063502](#).
- [72] S. Camera, M. Fornasa, N. Fornengo, M. Regis, A Novel Approach in the Weakly Interacting Massive Particle Quest: Cross-correlation of Gamma-Ray Anisotropies and Cosmic Shear, *Astrophys.J.* 771 (2013) L5. [arXiv:1212.5018](#), [doi:10.1088/2041-8205/771/1/L5](#).
- [73] S. Ando, A. Benoit-Lvy, E. Komatsu, Mapping dark matter in the gamma-ray sky with galaxy catalogs, *Phys.Rev. D* 90 (2014) 023514. [arXiv:1312.4403](#), [doi:10.1103/PhysRevD.90.023514](#).
- [74] S. Ando, Power spectrum tomography of dark matter annihilation with local galaxy distribution, *JCAP* 1410 (10) (2014) 061. [arXiv:1407.8502](#), [doi:10.1088/1475-7516/2014/10/061](#).
- [75] S. Camera, M. Fornasa, N. Fornengo, M. Regis, Tomographic-spectral approach for dark matter detection in the cross-correlation between cosmic shear and diffuse γ -ray emission, *JCAP* 1506 (06) (2015) 029. [arXiv:1411.4651](#), [doi:10.1088/1475-7516/2015/06/029](#).

- [76] M. Doro, et al., Dark Matter and Fundamental Physics with the Cherenkov Telescope Array, *Astropart.Phys.* 43 (2013) 189–214. [arXiv:1208.5356](#), [doi:10.1016/j.astropartphys.2012.08.002](#).
- [77] B. Acharya, M. Actis, T. Aghajani, G. Agnetta, J. Aguilar, et al., Introducing the CTA concept, *Astropart.Phys.* 43 (2013) 3–18. [doi:10.1016/j.astropartphys.2013.01.007](#).
- [78] W. Atwood, et al., The Large Area Telescope on the Fermi Gamma-ray Space Telescope Mission, *Astrophys.J.* 697 (2009) 1071–1102. [arXiv:0902.1089](#), [doi:10.1088/0004-637X/697/2/1071](#).
- [79] M. Ackermann, et al., Fermi-LAT Observations of the Diffuse Gamma-Ray Emission: Implications for Cosmic Rays and the Interstellar Medium, *Astrophys.J.* 750 (2012) 3. [arXiv:1202.4039](#), [doi:10.1088/0004-637X/750/1/3](#).
- [80] C. E. Fichtel, G. A. Simpson, D. J. Thompson, Diffuse gamma radiation, *Astrophys.J.* 222 (1978) 883–849.
- [81] A. W. Strong, I. V. Moskalenko, O. Reimer, A New estimate of the extragalactic gamma-ray background from EGRET data [arXiv:astro-ph/0306345](#).
- [82] A. Franceschini, G. Rodighiero, M. Vaccari, The extragalactic optical-infrared background radiations, their time evolution and the cosmic photon-photon opacity, *Astron.Astrophys.* 487 (2008) 837. [arXiv:0805.1841](#), [doi:10.1051/0004-6361:200809691](#).
- [83] A. Dominguez, J. Primack, D. Rosario, F. Prada, R. Gilmore, et al., Extragalactic Background Light Inferred from AEGIS Galaxy SED-type Fractions, *Mon.Not.Ray.Astron.Soc.* 410 (2011) 2556–2578. [arXiv:1007.1459](#).
- [84] M. Ackermann, et al., The Imprint of The Extragalactic Background Light in the Gamma-Ray Spectra of Blazars, *Science* 338 (2012) 1190–1192. [arXiv:1211.1671](#), [doi:10.1126/science.1227160](#).
- [85] A. Abramowski, et al., Measurement of the extragalactic background light imprint on the spectra of the brightest blazars observed with H.E.S.S., *Astron.Astrophys.* 550 (2013) 4. [arXiv:1212.3409](#), [doi:10.1051/0004-6361/201220355](#).
- [86] R. Gilmore, R. Somerville, J. Primack, A. Dominguez, Semi-analytic modeling of the EBL and consequences for extragalactic gamma-ray spectra, *Mon.Not.Roy.Astron.Soc.* 422 (2012) 3189. [arXiv:1104.0671](#), [doi:10.1111/j.1365-2966.2012.20841.x](#).
- [87] A. Domnguez, J. Finke, F. Prada, J. Primack, F. Kitaura, et al., Detection of the cosmic γ -ray horizon from multiwavelength observations of blazars, *Astrophys.J.* 770 (2013) 77. [arXiv:1305.2162](#), [doi:10.1088/0004-637X/770/1/77](#).
- [88] V. Khaire, R. Srianand, Star formation history, dust attenuation and extragalactic background light, *Astrophys.J.* 805 (1) (2015) 33. [arXiv:1405.7038](#), [doi:10.1088/0004-637X/805/1/33](#).
- [89] C. M. Urry, P. Padovani, Unified schemes for radio-loud active galactic nuclei, *Publ.Astron.Soc.Pac.* 107 (1995) 803. [arXiv:astro-ph/9506063](#), [doi:10.1086/133630](#).

- [90] R. D. Blandford, M. J. Rees, Extended and compact extragalactic radio sources - Interpretation and Theory, *Physics Scripta* 17 (1978) 1265–274.
- [91] G. Ghisellini, L. Maraschi, F. Tavecchio, The Fermi blazars’ divide, *Mon.Not.Roy.Astron.Soc.* 396 (2009) L105–109.
- [92] E. T. Meyer, G. Fossati, M. Georganopoulos, M. L. Lister, Collective evidence for Inverse Compton emission from External Photons in High-Power blazars, *Astrophys.J.* 752 (2012) L4. [arXiv:1203.4991](#).
- [93] M. Ackermann, et al., The Second Catalog of Active Galactic Nuclei detected by the Fermi Large Area Telescope, *Astrophys.J.* 743 (2011) 71. [arXiv:1108.1420](#).
- [94] P. Padovani, G. Ghisellini, A. C. Fabian, C. A., Radio-loud AGN and the extragalactic gamma-ray background, *Mon.Not.Roy.Astron.Soc.* 260 (1993) L21–L24.
- [95] T. M. Kneiske, K. Mannheim, BL Lac Contribution to the Extragalactic Gamma-Ray Background, *Astron.Astrophys.* 479 (2008) 41. [arXiv:0705.3778](#), [doi:10.1051/0004-6361:20065605](#).
- [96] R. C. Hartman, et al., The third EGRET Catalog of High-Energy Gamma-Ray Sources, *Astrophys.J.Suppl.* 123 (1999) 79–202.
- [97] H. Falcke, P. L. Biermann, The jet-disk symbiosis. 1. Radio to X-ray emission models for quasars, *Astron.Astrophys.* 293 (1995) 665. [arXiv:astro-ph/9411096](#).
- [98] H. Falcke, E. Koerding, S. Markoff, A Scheme to unify low - power accreting black holes: Jet - dominated accretion flows and the radio / x-ray correlation, *Astron.Astrophys.* 414 (2004) 895–903. [arXiv:astro-ph/0305335](#), [doi:10.1051/0004-6361:20031683](#).
- [99] A. Merloni, S. Heinz, T. Di Matteo, A Fundamental plane of black hole activity, *Mon.Not.Roy.Astron.Soc.* 345 (2003) 1057. [arXiv:astro-ph/0305261](#), [doi:10.1046/j.1365-2966.2003.07017.x](#).
- [100] E. Kording, R. Fender, S. Migliari, Jet-dominated advective systems: radio and x-ray luminosity dependence on the accretion rate, *Mon.Not.Roy.Astron.Soc.* 369 (2006) 1451–1458. [arXiv:astro-ph/0603731](#), [doi:10.1111/j.1365-2966.2006.10383.x](#).
- [101] G. Fossati, A. Celotti, G. Ghisellini, L. Maraschi, Unifying models for x-ray selected and radio selected BL Lac objects, *Mon.Not.Roy.Astron.Soc.* 289 (1997) 136. [arXiv:astro-ph/9704113](#), [doi:10.1093/mnras/289.1.136](#).
- [102] G. Fossati, L. Maraschi, A. Celotti, A. Comastri, G. Ghisellini, A Unifying view of the spectral energy distributions of blazars, *Mon.Not.Roy.Astron.Soc.* 299 (1998) 433–448. [arXiv:astro-ph/9804103](#), [doi:10.1046/j.1365-8711.1998.01828.x](#).
- [103] D. Donato, G. Ghisellini, G. Tagliaferri, G. Fossati, Hard X-ray properties of blazars, *Astron.Astrophys.* 375 (2001) 739–751. [arXiv:astro-ph/0105203](#).
- [104] Y. Ueda, M. Akiyama, K. Ohta, T. Miyaji, Cosmological evolution of the hard x-ray AGN luminosity function and the origin of the hard x-ray background, *Astrophys.J.* 598 (2003) 886–908. [arXiv:astro-ph/0308140](#), [doi:10.1086/378940](#).

- [105] G. Hasinger, T. Miyaji, M. Schmidt, Luminosity-dependent evolution of soft x-ray selected AGN: New Chandra and XMM-Newton surveys, *Astron.Astrophys.* 441 (2005) 417–434. [arXiv:astro-ph/0506118](#), [doi:10.1051/0004-6361:20042134](#).
- [106] R. Gilli, A. Comastri, G. Hasinger, The synthesis of the cosmic X-ray background in the Chandra and XMM-Newton era, *Astron.Astrophys.* [arXiv:astro-ph/0610939](#).
- [107] S. Ando, E. Komatsu, T. Narumoto, T. Totani, Angular power spectrum of gamma-ray sources for GLAST: Blazars and clusters of galaxies, *Mon.Not.Roy.Astron.Soc.* 376 (2007) 1635–1647. [arXiv:astro-ph/0610155](#), [doi:10.1111/j.1365-2966.2007.11421.x](#).
- [108] A. Abdo, et al., Fermi Large Area Telescope First Source Catalog, *Astrophys.J.Suppl.* 188 (2010) 405–436. [arXiv:1002.2280](#), [doi:10.1088/0067-0049/188/2/405](#).
- [109] M. Cavadini, R. Salvaterra, F. Haardt, A New model for the extragalactic γ -ray background [arXiv:1105.4613](#).
- [110] J. Dunlop, J. Peacock, The Redshift Cut-Off in the Luminosity Function of Radio Galaxies and Quasars, *Mon.Not.Roy.Astron.Soc.* 247 (1990) 19.
- [111] J. Chiang, R. Mukherjee, The Luminosity Function of the EGRET Gamma-Ray blazars, *Astrophys.J.* 496 (1998) 752.
- [112] Intensity and origin of the extragalactic gamma-ray background, for the 4th Fermi Symposium, <http://fermi.gsfc.nasa.gov/science/mtgs/symposia/2012/program/thu/MAckermann.pdf>.
- [113] A. Rau, et al., BL Lacertae objects beyond redshift 1.3 = UV-to-NIR photometry and photometric redshift for Fermi-LAT blazars, *Astron.Astrophys.* 538. [arXiv:1112.0025](#).
- [114] M. S. Shaw, R. W. Romani, G. Cotter, S. E. Healey, P. F. Michelson, et al., Spectroscopy of The Largest Ever Gamma-ray Selected BL Lac Sample, *Astrophys.J.* 764 (2013) 135. [arXiv:1301.0323](#), [doi:10.1088/0004-637X/764/2/135](#).
- [115] P. L. Nolan, et al., Fermi Large Area Telescope Second Source Catalog, *Astrophys.J.Suppl.* 199 (2012) 31. [arXiv:1108.1435](#), [doi:10.1088/0067-0049/199/2/31](#).
- [116] P. D. Barthel, Is every quasar beamed?, *Astrophys.J.* 336 (1989) 606. [doi:10.1086/167038](#).
- [117] B. L. Fanaroff, J. M. Riley, The morphology of extragalactic radio sources of high and low luminosity, *Mon.Not.Ray.Astron.Soc.* 167 (1974) 31P–36P.
- [118] A. A. Abdo, et al., Fermi Large Area Telescope observations of Misaligned Active Galactic Nuclei, *Astrophys.J.* 720 (2010) 912–922.
- [119] L. Maraschi, G. Ghisellini, A. Celotti, A jet model for the gamma-ray emitting blazar 3C 279, *Astrophys.J.* 397 (1992) L5–L9. [doi:10.1086/186531](#).

- [120] C. D. Dermer, R. Schlickeiser, Model for the high-energy emission from blazars, *Astrophys.J.* 416 (1993) 458. [doi:10.1086/173251](#).
- [121] G. Ghirlanda, G. Ghisellini, F. Tavecchio, L. Foschini, G. Bonnoli, The radio/gamma-ray connection in Fermi-blazars, *Mon.Not.Roy.Astron.Soc.* 413 (2011) 852–862. [arXiv:1007.2751](#).
- [122] C. J. Willott, S. Rawlings, K. M. Blundell, M. Lacy, S. A. Eales, The radio luminosity function from the low-frequency 3crr, 6ce and 7crs complete samples, *Mon.Not.Roy.Astron.Soc.* 322 (2001) 536–552. [arXiv:astro-ph/0010419](#), [doi:10.1046/j.1365-8711.2001.04101.x](#).
- [123] Z. Yuan, J. Wang, On the Evolution of the Cores of Radio Sources and Their Extended Radio Emission, *Astrophys.J.* 744 (2012) 84. [arXiv:1109.4028](#), [doi:10.1088/0004-637X/744/2/84](#).
- [124] L. Lara, G. Giovannini, W. Cotton, L. Feretti, J. Marcaide, et al., A New sample of large angular size radio galaxies. 3. Statistics and evolution of the grown population, *Astron.Astrophys.* 421 (2004) 899–911. [arXiv:astro-ph/0404373](#), [doi:10.1051/0004-6361:20035676](#).
- [125] A. A. Abdo, et al., Fermi Gamma-Ray Imaging of a Radio Galaxy, *Science* 328 (2010) 725.
- [126] A. A. Abdo, et al., Fermi Large Area Telescope observations of Local Group galaxies: Detection of M31 and search for M33, *Astron.Astrophys.* 523 (2010) A46. [arXiv:1012.1952](#).
- [127] A. Abdo, Observations of the Large Magellanic Cloud with Fermi, *Astron.Astrophys.* 512 (2010) A7. [arXiv:1001.3298](#), [doi:10.1051/0004-6361/200913474](#).
- [128] A. A. Abdo, et al., Detection of the Small Magellanic Cloud in gamma-rays with Fermi/LAT [arXiv:1008.2127](#).
- [129] M. Hayashida, . Stawarz, C. C. Cheung, K. Bechtol, G. M. Madejski, et al., Discovery of GeV Emission from the Circinus Galaxy with the Fermi Large Area Telescope, *Astrophys.J.* 779 (2013) 131. [arXiv:1310.1913](#), [doi:10.1088/0004-637X/779/2/131](#).
- [130] A. Abdo, Detection of Gamma-Ray Emission from the Starburst Galaxies M82 and NGC 253 with the Large Area Telescope on Fermi, *Astrophys.J.* 709 (2010) L152–L157. [arXiv:0911.5327](#), [doi:10.1088/2041-8205/709/2/L152](#).
- [131] A. Abdo, The First Catalog of Active Galactic Nuclei Detected by the Fermi Large Area Telescope, *Astrophys.J.* 715 (2010) 429–457. [arXiv:1002.0150](#), [doi:10.1088/0004-637X/715/1/429](#).
- [132] Q.-W. Tang, X.-Y. Wang, P.-H. Thomas Tam, Discovery of GeV emission from the direction of the luminous infrared galaxy NGC 2146, *Astrophys.J.* 794 (1) (2014) 26. [arXiv:1407.3391](#), [doi:10.1088/0004-637X/794/1/26](#).
- [133] J. Kennicutt, Robert C., Star formation in galaxies along the Hubble sequence, *Ann.Rev.Astron.Astrophys.* 36 (1998) 189–231. [arXiv:astro-ph/9807187](#), [doi:10.1146/annurev.astro.36.1.189](#).

- [134] V. L. Ginzburg, S. L. Syrovatskii, *The Origin of Cosmic Rays*, Pergamon Press, 1964.
- [135] A. Strong, T. Porter, S. Digel, G. Johannesson, P. Martin, et al., Global cosmic-ray related luminosity and energy budget of the Milky Way, *Astrophys.J.* 722 (2010) L58–L63. [arXiv:1008.4330](#), [doi:10.1088/2041-8205/722/1/L58](#).
- [136] E. E. Salpeter, The Luminosity function and stellar evolution, *Astrophys.J.* 121 (1955) 161–167. [doi:10.1086/145971](#).
- [137] N. Bastian, K. R. Covey, M. R. Meyer, A Universal Stellar Initial Mass Function? A Critical Look at Variations, *Ann.Rev.Astron.Astrophys.* 48 (2010) 339–389. [arXiv:1001.2965](#), [doi:10.1146/annurev-astro-082708-101642](#).
- [138] T. A. Thompson, E. Quataert, E. Waxman, The Starburst Contribution to the Extra-Galactic Gamma-Ray Background, *Astrophys.J.* 654 (2006) 219–225. [arXiv:astro-ph/0606665](#), [doi:10.1086/509068](#).
- [139] S. Cole, et al., The 2dF Galaxy Redshift Survey: Near infrared galaxy luminosity functions, *Mon.Not.Roy.Astron.Soc.* 326 (2001) 255. [arXiv:astro-ph/0012429](#), [doi:10.1046/j.1365-8711.2001.04591.x](#).
- [140] A. M. Hopkins, J. F. Beacom, On the normalisation of the cosmic star formation history, *Astrophys.J.* 651 (2006) 142–154. [arXiv:astro-ph/0601463](#), [doi:10.1086/506610](#).
- [141] S. Horiuchi, J. F. Beacom, E. Dwek, The Diffuse Supernova Neutrino Background is detectable in Super-Kamiokande, *Phys.Rev.* D79 (2009) 083013. [arXiv:0812.3157](#), [doi:10.1103/PhysRevD.79.083013](#).
- [142] M. Pohl, On the predictive power of the minimum energy condition. 2: Fractional calorimeter behaviour in the diffuse high energy gamma ray emission of spiral galaxies, *Astron.Astrophys.* 287 (1994) 453–462.
- [143] M. Persic, Y. Rephaeli, Cosmic rays in galaxies: a probe of star formation, *Mon.Not.Roy.Astron.Soc.* 403 (2010) 1569–1576. [arXiv:0912.4156](#), [doi:10.1111/j.1365-2966.2009.16218.x](#).
- [144] V. Pavlidou, B. D. Fields, The Guaranteed gamma-ray background, *Astrophys.J.* 575 (2002) L5–L8. [arXiv:astro-ph/0207253](#), [doi:10.1086/342670](#).
- [145] S. Ando, V. Pavlidou, Imprint of Galaxy Clustering in the Cosmic Gamma-Ray Background, *Mon.Not.Roy.Astron.Soc.* 400 (2009) 2122. [arXiv:0908.3890](#), [doi:10.1111/j.1365-2966.2009.15605.x](#).
- [146] B. C. Lacki, T. A. Thompson, E. Quataert, A. Loeb, E. Waxman, On The GeV and TeV Detections of the Starburst Galaxies M82 and NGC 253, *Astrophys.J.* 734 (2011) 107. [arXiv:1003.3257](#), [doi:10.1088/0004-637X/734/2/107](#).
- [147] M. Schmidt, The Rate of Star Formation, *Astrophys.J.* 129 (1959) 243. [doi:10.1086/146614](#).

- [148] J. Kennicutt, Robert C., P. B. Stetson, A. Saha, D. Kelson, D. M. Rawson, et al., The HST Key Project on the Extragalactic Distance Scale. 13. The Metallicity dependence of the Cepheid distance scale, *Astrophys.J.* 498 (1998) 181. [arXiv:astro-ph/9712055](#), [doi:10.1086/305538](#).
- [149] A. M. Hopkins, On the evolution of star forming galaxies, *Astrophys.J.* 615 (2004) 209. [arXiv:astro-ph/0407170](#), [doi:10.1086/424032](#).
- [150] O. Nakamura, M. Fukugita, J. Brinkmann, D. P. Schneider, The H-alpha luminosity function of morphologically classified galaxies in the Sloan Digital Sky Survey, *Astron.J.* 127 (2004) 2511–2521. [arXiv:astro-ph/0312519](#).
- [151] C. Papovich, S. L. Finkelstein, H. C. Ferguson, J. M. Lotz, M. Giavalisco, The Rising Star-Formation Histories of Distant Galaxies and Implications for Gas Accretion with Time, *Mon.Not.Roy.Astron.Soc.* 412 (2010) 1123–1136. [arXiv:1007.4554](#).
- [152] F. Elsner, G. Feulner, U. Hopp, The impact of Spitzer infrared data on stellar mass estimates - and a revised galaxy stellar mass function at $0 < z < 5$, *Astron.Astrophys.* 477 (2008) 503–5121. [arXiv:0711.0384](#).
- [153] A. K. Leroy, F. Walter, E. Brinks, F. Bigiel, W. de Blok, et al., The Star Formation Efficiency in Nearby Galaxies: Measuring Where Gas Forms Stars Effectively, *Astron.J.* 136 (2008) 2782–2845. [arXiv:0810.2556](#), [doi:10.1088/0004-6256/136/6/2782](#).
- [154] K. Nagamine, J. P. Ostriker, M. Fukugita, R. Cen, The history of cosmological star formation: three independent approaches and a critical test using the extragalactic background light, *Astrophys.J.* 653 (2006) 881–893. [arXiv:astro-ph/0603257](#), [doi:10.1086/508765](#).
- [155] M. S. Yun, N. A. Reddy, J. J. Condon, Radio properties of infrared selected galaxies in the IRAS 2 Jy sample, *Astrophys.J.* 554 (2001) 803. [arXiv:astro-ph/0102154](#), [doi:10.1086/323145](#).
- [156] H. Dole, G. Lagache, J.-L. Puget, K. I. Caputi, N. Fernandez-Conde, et al., The cosmic infrared background resolved by spitzer. contributions of mid-infrared galaxies to the far-infrared background, *Astron.Astrophys.* 451 (2006) 417–429. [arXiv:astro-ph/0603208](#), [doi:10.1051/0004-6361:20054446](#).
- [157] F. W. Stecker, Are Diffuse High Energy Neutrinos from Starburst Galaxies Observable?, *Astropart.Phys.* 26 (2007) 398–401. [arXiv:astro-ph/0607197](#), [doi:10.1016/j.astropartphys.2006.08.002](#).
- [158] P. F. Hopkins, J. D. Younger, C. C. Hayward, D. Narayanan, L. Hernquist, Mergers, AGN, and 'Normal' Galaxies: Contributions to the Distribution of Star Formation Rates and Infrared Luminosity Functions, *Mon.Not.Roy.Astron.Soc.* 402 (2010) 1693–1713. [arXiv:0911.1131](#).
- [159] M. Nagashima, Y. Yoshii, Hierarchical formation of galaxies with dynamical response to supernova - induced gas removal, *Astrophys.J.* 610 (2004) 23–44. [arXiv:astro-ph/0404485](#), [doi:10.1086/421484](#).

- [160] M. Nagashima, H. Yahagi, M. Enoki, Y. Yoshii, N. Gouda, Numerical galaxy catalog. 1. A Semi-analytic model of galaxy formation with N-body simulations, *Astrophys.J.* 634 (2005) 26–50. [arXiv:astro-ph/0508085](#), [doi:10.1086/496872](#).
- [161] I. Tamborra, S. Ando, K. Murase, Star-forming galaxies as the origin of diffuse high-energy backgrounds: Gamma-ray and neutrino connections, and implications for starburst history, *JCAP* 1409 (09) (2014) 043. [arXiv:1404.1189](#), [doi:10.1088/1475-7516/2014/09/043](#).
- [162] G. Rodighiero, et al., Mid- and far-infrared luminosity functions and galaxy evolution from multiwavelength Spitzer observations up to $z=2.5$, *Astron.Astrophys.* 515. [arXiv:0910.5649](#).
- [163] V. Acciari, E. Aliu, T. Arlen, T. Aune, M. Bautista, et al., A connection between star formation activity and cosmic rays in the starburst galaxy M 82, *Nature* 462 (2009) 770–772. [arXiv:0911.0873](#), [doi:10.1038/nature08557](#).
- [164] C. Gruppioni, P. F., R. G., et al., The Herschel PEP/HerMES luminosity function - I. Probing the evolution of PACS selected Galactic to $z=4$, *Mon.Not.Roy.Astron.Soc.* 432 (2013) 23–52. [arXiv:1302.5209](#).
- [165] M. J. Devlin, P. A. Ade, I. Aretxaga, J. J. Bock, E. L. Chapin, et al., Over half of the far-infrared background light comes from galaxies at $z < 1.2$, *Nature* 458 (2009) 737–739. [arXiv:0904.1201](#), [doi:10.1038/nature07918](#).
- [166] M. Bethermin, E. L. Floc'h, O. Ilbert, A. Conley, G. Lagache, et al., HerMES: deep number counts at 250, 350, and 500 microns in the COSMOS and GOODS-N fields and the build-up of the cosmic infrared background, *Astron.Astrophys.* 542. [arXiv:1203.1925](#).
- [167] A. Barger, W.-H. Wang, L. Cowie, F. Owen, C.-C. Chen, et al., Precise Identifications of Submillimeter Galaxies: Measuring the History of Massive Star-Forming Galaxies to $z < 5$, *Astrophys.J.* 761 (2012) 89. [arXiv:1209.1626](#), [doi:10.1088/0004-637X/761/2/89](#).
- [168] C.-Y. Ng, J. Takata, G. Leung, K. Cheng, P. Philippopoulos, High-Energy Emission of the First Millisecond Pulsar, *Astrophys.J.* 787 (2014) 167. [arXiv:1405.2148](#), [doi:10.1088/0004-637X/787/2/167](#).
- [169] T. Gregoire, J. Knudsen, Constraining the Galactic millisecond pulsar population using Fermi Large Area Telescope, *Astron.Astrophys.* 554 (2013) A62. [arXiv:1305.1584](#), [doi:10.1051/0004-6361/201219676](#).
- [170] A. Abdo, et al., The Second Fermi Large Area Telescope Catalog of Gamma-ray Pulsars, *Astrophys.J.Suppl.* 208 (2013) 17. [arXiv:1305.4385](#), [doi:10.1088/0067-0049/208/2/17](#).
- [171] G. Benford, R. Buschauer, Coherent pulsar radio radiation by antenna mechanisms - General theory, *Mon.Not.Roy.Astron.Soc.* 179 (1977) 189–207.
- [172] R. T. Gangadhara, Circular polarization in pulsars due to curvature radiation, *Astrophys.J.* 710 (2010) 29–44.

- [173] P. Wang, C. Wang, J. Han, Curvature Radiation in Rotating Pulsar Magnetosphere, *Mon.Not.Roy.Astron.Soc.* 423 (2012) 2464. [arXiv:1203.5995](#), [doi:10.1111/j.1365-2966.2012.21053.x](#).
- [174] M. Kerr, the Fermi-LAT Collaboration, Pulsars in gamma rays: what Fermi is teaching us, *IAU Symp.* 291 (2012) 307–312. [arXiv:1211.3726](#).
- [175] M. A. Alpar, A. F. Cheng, J. Ruderman, M. A. Shanan, A new class of radio pulsars, *Nature* 300 (1982) 728–730.
- [176] E. Phinney, S. Kulkarni, Binary and millisecond pulsars, *Ann.Rev.Astron.Astrophys.* 32 (1994) 591–639. [doi:10.1146/annurev.aa.32.090194.003111](#).
- [177] D. Lorimer, Binary and millisecond pulsars at the new millennium, *Living Rev.Rel.* 4 (2001) 5. [arXiv:astro-ph/0104388](#).
- [178] D. Lorimer, Binary and Millisecond Pulsars, *Living Rev.Rel.* 11 (2008) 8. [arXiv:0811.0762](#).
- [179] B. Kiziltan, S. E. Thorsett, Millisecond Pulsar Ages: Implications of Binary Evolution and a Maximum Spin Limit, *Astrophys.J.* 715 (2010) 335–341. [arXiv:0909.1562](#), [doi:10.1088/0004-637X/715/1/335](#).
- [180] A. G. Lyne, R. N. Manchester, D. R. Lorimer, M. Bailes, et al., The Parkes Southern Pulsar Survey - II. Final results and population analysis, *Mon.Not.Roy.Astron.Soc.* 295 (1998) 743–755.
- [181] J. Arons, Pulsars as gamma-ray sources, *Astron.Astrophys.Suppl.* 120 (1996) 49–60.
- [182] M. Ruderman, P. Sutherland, Theory of pulsars: Polar caps, sparks, and coherent microwave radiation, *Astrophys.J.* 196 (1975) 51. [doi:10.1086/153393](#).
- [183] A. K. Harding, Pulsar gamma-rays - Spectra, luminosities and efficiencies, *Astrophys.J.* 245 (1981) 267–273.
- [184] C.-A. Faucher-Giguere, V. M. Kaspi, Birth and evolution of isolated radio pulsars, *Astrophys.J.* 643 (2006) 332–355. [arXiv:astro-ph/0512585](#), [doi:10.1086/501516](#).
- [185] D. R. Lorimer, The Galactic Millisecond Pulsar Population, *IAU Symp.* 291 (2013) 237. [arXiv:1210.2746](#), [doi:10.1017/S1743921312023769](#).
- [186] M. McLaughlin, J. Cordes, The gamma-ray pulsar population, *Astrophys.J.* 538 (2000) 818. [arXiv:astro-ph/9912409](#), [doi:10.1086/309174](#).
- [187] J. Cordes, D. F. Chernoff, Neutron star population dynamics. I: Millisecond pulsars, *Astrophys.J.* 482 (1997) 971–992. [arXiv:astro-ph/9706162](#), [doi:10.1086/304179](#).
- [188] S. A. Story, P. L. Gonthier, A. K. Harding, Population synthesis of radio and gamma-ray millisecond pulsars from the Galactic disk, *Astrophys.J.* 671 (2007) 713–726. [arXiv:0706.3041](#), [doi:10.1086/521016](#).

- [189] R. N. Manchester, G. B. Hobbs, A. Teoh, M. Hobbs, The Australia Telescope National Facility pulsar catalogue, *Astron.J.* 129 (2005) 1993. [arXiv:astro-ph/0412641](#), [doi:10.1086/428488](#).
- [190] R. N. Manchester, L. A. G., N. D’Amico, M. Bailes, J. S., et al., The Parkes Southern Pulsar Survey - I. Observing and data analysis systems and initial results, *Mon.Not.Roy.Astron.Soc.* 279 (1996) 1235–1250.
- [191] G. M. Voit, S. T. Kay, G. L. Bryan, The baseline intracluster entropy profile from gravitational structure formation, *Mon.Not.Roy.Astron.Soc.* 364 (2005) 909–916. [arXiv:astro-ph/0511252](#), [doi:10.1111/j.1365-2966.2005.09621.x](#).
- [192] R. J. van Weerer, M. Bruggen, H. J. A. Rottgering, M. Hoeft, S. E. Nuza, H. T. Intema, Radio emission observations of new radio halos and relics from the NVSS and WENNS surveys. Relic orientations, cluster X-ray luminosities and redshift distribution, *Astron.Astrophys.* 533. [arXiv:1107.5597](#).
- [193] A., S. P. Oh, C. Pfrommer, Giant radio relics in galaxy clusters: reacceleration of fossil relativistic electrons?, *Mon.Not.Roy.Astron.Soc.* 435 (2013) 1061–10825. [arXiv:1301.5644](#).
- [194] B. M. Deis, W. Reich, H. Lesch, R. Wielebinski, The large-scale structure of the diffuse radio halo of the Coma cluster at 1.4 GHz, *Astron.Astrophys.* 321 (1997) 55–63. [arXiv:astro-ph/9609189](#).
- [195] S. Brown, L. Rudnick, Diffuse radio emission in/around the Coma cluster: beyond simple accretion, *Mon.Not.Roy.Astron.Soc.* 412 (2011) 2–12. [arXiv:1009.4258](#).
- [196] G. Brunetti, R. Cassano, K. Dolag, G. Setti, On the evolution of giant radio halos and their connection with cluster mergers, *Astron.Astrophys.* 507 (2009) 661. [arXiv:0909.2343](#), [doi:10.1051/0004-6361/200912751](#).
- [197] R. Cassano, S. Ettori, G. Brunetti, S. Giacintucci, G. Pratt, et al., Revisiting scaling relations for giant radio halos in galaxy clusters, *Astrophys.J.* 777 (2013) 141. [arXiv:1306.4379](#), [doi:10.1088/0004-637X/777/2/141](#).
- [198] A. Loeb, E. Waxman, Gamma-ray background from structure formation in the intergalactic medium, *Nature* 405 (2000) 156. [arXiv:astro-ph/0003447](#), [doi:10.1038/35012018](#).
- [199] T. Totani, T. Kitayama, Forming clusters of galaxies as the origin of unidentified GeV gamma-ray sources, *Astrophys.J.* 545 (2000) 572–577. [arXiv:astro-ph/0006176](#), [doi:10.1086/317872](#).
- [200] W. H. Press, P. Schechter, Formation of galaxies and clusters of galaxies by selfsimilar gravitational condensation, *Astrophys.J.* 187 (1974) 425–438. [doi:10.1086/152650](#).
- [201] A. Cooray, R. K. Sheth, Halo models of large scale structure, *Phys.Rept.* 372 (2002) 1–129. [arXiv:astro-ph/0206508](#), [doi:10.1016/S0370-1573\(02\)00276-4](#).
- [202] U. Keshet, E. Waxman, A. Loeb, V. Springel, L. Hernquist, Gamma-rays from intergalactic shocks, *Astrophys.J.* 585 (2003) 128–150. [arXiv:astro-ph/0202318](#), [doi:10.1086/345946](#).

- [203] C. Pfrommer, T. Ensslin, V. Springel, Simulating cosmic rays in clusters of galaxies - II. A unified scheme for radio halos and relics with predictions of the gamma-ray emission, *Mon.Not.Roy.Astron.Soc.* 385 (2008) 1211–1241. [arXiv:0707.1707](#).
- [204] S. Gabici, P. Blasi, The Gamma-ray background from large scale structure formation, *Astropart.Phys.* 19 (2003) 679–689. [arXiv:astro-ph/0211573](#), [doi:10.1016/S0927-6505\(03\)00106-3](#).
- [205] F. Miniati, Inter-Galactic shock acceleration and the cosmic gamma-ray background, *Mon.Not.Roy.Astron.Soc.* 337 (2002) 199. [arXiv:astro-ph/0203014](#), [doi:10.1046/j.1365-8711.2002.05903.x](#).
- [206] S. Gabici, P. Blasi, On the Detectability of gamma-rays from clusters of galaxies: Mergers versus secondary infall, *Astropart.Phys.* 20 (2004) 579–590. [arXiv:astro-ph/0306369](#), [doi:10.1016/j.astropartphys.2003.09.002](#).
- [207] K. Kashiyama, P. Meszaros, Galaxy Mergers as a Source of Cosmic Rays, Neutrinos, and Gamma Rays, *Astrophys.J.* 790 (2014) L14. [arXiv:1405.3262](#), [doi:10.1088/2041-8205/790/1/L14](#).
- [208] F. Zandanel, S. Ando, Constraints on diffuse gamma-ray emission from structure formation processes in the Coma cluster, *Mon.Not.Roy.Astron.Soc.* 440 (2014) 663–671. [arXiv:1312.1493](#), [doi:10.1093/mnras/stu324](#).
- [209] S. Colafrancesco, P. Blasi, Clusters of galaxies and the diffuse gamma-ray background, *Astropart.Phys.* 9 (1998) 227–246. [arXiv:astro-ph/9804262](#), [doi:10.1016/S0927-6505\(98\)00018-8](#).
- [210] S. Ando, D. Nagai, Gamma-ray probe of cosmic-ray pressure in galaxy clusters and cosmological implications, *Mon.Not.Roy.Astron.Soc.* 385 (2008) 2243–2253. [arXiv:0705.2588](#), [doi:10.1111/j.1365-2966.2008.12996.x](#).
- [211] F. Zandanel, F. Prada, A Phenomenological Model for the Intracluster Medium that matches X-ray and Sunyaev-Zel’dovich observations, *Mon.Not.Roy.Astron.Soc.* 438 (2014) 116–123. [arXiv:1311.4793](#), [doi:10.1093/mnras/stt2196](#).
- [212] G. Giovannini, M. Tordi, L. Feretti, Radio halo and relic candidates from the nrao vla sky survey, *New Astron.* 4 (1999) 141. [arXiv:astro-ph/9904210](#), [doi:10.1016/S1384-1076\(99\)00018-4](#).
- [213] J. Aleksic, et al., Constraining Cosmic Rays and Magnetic Fields in the Perseus Galaxy Cluster with TeV observations by the MAGIC telescopes, *Astron.Astrophys.* 541 (2012) A99. [arXiv:1111.5544](#), [doi:10.1051/0004-6361/201118502](#).
- [214] K. Greisen, End to the cosmic ray spectrum?, *Phys.Rev.Lett.* 16 (1966) 748–750. [doi:10.1103/PhysRevLett.16.748](#).
- [215] G. Zatsepin, V. Kuzmin, Upper limit of the spectrum of cosmic rays, *JETP Lett.* 4 (1966) 78–80.
- [216] P. S. Coppi, F. A. Aharonian, Constraints on the VHE emissivity of the universe from the diffuse GeV gamma-ray background, *Astrophys.J.* 487 (1997) L9–L12. [arXiv:astro-ph/9610176](#), [doi:10.1086/310883](#).

- [217] I. Cholis, D. Hooper, S. D. McDermott, Dissecting the Gamma-Ray Background in Search of Dark Matter, JCAP 1402 (2014) 014. [arXiv:1312.0608](#), [doi:10.1088/1475-7516/2014/02/014](#).
- [218] J. Whelan, I. J. Iben, Binaries and Supernovae of Type I, *Astrophys.J.* 186 (1973) 1007–1014.
- [219] J. Iben, I., A. Tutukov, Supernovae of type I as end products of the evolution of binaries with components of moderate initial mass (M not greater than about 9 solar masses), *Astrophys.J.Suppl.* 54 (1984) 335–372. [doi:10.1086/190932](#).
- [220] K. Ahn, E. Komatsu, P. Hoflich, Cosmic gamma-ray background from Type Ia supernovae revisited: Evidence for missing gamma-rays at MeV, *Phys.Rev.* D71 (2005) 121301. [arXiv:astro-ph/0506126](#), [doi:10.1103/PhysRevD.71.121301](#).
- [221] L. E. Strigari, J. F. Beacom, T. P. Walker, P. Zhang, The Concordance Cosmic Star Formation Rate: Implications from and for the supernova neutrino and gamma ray backgrounds, JCAP 0504 (2005) 017. [arXiv:astro-ph/0502150](#), [doi:10.1088/1475-7516/2005/04/017](#).
- [222] Y. Rasera, R. Teyssier, P. Sizun, B. Cordier, J. Paul, et al., Soft gamma-ray background and light dark matter annihilation, *Phys.Rev.* D73 (2006) 103518. [arXiv:astro-ph/0507707](#), [doi:10.1103/PhysRevD.73.103518](#).
- [223] M. G. Baring, A. K. Harding, Magnetic photon splitting: Computations of proper time rates and spectra, *Astrophys.J.* 482 (1997) 372. [arXiv:astro-ph/9704210](#), [doi:10.1086/304152](#).
- [224] Y. Lithwick, R. Sari, Lower limits on Lorentz factors in gamma-ray bursts, *Astrophys.J.* 555 (2001) 540–545. [arXiv:astro-ph/0011508](#), [doi:10.1086/321455](#).
- [225] B. Zhang, Y. Z. Fan, J. Dyks, S. Kobayashi, P. Meszaros, et al., Physical processes shaping GRB x-ray afterglow lightcurves: Theoretical implications from the SWIFT XRT observations, *Astrophys.J.* 642 (2006) 354–370. [arXiv:astro-ph/0508321](#), [doi:10.1086/500723](#).
- [226] P. Meszaros, The Fireball shock model of gamma-ray bursts, *AIP Conf.Proc.* 526 (2000) 514–518. [arXiv:astro-ph/9912474](#), [doi:10.1063/1.1361591](#).
- [227] S. Casanova, B. Dingus, B. Zhang, Contribution of GRB emission to the GeV extragalactic diffuse gamma-ray flux, *AIP Conf.Proc.* 1000 (2008) 40–43. [doi:10.1063/1.2943497](#).
- [228] T. Le, C. D. Dermer, Gamma-ray burst predictions for the Fermi Gamma Ray Space Telescope, *Astrophys.J.* 700 (2009) 1026–1033. [arXiv:0807.0355](#).
- [229] M. Schmidt, Luminosities and space densities of gamma-ray bursts, *Astrophys.J.* 523 (1999) L117–L120. [arXiv:astro-ph/9908206](#), [doi:10.1086/312281](#).
- [230] S. Ando, E. Nakar, R. Sari, GeV Emission from Prompt and Afterglow Phases of Gamma-Ray Bursts, *Astrophys.J.* 689 (2008) 1150. [arXiv:0807.0012](#), [doi:10.1086/592486](#).

- [231] I. V. Moskalenko, T. A. Porter, Isotropic Gamma-Ray Background: Cosmic-Ray Induced Albedo from Debris in the Solar System?, *Astrophys.J.* 692 (2009) 54–57. [arXiv:0901.0304](#), [doi:10.1088/0004-637X/692/1/L54](#).
- [232] R. Mahadevan, R. Narayan, J. Krolik, Gamma-ray emission from advection-dominated accretion flows around black holes: application to the Galactic Center, *Astrophys.J.* 486 (1997) 268–285. [arXiv:astro-ph/9704018](#).
- [233] K. Oka, T. Manmoto, Gamma-ray emission from an accretion flow around a Kerr black hole, *Mon.Not.Roy.Astron.Soc.* 340 (2003) 543–550.
- [234] S. H. Teng, R. F. Mushotzky, R. M. Sambruna, D. S. Davis, C. S. Reynolds, Fermi/LAT Observations of Swift/BAT Seyferts: on the Contribution of Radio-quiet AGN to the Extragalactic Gamma-ray Background, *Astrophys.J.* 742 (2011) 66. [arXiv:1109.2734](#), [doi:10.1088/0004-637X/742/2/66](#).
- [235] Y. Inoue, T. Totani, Y. Ueda, The Cosmic MeV Gamma-ray Background and Hard X-ray Spectra of Active Galactic Nuclei: Implications for the Origin of Hot AGN Coronae, *Astrophys.J.* 672 (2008) L5. [arXiv:0709.3877](#), [doi:10.1086/525848](#).
- [236] A. Galeev, R. Rosner, G. Vaiana, Structured coronae of accretion disks, *Astrophys.J.* 229 (1979) 318–326. [doi:10.1086/156957](#).
- [237] B. F. Liu, S. Mineshige, K. Shibata, A simple model for a magnetic reconnection-heated corona, *Astrophys.J.* 572 (2002) L173–L176. [arXiv:astro-ph/0205257](#).
- [238] U. Keshet, E. Waxman, A. Loeb, The Case for a low extragalactic gamma-ray background, *JCAP* 0404 (2004) 006. [arXiv:astro-ph/0306442](#), [doi:10.1088/1475-7516/2004/04/006](#).
- [239] R. Feldmann, D. Hooper, N. Y. Gnedin, Circum-Galactic Gas and the Isotropic Gamma Ray Background, *Astrophys.J.* 763 (2013) 21. [arXiv:1205.0249](#), [doi:10.1088/0004-637X/763/1/21](#).
- [240] M. E. Anderson, J. N. Bregman, Detection of a Hot Gaseous Halo Around the Giant Spiral Galaxy NGC 1961, *Astrophys.J.* 737 (2011) 22. [arXiv:1105.4614](#), [doi:10.1088/0004-637X/737/1/22](#).
- [241] N. Y. Gnedin, A. V. Kravtsov, Environmental Dependence of the Kennicutt-Schmidt Relation in Galaxies, *Astrophys.J.* 728 (2011) 88. [arXiv:1004.0003](#), [doi:10.1088/0004-637X/728/2/88](#).
- [242] R. Feldmann, N. Gnedin, A. Kravtsov, How Universal is the SFR - H₂ Relation?, *Astrophys.J.* 732 (2011) 115. [arXiv:1010.1539](#), [doi:10.1088/0004-637X/732/2/115](#).
- [243] N. I. Gnedin, J. P. Ostriker, Light elements nucleosynthesis - a false clue?, *Astrophys.J.* 400 (1992) 1–20.
- [244] D. N. Page, S. Hawking, Gamma rays from primordial black holes, *Astrophys.J.* 206 (1976) 1–7. [doi:10.1086/154350](#).
- [245] J. H. MacGibbon, B. J. Carr, Cosmic rays from primordial black holes, *Astrophys.J.* 371 (1991) 447–469. [doi:10.1086/169909](#).

- [246] F. Stecker, D. Morgan, J. Bredekamp, Possible evidence for the existence of antimatter on a cosmological scale in the universe, *Phys.Rev.Lett.* 27 (1971) 1469–1472. [doi:10.1103/PhysRevLett.27.1469](#).
- [247] P. Bhattacharjee, Q. Shafi, F. Stecker, TeV and superheavy mass scale particles from supersymmetric topological defects, the extragalactic gamma-ray background, and the highest energy cosmic rays, *Phys.Rev.Lett.* 80 (1998) 3698–3701. [arXiv:hep-ph/9710533](#), [doi:10.1103/PhysRevLett.80.3698](#).
- [248] T. Bringmann, F. Calore, M. Di Mauro, F. Donato, Constraining dark matter annihilation with the isotropic γ -ray background: updated limits and future potential, *Phys.Rev.* D89 (2014) 023012. [arXiv:1303.3284](#), [doi:10.1103/PhysRevD.89.023012](#).
- [249] M. Taoso, G. Bertone, A. Masiero, Dark Matter Candidates: A Ten-Point Test, *JCAP* 0803 (2008) 022. [arXiv:0711.4996](#), [doi:10.1088/1475-7516/2008/03/022](#).
- [250] G. Jungman, M. Kamionkowski, K. Griest, Supersymmetric dark matter, *Phys.Rept.* 267 (1996) 195–373. [arXiv:hep-ph/9506380](#), [doi:10.1016/0370-1573\(95\)00058-5](#).
- [251] S. P. Martin, A Supersymmetry primer, *Adv.Ser.Direct.High Energy Phys.* 21 (2010) 1–153. [arXiv:hep-ph/9709356](#), [doi:10.1142/9789814307505_0001](#).
- [252] D. Hooper, S. Profumo, Dark matter and collider phenomenology of universal extra dimensions, *Phys.Rept.* 453 (2007) 29–115. [arXiv:hep-ph/0701197](#), [doi:10.1016/j.physrep.2007.09.003](#).
- [253] G. Bertone, The moment of truth for WIMP Dark Matter, *Nature* 468 (2010) 389–393. [arXiv:1011.3532](#), [doi:10.1038/nature09509](#).
- [254] P. Ade, et al., Planck 2013 results. XVI. Cosmological parameters, *Astron.Astrophys.* [arXiv:1303.5076](#), [doi:10.1051/0004-6361/201321591](#).
- [255] S. Palomares-Ruiz, J. M. Siegal-Gaskins, Annihilation vs. Decay: Constraining dark matter properties from a gamma-ray detection, *JCAP* 1007 (2010) 023. [arXiv:1003.1142](#), [doi:10.1088/1475-7516/2010/07/023](#).
- [256] S. Campbell, B. Dutta, E. Komatsu, Effects of Velocity-Dependent Dark Matter Annihilation on the Energy Spectrum of the Extragalactic Gamma-ray Background, *Phys.Rev.* D82 (2010) 095007. [arXiv:1009.3530](#), [doi:10.1103/PhysRevD.82.095007](#).
- [257] S. Campbell, B. Dutta, Effects of P-wave Annihilation on the Angular Power Spectrum of Extragalactic Gamma-rays from Dark Matter Annihilation, *Phys.Rev.* D84 (2011) 075004. [arXiv:1106.4621](#), [doi:10.1103/PhysRevD.84.075004](#).
- [258] S. Hofmann, D. J. Schwarz, H. Stoecker, Damping scales of neutralino cold dark matter, *Phys.Rev.* D64 (2001) 083507. [arXiv:astro-ph/0104173](#), [doi:10.1103/PhysRevD.64.083507](#).
- [259] A. Loeb, M. Zaldarriaga, The Small-scale power spectrum of cold dark matter, *Phys.Rev.* D71 (2005) 103520. [arXiv:astro-ph/0504112](#), [doi:10.1103/PhysRevD.71.103520](#).

- [260] A. M. Green, S. Hofmann, D. J. Schwarz, The First wimpy halos, JCAP 0508 (2005) 003. [arXiv:astro-ph/0503387](#), [doi:10.1088/1475-7516/2005/08/003](#).
- [261] T. Bringmann, Particle Models and the Small-Scale Structure of Dark Matter, New J.Phys. 11 (2009) 105027. [arXiv:0903.0189](#), [doi:10.1088/1367-2630/11/10/105027](#).
- [262] S. Profumo, K. Sigurdson, P. Ullio, M. Kamionkowski, A Running spectral index in supersymmetric dark-matter models with quasi-stable charged particles, Phys.Rev. D71 (2005) 023518. [arXiv:astro-ph/0410714](#), [doi:10.1103/PhysRevD.71.023518](#).
- [263] J. M. Cornell, S. Profumo, W. Shepherd, Kinetic Decoupling and Small-Scale Structure in Effective Theories of Dark Matter, Phys.Rev. D88 (1) (2013) 015027. [arXiv:1305.4676](#), [doi:10.1103/PhysRevD.88.015027](#).
- [264] E. Sefusatti, G. Zaharijas, P. D. Serpico, D. Theurel, M. Gustafsson, Extragalactic gamma-ray signal from dark matter annihilation: an appraisal, Mon.Not.Roy.Astron.Soc. 441 (2014) 1861–1878. [arXiv:1401.2117](#), [doi:10.1093/mnras/stu686](#).
- [265] J. S. Bullock, T. S. Kolatt, Y. Sigad, R. S. Somerville, A. V. Kravtsov, et al., Profiles of dark haloes. Evolution, scatter, and environment, Mon.Not.Roy.Astron.Soc. 321 (2001) 559–575. [arXiv:astro-ph/9908159](#), [doi:10.1046/j.1365-8711.2001.04068.x](#).
- [266] A. V. Maccio', A. A. Dutton, F. C. d. Bosch, Concentration, Spin and Shape of Dark Matter Haloes as a Function of the Cosmological Model: WMAP1, WMAP3 and WMAP5 results, Mon.Not.Roy.Astron.Soc. 391 (2008) 1940–1954. [arXiv:0805.1926](#), [doi:10.1111/j.1365-2966.2008.14029.x](#).
- [267] F. Prada, A. A. Klypin, A. J. Cuesta, J. E. Betancort-Rijo, J. Primack, Halo concentrations in the standard LCDM cosmology, Mon.Not.Roy.Astron.Soc. 428 (2012) 3018–3030. [arXiv:1104.5130](#), [doi:10.1111/j.1365-2966.2012.21007.x](#).
- [268] R. H. Wechsler, J. S. Bullock, J. R. Primack, A. V. Kravtsov, A. Dekel, Concentrations of dark halos from their assembly histories, Astrophys.J. 568 (2002) 52–70. [arXiv:astro-ph/0108151](#), [doi:10.1086/338765](#).
- [269] K. Dolag, M. Bartelmann, F. Perrotta, C. Baccigalupi, L. Moscardini, et al., Numerical study of halo concentrations in dark - energy cosmologies, Astron.Astrophys. 416 (2004) 853–864. [arXiv:astro-ph/0309771](#), [doi:10.1051/0004-6361:20031757](#).
- [270] M. Kuhlen, M. Vogelsberger, R. Angulo, Numerical Simulations of the Dark Universe: State of the Art and the Next Decade, Phys.Dark Univ. 1 (2012) 50–93. [arXiv:1209.5745](#), [doi:10.1016/j.dark.2012.10.002](#).
- [271] V. Springel, J. Wang, M. Vogelsberger, A. Ludlow, A. Jenkins, et al., The Aquarius Project: the subhalos of galactic halos, Mon.Not.Roy.Astron.Soc. 391 (2008) 1685–1711. [arXiv:0809.0898](#), [doi:10.1111/j.1365-2966.2008.14066.x](#).

- [272] A. F. Neto, L. Gao, P. Bett, S. Cole, J. F. Navarro, et al., The statistics of Λ CDM Halo Concentrations, *Mon.Not.Roy.Astron.Soc.* 381 (2007) 1450–1462. [arXiv:0706.2919](#), [doi:10.1111/j.1365-2966.2007.12381.x](#).
- [273] A. R. Duffy, J. Schaye, S. T. Kay, C. Dalla Vecchia, Dark matter halo concentrations in the Wilkinson Microwave Anisotropy Probe year 5 cosmology, *Mon.Not.Roy.Astron.Soc.* 390 (2008) L64. [arXiv:0804.2486](#).
- [274] L. Pieri, G. Bertone, E. Branchini, Dark Matter Annihilation in Substructures Revised, *Mon.Not.Roy.Astron.Soc.* 384 (2008) 1627. [arXiv:0706.2101](#), [doi:10.1111/j.1365-2966.2007.12828.x](#).
- [275] A. Pinzke, C. Pfrommer, L. Bergstrom, Prospects of detecting gamma-ray emission from galaxy clusters: cosmic rays and dark matter annihilations, *Phys.Rev. D* 84 (2011) 123509. [arXiv:1105.3240](#), [doi:10.1103/PhysRevD.84.123509](#).
- [276] L. Gao, C. Frenk, A. Jenkins, V. Springel, S. White, Where will supersymmetric dark matter first be seen?, *Mon.Not.Roy.Astron.Soc.* 419 (2012) 1721. [arXiv:1107.1916](#), [doi:10.1111/j.1365-2966.2011.19836.x](#).
- [277] T. Ishiyama, Hierarchical Formation of Dark Matter Halos and the Free Streaming Scale, *Astrophys.J.* 788 (2014) 27. [arXiv:1404.1650](#), [doi:10.1088/0004-637X/788/1/27](#).
- [278] J. Diemand, B. Moore, J. Stadel, Earth-mass dark-matter haloes as the first structures in the early Universe, *Nature* 433 (2005) 389–391. [arXiv:astro-ph/0501589](#), [doi:10.1038/nature03270](#).
- [279] D. Anderhalden, J. Diemand, Density Profiles of CDM Microhalos and their Implications for Annihilation Boost Factors, *JCAP* 1304 (2013) 009. [arXiv:1302.0003](#), [doi:10.1088/1475-7516/2013/04/009](#), [doi:10.1088/1475-7516/2013/08/E02](#).
- [280] M. A. Sanchez-Conde, F. Prada, The flattening of the concentration-mass relation towards low halo masses and its implications for the annihilation signal boost, *Mon.Not.Roy.Astron.Soc.* 442 (2014) 2271–2277. [arXiv:1312.1729](#).
- [281] A. D. Ludlow, J. F. Navarro, R. E. Angulo, M. Boylan-Kolchin, V. Springel, et al., The Mass-Concentration-Redshift Relation of Cold Dark Matter Halos, *Mon.Not.Roy.Astron.Soc.* 441 (2013) 378–388. [arXiv:1312.0945](#).
- [282] K. J. Mack, Known Unknowns of Dark Matter Annihilation over Cosmic Time, *Mon.Not.Roy.Astron.Soc.* 439 (2014) 2728. [arXiv:1309.7783](#), [doi:10.1093/mnras/stu129](#).
- [283] A. Jenkins, C. Frenk, S. D. White, J. Colberg, S. Cole, et al., The Mass function of dark matter halos, *Mon.Not.Roy.Astron.Soc.* 321 (2001) 372. [arXiv:astro-ph/0005260](#), [doi:10.1046/j.1365-8711.2001.04029.x](#).
- [284] V. Springel, S. D. White, A. Jenkins, C. S. Frenk, N. Yoshida, et al., Simulating the joint evolution of quasars, galaxies and their large-scale distribution, *Nature* 435 (2005) 629–636. [arXiv:astro-ph/0504097](#), [doi:10.1038/nature03597](#).
- [285] J. Bond, S. Cole, G. Efstathiou, N. Kaiser, Excursion set mass functions for hierarchical Gaussian fluctuations, *Astrophys.J.* 379 (1991) 440. [doi:10.1086/170520](#).

- [286] C. G. Lacey, S. Cole, Merger rates in hierarchical models of galaxy formation, *Mon.Not.Roy.Astron.Soc.* 262 (1993) 627–649.
- [287] R. K. Sheth, H. Mo, G. Tormen, Ellipsoidal collapse and an improved model for the number and spatial distribution of dark matter haloes, *Mon.Not.Roy.Astron.Soc.* 323 (2001) 1. [arXiv:astro-ph/9907024](#), [doi:10.1046/j.1365-8711.2001.04006.x](#).
- [288] R. K. Sheth, G. Tormen, An Excursion set model of hierarchical clustering : Ellipsoidal collapse and the moving barrier, *Mon.Not.Roy.Astron.Soc.* 329 (2002) 61. [arXiv:astro-ph/0105113](#), [doi:10.1046/j.1365-8711.2002.04950.x](#).
- [289] J. L. Tinker, A. V. Kravtsov, A. Klypin, K. Abazajian, M. S. Warren, et al., Toward a halo mass function for precision cosmology: The Limits of universality, *Astrophys.J.* 688 (2008) 709–728. [arXiv:0803.2706](#), [doi:10.1086/591439](#).
- [290] A. Knebe, S. R. Knollmann, S. I. Muldrew, F. R. Pearce, M. A. Aragon-Calvo, et al., Haloes gone MAD: The Halo-Finder Comparison Project, *Mon.Not.Roy.Astron.Soc.* 415 (2011) 2293–2318. [arXiv:1104.0949](#), [doi:10.1111/j.1365-2966.2011.18858.x](#).
- [291] J. F. Navarro, C. S. Frenk, S. D. White, The Structure of cold dark matter halos, *Astrophys.J.* 462 (1996) 563–575. [arXiv:astro-ph/9508025](#), [doi:10.1086/177173](#).
- [292] J. Einasto, On the construction of a composite model for the Galaxy and on the determination of the system of Galactic parameters, *Trudy Inst. Astroz. Alma-Ata* 51.
- [293] A. W. Graham, D. Merritt, B. Moore, J. Diemand, B. Terzic, Empirical models for Dark Matter Halos. I. Nonparametric Construction of Density Profiles and Comparison with Parametric Models, *Astron.J.* 132 (2006) 2685–2700. [arXiv:astro-ph/0509417](#), [doi:10.1086/508988](#).
- [294] J. F. Navarro, A. Ludlow, V. Springel, J. Wang, M. Vogelsberger, et al., The Diversity and Similarity of Cold Dark Matter Halos, *Mon.Not.Roy.Astron.Soc.* 402 (2010) 21. [arXiv:0810.1522](#), [doi:10.1111/j.1365-2966.2009.15878.x](#).
- [295] L. Hernquist, An Analytical Model for Spherical Galaxies and Bulges, *Astrophys.J.* 356 (1990) 359. [doi:10.1086/168845](#).
- [296] B. Moore, T. R. Quinn, F. Governato, J. Stadel, G. Lake, Cold collapse and the core catastrophe, *Mon.Not.Roy.Astron.Soc.* 310 (1999) 1147–1152. [arXiv:astro-ph/9903164](#), [doi:10.1046/j.1365-8711.1999.03039.x](#).
- [297] W. Dehnen, D. McLaughlin, Dynamical insight into dark-matter haloes, *Mon.Not.Roy.Astron.Soc.* 363 (2005) 1057–1068. [arXiv:astro-ph/0506528](#), [doi:10.1111/j.1365-2966.2005.09510.x](#).
- [298] J. F. Navarro, E. Hayashi, C. Power, A. Jenkins, C. S. Frenk, et al., The Inner structure of Lambda-CDM halos 3: Universality and asymptotic slopes, *Mon.Not.Roy.Astron.Soc.* 349 (2004) 1039. [arXiv:astro-ph/0311231](#), [doi:10.1111/j.1365-2966.2004.07586.x](#).

- [299] D. Merritt, J. F. Navarro, A. Ludlow, A. Jenkins, A Universal density profile for dark and luminous matter?, *Astrophys.J.* 624 (2005) L85–L88. [arXiv:astro-ph/0502515](#), [doi:10.1086/430636](#).
- [300] J. Stadel, D. Potter, B. Moore, J. Diemand, P. Madau, et al., Quantifying the heart of darkness with GHALO - a multi-billion particle simulation of our galactic halo, *Mon.Not.Roy.Astron.Soc.* 398 (2009) L21–L25. [arXiv:0808.2981](#), [doi:10.1111/j.1745-3933.2009.00699.x](#).
- [301] R. A. Flores, J. R. Primack, Observational and theoretical constraints on singular dark matter halos, *Astrophys.J.* 427 (1994) L1–4. [arXiv:astro-ph/9402004](#), [doi:10.1086/187350](#).
- [302] A. Burkert, The Structure of dark matter halos in dwarf galaxies, *IAU Symp.* 171 (1996) 175. [arXiv:astro-ph/9504041](#), [doi:10.1086/309560](#).
- [303] W. de Blok, S. McGaugh, J. van der Hulst, Hi observations of low surface brightness galaxies: probing low density galaxies, *Mon.Not.Roy.Astron.Soc.* 283 (1996) 18–54. [arXiv:astro-ph/9605069](#), [doi:10.1093/mnras/283.1.18](#).
- [304] S. S. McGaugh, V. C. Rubin, W. de Blok, High - resolution rotation curves of low surface brightness galaxies: Data, *Astron.J.* 122 (2001) 2381–2395. [arXiv:astro-ph/0107326](#), [doi:10.1086/323448](#).
- [305] W. de Blok, A. Bosma, High-resolution rotation curves of low surface brightness galaxies, *Astron.Astrophys.* 385 (2002) 816. [arXiv:astro-ph/0201276](#), [doi:10.1051/0004-6361:20020080](#).
- [306] G. Gentile, P. Salucci, U. Klein, D. Vergani, P. Kalberla, The Cored distribution of dark matter in spiral galaxies, *Mon.Not.Roy.Astron.Soc.* 351 (2004) 903. [arXiv:astro-ph/0403154](#), [doi:10.1111/j.1365-2966.2004.07836.x](#).
- [307] J. D. Simon, A. D. Bolatto, A. Leroy, L. Blitz, E. L. Gates, High-resolution measurements of the halos of four dark matter-dominated galaxies: Deviations from a universal density profile, *Astrophys.J.* 621 (2005) 757–776. [arXiv:astro-ph/0412035](#), [doi:10.1086/427684](#).
- [308] P. Salucci, A. Lapi, C. Tonini, G. Gentile, I. Yegorova, et al., The Universal Rotation Curve of Spiral Galaxies. 2. The Dark Matter Distribution out to the Virial Radius, *Mon.Not.Roy.Astron.Soc.* 378 (2007) 41–47. [arXiv:astro-ph/0703115](#), [doi:10.1111/j.1365-2966.2007.11696.x](#).
- [309] N. Li, D.-M. Chen, Cusp-core problem and strong gravitational lensing, *Res.Astron.Astrophys.* 9 (2009) 1173–1184. [arXiv:0905.3041](#), [doi:10.1088/1674-4527/9/11/001](#).
- [310] J. Guedes, S. Callegari, P. Madau, L. Mayer, Forming Realistic Late-Type Spirals in a LCDM Universe: The Eris Simulation, *Astrophys.J.* 742 (2011) 76. [arXiv:1103.6030](#), [doi:10.1088/0004-637X/742/2/76](#).
- [311] M. Kuhlen, A. Pillepich, J. Guedes, P. Madau, The Distribution of Dark Matter in the Milky Way’s Disk, *Astrophys.J.* 784 (2014) 161. [arXiv:1308.1703](#), [doi:10.1088/0004-637X/784/2/161](#).

- [312] M. Gustafsson, M. Fairbairn, J. Sommer-Larsen, Baryonic Pinching of Galactic Dark Matter Haloes, *Phys.Rev. D* 74 (2006) 123522. [arXiv:astro-ph/0608634](#), [doi:10.1103/PhysRevD.74.123522](#).
- [313] P. Colin, O. Valenzuela, A. Klypin, Bars and cold dark matter halos, *Astrophys.J.* 644 (2006) 687–700. [arXiv:astro-ph/0506627](#), [doi:10.1086/503791](#).
- [314] P. B. Tissera, S. D. White, S. Pedrosa, C. Scannapieco, Dark matter response to galaxy formation, *Mon. Not. Roy. Astron. Soc.* 406 (2010) 922. [arXiv:0911.2316](#), [doi:10.1111/j.1365-2966.2010.16777.x](#).
- [315] O. Y. Gnedin, D. Ceverino, N. Y. Gnedin, A. A. Klypin, A. V. Kravtsov, et al., Halo Contraction Effect in Hydrodynamic Simulations of Galaxy Formation [arXiv:1108.5736](#).
- [316] J. Sommer-Larsen, M. Limousin, Moderate Steepening of Galaxy Cluster Dark Matter Profiles by Baryonic Pinching, *Mon. Not. Roy. Astron. Soc.* 408 (2010) 1998. [arXiv:0906.0573](#), [doi:10.1111/j.1365-2966.2010.17260.x](#).
- [317] S. Mashchenko, J. Wadsley, H. Couchman, Stellar Feedback in Dwarf Galaxy Formation, *Science* 319 (2008) 174. [arXiv:0711.4803](#), [doi:10.1126/science.1148666](#).
- [318] A. Pontzen, F. Governato, How supernova feedback turns dark matter cusps into cores, *Mon.Not.Roy.Astron.Soc.* 421 (2012) 3464. [arXiv:1106.0499](#), [doi:10.1111/j.1365-2966.2012.20571.x](#).
- [319] F. Governato, C. Brook, L. Mayer, A. Brooks, G. Rhee, et al., At the heart of the matter: the origin of bulgeless dwarf galaxies and Dark Matter cores, *Nature* 463 (2010) 203–206. [arXiv:0911.2237](#), [doi:10.1038/nature08640](#).
- [320] A. V. Maccio', G. Stinson, C. B. Brook, J. Wadsley, H. Couchman, et al., Halo expansion in cosmological hydro simulations: towards a baryonic solution of the cusp/core problem in massive spirals, *Astrophys.J.* 744 (2012) L9. [arXiv:1111.5620](#), [doi:10.1088/2041-8205/744/1/L9](#).
- [321] S. Profumo, T. E. Jeltema, Extragalactic Inverse Compton Light from Dark Matter Annihilation and the Pamela Positron Excess, *JCAP* 0907 (2009) 020. [arXiv:0906.0001](#), [doi:10.1088/1475-7516/2009/07/020](#).
- [322] L. E. Strigari, S. M. Koushiappas, J. S. Bullock, M. Kaplinghat, Precise constraints on the dark matter content of Milky Way dwarf galaxies for gamma-ray experiments, *Phys.Rev. D* 75 (2007) 083526. [arXiv:astro-ph/0611925](#), [doi:10.1103/PhysRevD.75.083526](#).
- [323] M. Kuhlen, J. Diemand, P. Madau, The Dark Matter Annihilation Signal from Galactic Substructure: Predictions for GLAST, *Astrophys.J.* 686 (2008) 262. [arXiv:0805.4416](#).
- [324] J. Lavalle, Q. Yuan, D. Maurin, X. Bi, Full Calculation of Clumpiness Boost factors for Antimatter Cosmic Rays in the light of Lambda-CDM N-body simulation results. Abandoning hope in clumpiness enhancement?, *Astron.Astrophys.* 479 (2008) 427–452. [arXiv:0709.3634](#), [doi:10.1051/0004-6361:20078723](#).

- [325] V. Springel, S. D. White, C. S. Frenk, J. F. Navarro, A. Jenkins, et al., A blueprint for detecting supersymmetric dark matter in the Galactic halo, *Nature* (2008) 73–76 [arXiv:0809.0894](#).
- [326] G. D. Martinez, J. S. Bullock, M. Kaplinghat, L. E. Strigari, R. Trotta, Indirect Dark Matter Detection from Dwarf Satellites: Joint Expectations from Astrophysics and Supersymmetry, *JCAP* 0906 (2009) 014. [arXiv:0902.4715](#), [doi:10.1088/1475-7516/2009/06/014](#).
- [327] M. Kamionkowski, S. M. Koushiappas, M. Kuhlen, Galactic Substructure and Dark Matter Annihilation in the Milky Way Halo, *Phys.Rev. D* 81 (2010) 043532. [arXiv:1001.3144](#), [doi:10.1103/PhysRevD.81.043532](#).
- [328] A. Charbonnier, C. Combet, M. Daniel, S. Funk, J. Hinton, et al., Dark matter profiles and annihilation in dwarf spheroidal galaxies: prospectives for present and future gamma-ray observatories - I. The classical dSphs, *Mon.Not.Roy.Astron.Soc.* 418 (2011) 1526–1556. [arXiv:1104.0412](#), [doi:10.1111/j.1365-2966.2011.19387.x](#).
- [329] M. A. Sanchez-Conde, M. Cannoni, F. Zandanel, M. E. Gomez, F. Prada, Dark matter searches with Cherenkov telescopes: nearby dwarf galaxies or local galaxy clusters?, *JCAP* 1112 (2011) 011. [arXiv:1104.3530](#), [doi:10.1088/1475-7516/2011/12/011](#).
- [330] E. Nezri, R. White, C. Combet, D. Maurin, E. Pointecouteau, et al., gamma-rays from annihilating dark matter in galaxy clusters: stacking vs single source analysis, *Mon.Not.Roy.Astron.Soc.* 425 (2012) 477. [arXiv:1203.1165](#), [doi:10.1111/j.1365-2966.2012.21484.x](#).
- [331] J. Zavala, N. Afshordi, Clustering in the Phase Space of Dark Matter Haloes. II. Stable Clustering and Dark Matter Annihilation, *MNRAS* 441 (2014) 1329–1339. [arXiv:1311.3296](#), [doi:10.1093/mnras/stu506](#).
- [332] J. Diemand, M. Kuhlen, P. Madau, Dark matter substructure and gamma-ray annihilation in the Milky Way halo, *Astrophys.J.* 657 (2007) 262–270. [arXiv:astro-ph/0611370](#), [doi:10.1086/510736](#).
- [333] F. C. van den Bosch, G. Tormen, C. Giocoli, The Mass function and average mass loss rate of dark matter subhaloes, *Mon.Not.Roy.Astron.Soc.* 359 (2005) 1029–1040. [arXiv:astro-ph/0409201](#), [doi:10.1111/j.1365-2966.2005.08964.x/abs/](#).
- [334] C. Giocoli, G. Tormen, F. C. d. Bosch, The Population of Dark Matter Subhaloes: Mass Functions and Average Mass Loss Rates, *Mon.Not.Roy.Astron.Soc.* 386 (2008) 2135–2144. [arXiv:0712.1563](#), [doi:10.1111/j.1365-2966.2008.13182.x](#).
- [335] S. Blanchet, J. Lavalle, Diffuse gamma-ray constraints on dark matter revisited. I: the impact of subhalos, *JCAP* 1211 (2012) 021. [arXiv:1207.2476](#), [doi:10.1088/1475-7516/2012/11/021](#).
- [336] J. Diemand, M. Kuhlen, P. Madau, Formation and evolution of galaxy dark matter halos and their substructure, *Astrophys.J.* 667 (2007) 859–877. [arXiv:astro-ph/0703337](#), [doi:10.1086/520573](#).

- [337] J. Diemand, M. Kuhlen, P. Madau, M. Zemp, B. Moore, et al., Clumps and streams in the local dark matter distribution, *Nature* 454 (2008) 735–738. [arXiv:0805.1244](#), [doi:10.1038/nature07153](#).
- [338] A. Klypin, S. Trujillo-Gomez, J. Primack, Halos and galaxies in the standard cosmological model: results from the Bolshoi simulation, *Astrophys.J.* 740 (2011) 102. [arXiv:1002.3660](#), [doi:10.1088/0004-637X/740/2/102](#).
- [339] S. Ando, E. Komatsu, Constraints on the annihilation cross section of dark matter particles from anisotropies in the diffuse gamma-ray background measured with Fermi-LAT, *Phys.Rev. D* 87 (12) (2013) 123539. [arXiv:1301.5901](#), [doi:10.1103/PhysRevD.87.123539](#).
- [340] P. D. Serpico, E. Sefusatti, M. Gustafsson, G. Zaharijas, Extragalactic gamma-ray signal from Dark Matter annihilation: a power spectrum based computation, *Mon.Not.Roy.Astron.Soc.* 421 (2012) L87–L91. [arXiv:1109.0095](#), [doi:10.1111/j.1745-3933.2011.01212.x](#).
- [341] M. P. van Daalen, J. Schaye, The contributions of matter inside and outside of haloes to the matter power spectrum, *Mon.Not.Roy.Astron.Soc.* 452 (2015) 2247–2257. [arXiv:1501.05950](#).
- [342] J. Zavala, N. Afshordi, Clustering in the Phase Space of Dark Matter Haloes. I. Results from the Aquarius simulations, *MNRAS* 441 (2013) 1317–1328. [arXiv:1308.1098](#), [doi:10.1093/mnras/stu678](#).
- [343] M. Boylan-Kolchin, V. Springel, S. D. White, A. Jenkins, G. Lemson, Resolving Cosmic Structure Formation with the Millennium-II Simulation, *Mon.Not.Roy.Astron.Soc.* 398 (2009) 1150. [arXiv:0903.3041](#), [doi:10.1111/j.1365-2966.2009.15191.x](#).
- [344] K. C. Y. Ng, R. Laha, S. Campbell, S. Horiuchi, B. Dasgupta, et al., Resolving small-scale dark matter structures using multisource indirect detection, *Phys.Rev. D* 89 (8) (2014) 083001. [arXiv:1310.1915](#), [doi:10.1103/PhysRevD.89.083001](#).
- [345] F. Stecker, The Cosmic Gamma-Ray Background from the Annihilation of Primordial Stable Neutral Heavy Leptons, *Astrophys.J.* 223 (1978) 1032–1036. [doi:10.1086/156336](#).
- [346] Y.-T. Gao, F. W. Stecker, D. B. Cline, The Lightest supersymmetric particle and the extragalactic gamma-ray background, *Astron.Astrophys.* 249 (1991) 1–4.
- [347] L. Bergstrom, J. Edsjo, P. Ullio, Spectral gamma-ray signatures of cosmological dark matter annihilation, *Phys.Rev.Lett.* 87 (2001) 251301. [arXiv:astro-ph/0105048](#), [doi:10.1103/PhysRevLett.87.251301](#).
- [348] D. Elsaesser, K. Mannheim, Supersymmetric dark matter and the extragalactic gamma-ray background, *Phys.Rev.Lett.* 94 (2005) 171302. [arXiv:astro-ph/0405235](#), [doi:10.1103/PhysRevLett.94.171302](#).
- [349] D. Elsaesser, K. Mannheim, Cosmological gamma ray and neutrino backgrounds due to neutralino dark matter annihilation, *Astropart.Phys.* 22 (2004) 65–72. [arXiv:astro-ph/0405347](#), [doi:10.1016/j.astropartphys.2004.05.003](#).

- [350] K. Ahn, E. Komatsu, Cosmological lower bound on dark matter masses from the soft gamma-ray background, *Phys.Rev. D* 71 (2005) 021303. [arXiv:astro-ph/0412630](#), [doi:10.1103/PhysRevD.71.021303](#).
- [351] T. Oda, T. Totani, M. Nagashima, Gamma-ray background from neutralino annihilation in the first cosmological objects, *Astrophys.J.* 633 (2005) L65–L68. [arXiv:astro-ph/0504096](#), [doi:10.1086/497691](#).
- [352] S. Horiuchi, S. Ando, Dark matter annihilation from intermediate-mass black holes: Contribution to the extragalactic gamma-ray background, *Phys.Rev. D* 74 (2006) 103504. [arXiv:astro-ph/0607042](#), [doi:10.1103/PhysRevD.74.103504](#).
- [353] W. de Boer, C. Sander, V. Zhukov, A. Gladyshev, D. Kazakov, Egret excess of diffuse galactic gamma rays interpreted as a signal of dark matter annihilation, *Phys.Rev.Lett.* 95 (2005) 209001. [arXiv:astro-ph/0602325](#), [doi:10.1103/PhysRevLett.95.209001](#).
- [354] E.-J. Ahn, G. Bertone, D. Merritt, Impact of astrophysical processes on the gamma-ray background from dark matter annihilations, *Phys.Rev. D* 76 (2007) 023517. [arXiv:astro-ph/0703236](#), [doi:10.1103/PhysRevD.76.023517](#).
- [355] M. Fornasa, G. Bertone, Black Holes as Dark Matter Annihilation Boosters, *Int.J.Mod.Phys. D* 17 (2008) 1125–1157. [arXiv:0711.3148](#), [doi:10.1142/S0218271808012747](#).
- [356] A. Cuoco, J. Brandbyge, S. Hannestad, T. Haugboelle, G. Miele, Angular Signatures of Annihilating Dark Matter in the Cosmic Gamma-Ray Background, *Phys.Rev. D* 77 (2008) 123518. [arXiv:0710.4136](#), [doi:10.1103/PhysRevD.77.123518](#).
- [357] W. de Boer, A. Nordt, C. Sander, V. Zhukov, A New Determination of the Extragalactic Background of Diffuse Gamma Rays taking into account Dark Matter Annihilation, *Astron.Astrophys.* 470 (2007) 61–66. [arXiv:0705.0094](#), [doi:10.1051/0004-6361:20054613](#).
- [358] E. Baltz, B. Berenji, G. Bertone, L. Bergstrom, E. Bloom, et al., Pre-launch estimates for GLAST sensitivity to Dark Matter annihilation signals, *JCAP* 0807 (2008) 013. [arXiv:0806.2911](#), [doi:10.1088/1475-7516/2008/07/013](#).
- [359] J. M. Siegal-Gaskins, V. Pavlidou, Robust identification of isotropic diffuse gamma rays from Galactic dark matter, *Phys.Rev.Lett.* 102 (2009) 241301. [arXiv:0901.3776](#), [doi:10.1103/PhysRevLett.102.241301](#).
- [360] A. V. Belikov, D. Hooper, The Contribution Of Inverse Compton Scattering To The Diffuse Extragalactic Gamma-Ray Background From Annihilating Dark Matter, *Phys.Rev. D* 81 (2010) 043505. [arXiv:0906.2251](#), [doi:10.1103/PhysRevD.81.043505](#).
- [361] M. Kawasaki, K. Kohri, K. Nakayama, Diffuse gamma-ray background and cosmic-ray positrons from annihilating dark matter, *Phys.Rev. D* 80 (2009) 023517. [arXiv:0904.3626](#), [doi:10.1103/PhysRevD.80.023517](#).

- [362] F.-Y. Cyr-Racine, S. Profumo, K. Sigurdson, Protohalo Constraints to the Resonant Annihilation of Dark Matter, *Phys.Rev. D*80 (2009) 081302. [arXiv:0904.3933](#), [doi:10.1103/PhysRevD.80.081302](#).
- [363] G. Huetsi, A. Hektor, M. Raidal, Constraints on leptonically annihilating Dark Matter from reionization and extragalactic gamma background, *Astron.Astrophys.* 505 (2009) 999–1005. [arXiv:0906.4550](#), [doi:10.1051/0004-6361/200912760](#).
- [364] S. Dodelson, A. V. Belikov, D. Hooper, P. Serpico, Identifying Dark Matter Annihilation Products In The Diffuse Gamma Ray Background, *Phys.Rev. D*80 (2009) 083504. [arXiv:0903.2829](#), [doi:10.1103/PhysRevD.80.083504](#).
- [365] K. N. Abazajian, P. Agrawal, Z. Chacko, C. Kilic, Conservative Constraints on Dark Matter from the Fermi-LAT Isotropic Diffuse Gamma-Ray Background Spectrum, *JCAP* 1011 (2010) 041. [arXiv:1002.3820](#), [doi:10.1088/1475-7516/2010/11/041](#).
- [366] A. Cuoco, A. Sella, J. Conrad, S. Hannestad, Anisotropies in the Diffuse Gamma-Ray Background from Dark Matter with Fermi LAT: a closer look, *Mon.Not.Roy.Astron.Soc.* 414 (2011) 2040–2054. [arXiv:1005.0843](#), [doi:10.1111/j.1365-2966.2011.18525.x](#).
- [367] K. N. Abazajian, S. Blanchet, J. P. Harding, Current and Future Constraints on Dark Matter from Prompt and Inverse-Compton Photon Emission in the Isotropic Diffuse Gamma-ray Background, *Phys.Rev. D*85 (2012) 043509. [arXiv:1011.5090](#), [doi:10.1103/PhysRevD.85.043509](#).
- [368] J. Aleks, S. Ansoldi, L. Antonelli, P. Antoranz, A. Babic, et al., Optimized dark matter searches in deep observations of Segue 1 with MAGIC, *JCAP* 1402 (2014) 008. [arXiv:1312.1535](#), [doi:10.1088/1475-7516/2014/02/008](#).
- [369] A. Abramowski, et al., Search for a Dark Matter annihilation signal from the Galactic Center halo with H.E.S.S., *Phys.Rev.Lett.* 106 (2011) 161301. [arXiv:1103.3266](#), [doi:10.1103/PhysRevLett.106.161301](#).
- [370] M. Ackermann, et al., Searching for Dark Matter Annihilation from Milky Way Dwarf Spheroidal Galaxies with Six Years of Fermi-LAT Data [arXiv:1503.02641](#).
- [371] M. Ackermann, et al., Search for Dark Matter Satellites using the FERMI-LAT, *Astrophys.J.* 747 (2012) 121. [arXiv:1201.2691](#), [doi:10.1088/0004-637X/747/2/121](#).
- [372] H.-S. Zechlin, D. Horns, Unidentified sources in the Fermi-LAT second source catalog: the case for DM subhalos, *JCAP* 1211 (2012) 050. [arXiv:1210.3852](#), [doi:10.1088/1475-7516/2012/11/050](#).
- [373] M. Bolz, A. Brandenburg, W. Buchmuller, Thermal production of gravitinos, *Nucl.Phys. B*606 (2001) 518–544. [arXiv:hep-ph/0012052](#), [doi:10.1016/S0550-3213\(01\)00132-8](#), [10.1016/j.nuclphysb.2007.09.020](#).
- [374] K.-Y. Choi, D. E. Lopez-Fogliani, C. Munoz, R. R. de Austri, Gamma-ray detection from gravitino dark matter decay in the $\mu\mu$ SSM, *JCAP* 1003 (2010) 028. [arXiv:0906.3681](#), [doi:10.1088/1475-7516/2010/03/028](#).

- [375] A. Arvanitaki, S. Dimopoulos, S. Dubovsky, P. W. Graham, R. Harnik, et al., Decaying Dark Matter as a Probe of Unification and TeV Spectroscopy, *Phys.Rev. D* 80 (2009) 055011. [arXiv:0904.2789](#), [doi:10.1103/PhysRevD.80.055011](#).
- [376] M. Cirelli, M. Kadastik, M. Raidal, A. Strumia, Model-independent implications of the e^+e^- , anti-proton cosmic ray spectra on properties of Dark Matter, *Nucl.Phys. B* 813 (2009) 1–21. [arXiv:0809.2409](#), [doi:10.1016/j.nuclphysb.2013.05.002](#), [10.1016/j.nuclphysb.2008.11.031](#).
- [377] G. Bertone, W. Buchmuller, L. Covi, A. Ibarra, Gamma-Rays from Decaying Dark Matter, *JCAP* 0711 (2007) 003. [arXiv:0709.2299](#), [doi:10.1088/1475-7516/2007/11/003](#).
- [378] A. Ibarra, D. Tran, Gamma Ray Spectrum from Gravitino Dark Matter Decay, *Phys.Rev.Lett.* 100 (2008) 061301. [arXiv:0709.4593](#), [doi:10.1103/PhysRevLett.100.061301](#).
- [379] W. Buchmuller, L. Covi, K. Hamaguchi, A. Ibarra, T. Yanagida, Gravitino Dark Matter in R-Parity Breaking Vacua, *JHEP* 0703 (2007) 037. [arXiv:hep-ph/0702184](#), [doi:10.1088/1126-6708/2007/03/037](#).
- [380] X. Huang, G. Vertongen, C. Weniger, Probing Dark Matter Decay and Annihilation with Fermi LAT Observations of Nearby Galaxy Clusters, *JCAP* 1201 (2012) 042. [arXiv:1110.1529](#), [doi:10.1088/1475-7516/2012/01/042](#).
- [381] A. Ibarra, S. Lopez Gehler, M. Pato, Dark matter constraints from box-shaped gamma-ray features, *JCAP* 1207 (2012) 043. [arXiv:1205.0007](#), [doi:10.1088/1475-7516/2012/07/043](#).
- [382] L. Zhang, C. Weniger, L. Maccione, J. Redondo, G. Sigl, Constraining Decaying Dark Matter with Fermi LAT Gamma-rays, *JCAP* 1006 (2010) 027. [arXiv:0912.4504](#), [doi:10.1088/1475-7516/2010/06/027](#).
- [383] C.-R. Chen, S. K. Mandal, F. Takahashi, Gamma-ray Constraints on Hadronic and Leptonic Activities of Decaying Dark Matter, *JCAP* 1001 (2010) 023. [arXiv:0910.2639](#), [doi:10.1088/1475-7516/2010/01/023](#).
- [384] M. Papucci, A. Strumia, Robust implications on Dark Matter from the first FERMI sky gamma map, *JCAP* 1003 (2010) 014. [arXiv:0912.0742](#), [doi:10.1088/1475-7516/2010/03/014](#).
- [385] M. Cirelli, P. Panci, P. D. Serpico, Diffuse gamma ray constraints on annihilating or decaying Dark Matter after Fermi, *Nucl.Phys. B* 840 (2010) 284–303. [arXiv:0912.0663](#), [doi:10.1016/j.nuclphysb.2010.07.010](#).
- [386] M. Cirelli, E. Moulin, P. Panci, P. D. Serpico, A. Viana, Gamma ray constraints on Decaying Dark Matter, *Phys.Rev. D* 86 (2012) 083506. [arXiv:1205.5283](#), [doi:10.1103/PhysRevD.86.083506](#), [10.1103/PhysRevD.86.109901](#).
- [387] S. Ando, K. Ishiwata, Constraints on decaying dark matter from the extragalactic gamma-ray background, *JCAP* 1505 (05) (2015) 024. [arXiv:1502.02007](#), [doi:10.1088/1475-7516/2015/05/024](#).

- [388] L. Dugger, T. E. Jeltema, S. Profumo, Constraints on Decaying Dark Matter from Fermi Observations of Nearby Galaxies and Clusters, JCAP 1012 (2010) 015. [arXiv:1009.5988](#), [doi:10.1088/1475-7516/2010/12/015](#).
- [389] M. Ackermann, et al., Constraints on the Galactic Halo Dark Matter from Fermi-LAT Diffuse Measurements, Astrophys.J. 761 (2012) 91. [arXiv:1205.6474](#), [doi:10.1088/0004-637X/761/2/91](#).
- [390] T. Asaka, J. Hashiba, M. Kawasaki, T. Yanagida, Spectrum of background x-rays from moduli dark matter, Phys.Rev. D58 (1998) 023507. [arXiv:hep-ph/9802271](#), [doi:10.1103/PhysRevD.58.023507](#).
- [391] F. Takayama, M. Yamaguchi, Gravitino dark matter without R-parity, Phys.Lett. B485 (2000) 388–392. [arXiv:hep-ph/0005214](#), [doi:10.1016/S0370-2693\(00\)00726-7](#).
- [392] J. M. Overduin, P. Wesson, Dark matter and background light, Phys.Rept. 402 (2004) 267–406. [arXiv:astro-ph/0407207](#), [doi:10.1016/j.physrep.2004.07.006](#).
- [393] S. Matsumoto, K. Ishiwata, T. Moroi, Cosmic Gamma-ray from Inverse Compton Process in Unstable Dark Matter Scenario, Phys.Lett. B679 (2009) 1–5. [arXiv:0905.4593](#), [doi:10.1016/j.physletb.2009.07.004](#).
- [394] A. Ibarra, D. Tran, C. Weniger, Decaying Dark Matter in Light of the PAMELA and Fermi LAT Data, JCAP 1001 (2010) 009. [arXiv:0906.1571](#), [doi:10.1088/1475-7516/2010/01/009](#).
- [395] C. Arina, T. Hambye, A. Ibarra, C. Weniger, Intense Gamma-Ray Lines from Hidden Vector Dark Matter Decay, JCAP 1003 (2010) 024. [arXiv:0912.4496](#), [doi:10.1088/1475-7516/2010/03/024](#).
- [396] K. Ishiwata, S. Matsumoto, T. Moroi, Decaying Dark Matter in Supersymmetric Model and Cosmic-Ray Observations, JHEP 1012 (2010) 006. [arXiv:1008.3636](#), [doi:10.1007/JHEP12\(2010\)006](#).
- [397] A. Ibarra, D. Tran, C. Weniger, Indirect Searches for Decaying Dark Matter, Int.J.Mod.Phys. A28 (2013) 1330040. [arXiv:1307.6434](#), [doi:10.1142/S0217751X13300408](#).
- [398] M. Ave, L. Cazon, J. Cronin, J. M. Neto, A. Olinto, et al., The 2pt+: an enhanced 2 point correlation function, JCAP 0907 (2009) 023. [arXiv:0905.2192](#), [doi:10.1088/1475-7516/2009/07/023](#).
- [399] J.-Q. Xia, A. Cuoco, E. Branchini, M. Fornasa, M. Viel, A cross-correlation study of the Fermi-LAT γ -ray diffuse extragalactic signal, Mon.Not.Roy.Astron.Soc. 416 (2011) 2247–2264. [arXiv:1103.4861](#).
- [400] A. M. Soltan, The nearest neighbor statistics for X-ray source counts I.The method [arXiv:1101.0256](#).
- [401] T. R. Slatyer, D. P. Finkbeiner, A statistical test of emission from unresolved point sources, Mon.Not.Roy.Astron.Soc. 405 (2009) 1777–1786. [arXiv:0910.0482](#).

- [402] K. Gorski, E. Hivon, A. Banday, B. Wandelt, F. Hansen, et al., HEALPix - A Framework for high resolution discretization, and fast analysis of data distributed on the sphere, *Astrophys.J.* 622 (2005) 759–771. [arXiv:astro-ph/0409513](#), [doi:10.1086/427976](#).
- [403] E. Komatsu, B. D. Wandelt, D. N. Spergel, A. J. Banday, K. M. Gorski, Measurement of the cosmic microwave background bispectrum on the COBE DMR sky maps, *Astrophys.J.* 566 (2002) 19–29. [arXiv:astro-ph/0107605](#), [doi:10.1086/337963](#).
- [404] L. Knox, Determination of inflationary observables by cosmic microwave background anisotropy experiments, *Phys.Rev.* D52 (1995) 4307–4318. [arXiv:astro-ph/9504054](#), [doi:10.1103/PhysRevD.52.4307](#).
- [405] S. S. Campbell, Angular Power Spectra with Finite Counts, *Mon.Not.Roy.Astron.Soc.* 448 (3) (2015) 2854–2878. [arXiv:1411.4031](#), [doi:10.1093/mnras/stv135](#).
- [406] N. Fornengo, M. Regis, Particle dark matter searches in the anisotropic sky, *Front. Physics* 2 (2014) 6. [arXiv:1312.4835](#), [doi:10.3389/fphy.2014.00006](#).
- [407] B. S. Hensley, J. M. Siegal-Gaskins, V. Pavlidou, The detectability of dark matter annihilation with Fermi using the anisotropy energy spectrum of the gamma-ray background, *Astrophys.J.* 723 (2010) 277–284. [arXiv:0912.1854](#), [doi:10.1088/0004-637X/723/1/277](#).
- [408] B. S. Hensley, V. Pavlidou, J. M. Siegal-Gaskins, Novel Techniques for Decomposing Diffuse Backgrounds, *Mon.Not.Roy.Astron.Soc.* 433 (2013) 591. [arXiv:1210.7239](#), [doi:10.1093/mnras/stt746](#).
- [409] A. E. Broderick, C. Pfrommer, E. Puchwein, K. M. Smith, P. Chang, Lower Limits upon the Anisotropy of the Extragalactic Gamma-Ray Background implied by the 2FGL and 1FHL Catalogs, *Astrophys.J.* 796 (1) (2014) 12. [arXiv:1308.0015](#), [doi:10.1088/0004-637X/796/1/12](#).
- [410] D. N. Limber, The Analysis of Counts of the Extragalactic Nebulae in Terms of a Fluctuating Density Field. II, *Astrophys.J.* 119 (1954) 655. [doi:10.1086/145870](#).
- [411] N. Kaiser, Clustering in real space and in redshift space, *Mon.Not.Roy.Astron.Soc.* 227 (1987) 1–27.
- [412] N. Afshordi, Y.-S. Loh, M. A. Strauss, Cross - correlation of the Cosmic Microwave Background with the 2MASS galaxy survey: Signatures of dark energy, hot gas, and point sources, *Phys.Rev.* D69 (2004) 083524. [arXiv:astro-ph/0308260](#), [doi:10.1103/PhysRevD.69.083524](#).
- [413] P.-J. Zhang, J. F. Beacom, Angular correlations of the MeV cosmic gamma ray background, *Astrophys.J.* 614 (2004) 37–42. [arXiv:astro-ph/0401351](#), [doi:10.1086/423329](#).
- [414] V. Berezhinsky, P. Blasi, V. Ptuskin, Clusters of galaxies as a storage room for cosmic rays, *Astrophys J.* 487 (1997) 529–535. [arXiv:astro-ph/9609048](#), [doi:10.1086/304622](#).

- [415] E. Waxman, A. Loeb, Fluctuations in the radio background from intergalactic synchrotron emission, *Astrophys.J.* 545 (2000) L11–L14. [arXiv:astro-ph/0007049](#), [doi:10.1086/317326](#).
- [416] U. Keshet, E. Waxman, A. Loeb, Imprint of intergalactic shocks on the low - frequency radio sky, *Astrophys.J.* 617 (2004) 281–302. [arXiv:astro-ph/0402320](#), [doi:10.1086/424837](#).
- [417] S. S. Campbell, J. F. Beacom, Combined Flux and Anisotropy Searches Improve Sensitivity to Gamma Rays from Dark Matter [arXiv:1312.3945](#).
- [418] M. Taoso, S. Ando, G. Bertone, S. Profumo, Angular correlations in the cosmic gamma-ray background from dark matter annihilation around intermediate-mass black holes, *Phys.Rev. D* 79 (2009) 043521. [arXiv:0811.4493](#), [doi:10.1103/PhysRevD.79.043521](#).
- [419] F. Calore, V. De Romeri, M. Di Mauro, F. Donato, J. Herpich, et al., Gamma-ray anisotropies from dark matter in the Milky Way: the role of the radial distribution, *Mon.Not.Roy.Astron.Soc.* 442 (2014) 1151–1156. [arXiv:1402.0512](#), [doi:10.1093/mnras/stu912](#).
- [420] G. Gomez-Vargas, et al., Dark matter implications of Fermi-LAT measurement of anisotropies in the diffuse gamma-ray background, *Nucl.Instrum.Meth.* A742 (2014) 149–153. [doi:10.1016/j.nima.2013.11.009](#).
- [421] P. G. Hoel, S. Port, C. Stone, Introduction to probability theory, Houghton Mifflin, 1972.
- [422] S. K. Lee, S. Ando, M. Kamionkowski, The Gamma-Ray-Flux Probability Distribution Function from Galactic Halo Substructure, *JCAP* 0907 (2009) 007. [arXiv:0810.1284](#), [doi:10.1088/1475-7516/2009/07/007](#).
- [423] E. J. Baxter, S. Dodelson, S. M. Koushiappas, L. E. Strigari, Constraining Dark Matter in Galactic Substructure, *Phys.Rev. D* 82 (2010) 123511. [arXiv:1006.2399](#), [doi:10.1103/PhysRevD.82.123511](#).
- [424] M. R. Feyereisen, S. Ando, S. K. Lee, Modelling the flux distribution function of the extragalactic gamma-ray background from dark matter annihilation [arXiv:1506.05118](#).
- [425] G. T. Richards, A. D. Myers, A. G. Gray, R. N. Riegel, R. C. Nichol, et al., Efficient Photometric Selection of Quasars from the Sloan Digital Sky Survey: II. 1,000,000 Quasars from Data Release Six, *Astrophys.J.Suppl.* 180 (2009) 67–83. [arXiv:0809.3952](#), [doi:10.1088/0067-0049/180/1/67](#).
- [426] T. Jarrett, T. Chester, R. Cutri, S. Schneider, J. L. Rosenberg, et al., 2mass extended sources in the zone of avoidance, *Astron.J.* 120 (2000) 298–313. [arXiv:astro-ph/0005017](#), [doi:10.1086/301426](#).
- [427] J. J. Condon, W. Cotton, E. Greisen, Q. Yin, R. Perley, et al., The NRAO VLA Sky survey, *Astron.J.* 115 (1998) 1693–1716. [doi:10.1086/300337](#).
- [428] F. B. Abdalla, M. Banerji, O. Lahav, V. Rashkov, A Comparison of Six Photometric Redshift Methods Applied to 1.5 Million Luminous Red Galaxies, *Mon.Not.Roy.Astron.Soc.* 417 (2011) 1891. [arXiv:0812.3831](#).

- [429] H. Aihara, et al., The Eighth Data Release of the Sloan Digital Sky Survey: First Data from SDSS-III, *Astrophys.J.Suppl.* 193 (2011) 29. [arXiv:1101.1559](#), [doi:10.1088/0067-0049/193/2/29](#).
- [430] A. Cuoco, J.-Q. Xia, M. Regis, E. Branchini, N. Fornengo, et al., Dark matter searches in the gamma-ray extragalactic background via cross-correlations with galaxy catalogues [arXiv:1506.01030](#).
- [431] A. Lewis, S. Bridle, Cosmological parameters from CMB and other data: A Monte Carlo approach, *Phys.Rev. D* 66 (2002) 103511. [arXiv:astro-ph/0205436](#), [doi:10.1103/PhysRevD.66.103511](#).
- [432] R. Smith, et al., Stable clustering, the halo model and nonlinear cosmological power spectra, *Mon.Not.Roy.Astron.Soc.* 341 (2003) 1311. [arXiv:astro-ph/0207664](#), [doi:10.1046/j.1365-8711.2003.06503.x](#).
- [433] J. P. Huchra, L. M. Macri, K. L. Masters, T. H. Jarrett, P. Berlind, et al., The 2MASS Redshift Survey - Description and Data Release, *Astrophys.J.Suppl.* 199 (2012) 26. [arXiv:1108.0669](#), [doi:10.1088/0067-0049/199/2/26](#).
- [434] U. Seljak, Analytic model for galaxy and dark matter clustering, *Mon.Not.Roy.Astron.Soc.* 318 (2000) 203. [arXiv:astro-ph/0001493](#), [doi:10.1046/j.1365-8711.2000.03715.x](#).
- [435] Z. Zheng, A. A. Berlind, D. H. Weinberg, A. J. Benson, C. M. Baugh, et al., Theoretical models of the halo occupation distribution: Separating central and satellite galaxies, *Astrophys.J.* 633 (2005) 791–809. [arXiv:astro-ph/0408564](#), [doi:10.1086/466510](#).
- [436] M. Regis, J.-Q. Xia, A. Cuoco, E. Branchini, N. Fornengo, et al., Particle dark matter searches outside the Local Group, *Phys.Rev.Lett.* 114 (24) (2015) 241301. [arXiv:1503.05922](#), [doi:10.1103/PhysRevLett.114.241301](#).
- [437] M. Bartelmann, P. Schneider, Weak gravitational lensing, *Phys.Rept.* 340 (2001) 291–472. [arXiv:astro-ph/9912508](#), [doi:10.1016/S0370-1573\(00\)00082-X](#).
- [438] N. Kaiser, Weak lensing and cosmology, *Astrophys.J.* 498 (1998) 26. [arXiv:astro-ph/9610120](#), [doi:10.1086/305515](#).
- [439] T. Abbott, et al., The dark energy survey [arXiv:astro-ph/0510346](#).
- [440] R. Laureijs, et al., Euclid Definition Study Report [arXiv:1110.3193](#).
- [441] L. Amendola, et al., Cosmology and fundamental physics with the Euclid satellite, *Living Rev.Rel.* 16 (2013) 6. [arXiv:1206.1225](#).
- [442] C. Heymans, L. Van Waerbeke, L. Miller, T. Erben, H. Hildebrandt, et al., CFHTLenS: The Canada-France-Hawaii Telescope Lensing Survey, *Mon.Not.Roy.Astron.Soc.* 427 (2012) 146. [arXiv:1210.0032](#), [doi:10.1111/j.1365-2966.2012.21952.x](#).
- [443] L. Miller, C. Heymans, T. Kitching, L. Van Waerbeke, T. Erben, et al., Bayesian Galaxy Shape Measurement for Weak Lensing Surveys - III. Application to the Canada-France-Hawaii Telescope Lensing Survey, *Mon.Not.Roy.Astron.Soc.* 429 (2013) 2858–2880. [arXiv:1210.8201](#), [doi:10.1093/mnras/sts454](#).

- [444] E. Komatsu, et al., Seven-Year Wilkinson Microwave Anisotropy Probe (WMAP) Observations: Cosmological Interpretation, *Astrophys.J.Suppl.* 192 (2011) 18. [arXiv:1001.4538](#), [doi:10.1088/0067-0049/192/2/18](#).
- [445] R. Sachs, A. Wolfe, Perturbations of a cosmological model and angular variations of the microwave background, *Astrophys.J.* 147 (1967) 73–90. [doi:10.1007/s10714-007-0448-9](#).
- [446] N. Fornengo, L. Perotto, M. Regis, S. Camera, Evidence of Cross-correlation between the CMB Lensing and the Γ -ray sky, *Astrophys.J.* 802 (1) (2015) L1. [arXiv:1410.4997](#), [doi:10.1088/2041-8205/802/1/L1](#).
- [447] P. Ade, et al., Planck 2013 results. XII. Component separation, *Astron.Astrophys.* 571 (2014) A12. [arXiv:1303.5072](#), [doi:10.1051/0004-6361/201321580](#).
- [448] A. Blanchard, J. Schneider, Gravitational lensing effect on the fluctuations of the cosmic microwave background, *Astron.Astrophys.* 184.
- [449] A. Lewis, A. Challinor, Weak gravitational lensing of the cmb, *Phys.Rept.* 429 (2006) 1–65. [arXiv:astro-ph/0601594](#), [doi:10.1016/j.physrep.2006.03.002](#).
- [450] T. Okamoto, W. Hu, CMB lensing reconstruction on the full sky, *Phys.Rev.* D67 (2003) 083002. [arXiv:astro-ph/0301031](#), [doi:10.1103/PhysRevD.67.083002](#).
- [451] P. Ade, et al., Planck 2013 results. XVII. Gravitational lensing by large-scale structure, *Astron.Astrophys.* 571 (2013) A17. [arXiv:1303.5077](#).
- [452] V. Springel, The Cosmological simulation code GADGET-2, *Mon.Not.Roy.Astron.Soc.* 364 (2005) 1105–1134. [arXiv:astro-ph/0505010](#), [doi:10.1111/j.1365-2966.2005.09655.x](#).
- [453] R. Angulo, V. Springel, S. White, A. Jenkins, C. Baugh, et al., Scaling relations for galaxy clusters in the Millennium-XXL simulation, *Mon.Not.Roy.Astron.Soc.* 426 (2012) 2046–2062. [arXiv:1203.3216](#), [doi:10.1111/j.1365-2966.2009.15191.x](#).
- [454] J.-M. Alimi, V. Bouillot, Y. Rasera, V. Reverdy, P.-S. Corasaniti, et al., DEUS Full Observable Λ CDM Universe Simulation: the numerical challenge [arXiv:1206.2838](#).
- [455] G. Dubus, J. Contreras, S. Funk, Y. Gallant, T. Hassan, et al., Surveys with the Cherenkov Telescope Array, *Astropart.Phys.* 43 (2013) 317–330. [arXiv:1208.5686](#), [doi:10.1016/j.astropartphys.2012.05.020](#).
- [456] J. Ripken, A. Cuoco, H.-S. Zechlin, J. Conrad, D. Horns, The sensitivity of Cherenkov telescopes to dark matter and astrophysical anisotropies in the diffuse gamma-ray background, *JCAP* 1401 (01) (2014) 049. [arXiv:1211.6922](#), [doi:10.1088/1475-7516/2014/01/049](#).
- [457] D. Schlegel, et al., The BigBOSS Experiment [arXiv:1106.1706](#).
- [458] F. A. Harrison, W. W. Craig, F. E. Christensen, C. J. Hailey, W. W. Zhang, et al., The Nuclear Spectroscopic Telescope Array (NuSTAR) High-Energy X-Ray Mission, *Astrophys.J.* 770 (2013) 103. [arXiv:1301.7307](#), [doi:10.1088/0004-637X/770/2/103](#).

- [459] T. Takahashi, K. Mitsuda, R. Kelley, H. Aharonian, F. Aarts, et al., The ASTRO-H X-ray Observatory, Proc.SPIE Int.Soc.Opt.Eng. 8443 (2012) 1Z. [arXiv:1210.4378](#), [doi:10.1117/12.926190](#).
- [460] T. Kitayama, M. Bautz, M. Markevitch, K. Matsushita, S. Allen, et al., ASTRO-H White Paper - Clusters of Galaxies and Related Science [arXiv:1412.1176](#).
- [461] M. Aartsen, et al., First observation of PeV-energy neutrinos with IceCube, Phys.Rev.Lett. 111 (2013) 021103. [arXiv:1304.5356](#), [doi:10.1103/PhysRevLett.111.021103](#).
- [462] M. Aartsen, et al., Evidence for High-Energy Extraterrestrial Neutrinos at the IceCube Detector, Science 342 (2013) 1242856. [arXiv:1311.5238](#), [doi:10.1126/science.1242856](#).
- [463] M. Aartsen, et al., Observation of High-Energy Astrophysical Neutrinos in Three Years of IceCube Data, Phys.Rev.Lett. 113 (2014) 101101. [arXiv:1405.5303](#), [doi:10.1103/PhysRevLett.113.101101](#).
- [464] IceCube’s Neutrinos: The beginning of extra-Galactic neutrino astrophysics? [arXiv:1312.0558](#).
- [465] L. A. Anchordoqui, V. Barger, I. Cholis, H. Goldberg, D. Hooper, et al., Cosmic Neutrino Pevatrons: A Brand New Pathway to Astronomy, Astrophysics, and Particle Physics, JHEAp 1-2 (2014) 1–30. [arXiv:1312.6587](#), [doi:10.1016/j.jheap.2014.01.001](#).
- [466] A. Loeb, E. Waxman, The Cumulative background of high energy neutrinos from starburst galaxies, JCAP 0605 (2006) 003. [arXiv:astro-ph/0601695](#), [doi:10.1088/1475-7516/2006/05/003](#).
- [467] F. W. Stecker, PeV neutrinos observed by IceCube from cores of active galactic nuclei, Phys.Rev. D88 (4) (2013) 047301. [arXiv:1305.7404](#), [doi:10.1103/PhysRevD.88.047301](#).
- [468] K. Murase, Y. Inoue, C. D. Dermer, Diffuse Neutrino Intensity from the Inner Jets of Active Galactic Nuclei: Impacts of External Photon Fields and the Blazar Sequence, Phys.Rev. D90 (2014) 023007. [arXiv:1403.4089](#), [doi:10.1103/PhysRevD.90.023007](#).
- [469] P. Padovani, E. Resconi, Are both BL Lacs and pulsar wind nebulae the astrophysical counterparts of IceCube neutrino events?, Mon.Not.Roy.Astron.Soc. 443 (2014) 474–484. [arXiv:1406.0376](#), [doi:10.1093/mnras/stu1166](#).
- [470] K. Murase, M. Ahlers, B. C. Lacki, Testing the Hadronuclear Origin of PeV Neutrinos Observed with IceCube, Phys.Rev. D88 (12) (2013) 121301. [arXiv:1306.3417](#), [doi:10.1103/PhysRevD.88.121301](#).
- [471] M. Ahlers, K. Murase, Probing the Galactic Origin of the IceCube Excess with Gamma-Rays, Phys.Rev. D90 (2) (2014) 023010. [arXiv:1309.4077](#), [doi:10.1103/PhysRevD.90.023010](#).

- [472] R.-Y. Liu, X.-Y. Wang, S. Inoue, R. Crocker, F. Aharonian, Diffuse PeV neutrinos from EeV cosmic ray sources: semi-relativistic hypernova remnants in star-forming galaxies, *Phys.Rev. D*89 (2014) 083004. [arXiv:1310.1263](#), [doi:10.1103/PhysRevD.89.083004](#).
- [473] L. A. Anchordoqui, T. C. Paul, L. H. M. da Silva, D. F. Torres, B. J. Vlcek, What IceCube data tell us about neutrino emission from star-forming galaxies (so far), *Phys.Rev. D*89 (2014) 127304. [arXiv:1405.7648](#), [doi:10.1103/PhysRevD.89.127304](#).